Impact of HIF-1α-signalling in cardiac fibroblasts on the healing process after myocardial infarction

Inaugural dissertation

Submitted to the

Faculty of Mathematics and Natural Science

of the Heinrich Heine University of Düsseldorf, Germany

for the degree of

Doctor of Natural Science

Submitted by

Julia Steinhausen

born in Wuppertal, Germany

Düsseldorf, November 2024

From the Department of Molecular Cardiology, Medical Faculty and University Hospital Düsseldorf, Heinrich Heine University Düsseldorf

Printed with the permission of the Faculty of Mathematics and Natural Science of the Heinrich Heine University Düsseldorf

1. Assessor: Prof. Dr. Jürgen Schrader

Department of Molecular Cardiology, Heinrich Heine University Düsseldorf

Universitätsstraße 1

40225 Düsseldorf

2. Assessor: Prof. Dr. Eckhard Lammert

Department of Metabolic Physiology, Heinrich Heine University Düsseldorf

Universitätsstraße 1

40225 Düsseldorf

Day of oral exam: 31/03/2025

Summary

Ischemic heart diseases including myocardial infarction (MI) are representing the leading cause of death worldwide. MI is associated with cardiac fibrosis that results in extensive extracellular matrix (ECM) deposition, leading to cardiac stiffness, severe impairment of cardiac function and eventually heart failure (HF) and death. Key players in cardiac tissue remodelling post MI are cardiac fibroblasts (CFs), which become activated (aCFs), mediate ECM deposition, and orchestrate the cellular response by secreting paracrine signals. During an ischemic event such as MI, the transcription factor hypoxia-inducible factor 1 (HIF-1) plays a crucial role in the adaption of cells to hypoxia, for example by switching the energy metabolism to glycolysis. HIF-1 is a dimer of an α-subunit (HIF-1α), which is usually subject to proteasomal degradation under normoxic conditions, and a steadily expressed β-subunit (HIF-1β). Several studies have shown that the stabilisation of HIF-1α has cardioprotective potential and can improve cardiac outcome post MI. The specific role of HIF-1α stabilisation in aCFs post MI, however, has not been explored so far. Thus, the aim of this study was to characterise HIF-1 signalling in CFs and aCFs to explore differences in their response, especially with respect to HIF-1-controlled expression of glycolytic enzymes, ECM proteins and paracrine factors.

Using an MI mouse model (50 min ischemia followed by reperfusion) to activate CFs, three different hypoxia-dependent or -independent approaches were applied to induce HIF-1α expression *in vitro* as well as *in vivo.* In addition, HIF-1-mediated effects were analysed in aCFs in comparison to CFs at the level of gene expression but also functionally. (I) Seahorse extracellular flux analysis showed that in vitro HIF-1α induction by adenosine receptor $A_{2B}R$ activation for 24 h increased the glycolytic rate and decreased oxygen consumption in both CFs (from healthy hearts) and aCFs (from hearts 5 days post MI (dpMI)) to a similar extent. Without exogenous HIF-1α induction, however, aCFs showed a higher glycolytic rate than CFs, which might be a consequence of the higher proliferation rate of aCFs. (II) Quantitative Real-Time PCR (qRT-PCR) analysis revealed that *in vitro* HIF-1α induction by incubation at 1% O_2 for 6 h enhanced gene expression of glycolytic enzymes in aCFs more profoundly than in CFs, which suggests a faster HIF-1-mediated adaption to hypoxia in aCFs. (III) Single-cell RNA sequencing (scRNAseq) at 5 dpMI revealed that *in vivo* aCF-specific HIF-1α induction by expression of a mutated HIF-1α protein escaping proteasomal

degradation in a transgenic mouse line (Postn-Hif-1αdPA) increased the number of aCFs and intensified the expression of ECM proteins as well as paracrine pro-angiogenic factors. This was accompanied by a transient improvement of cardiac function parameters at 1 dpMI in comparison to mice without Hif-1αdPA expression as assessed by magnetic resonance imaging (MRI).

Together, this study identified a variety of similarities and differences in the HIF-1 response between CFs and aCFs. HIF-1α induction in both CFs and aCFs switched their energy metabolism to cell-protective glycolysis, but aCFs seemed to be more susceptible to regulation of glycolytic enzyme gene expression. HIF-1 induction in post-MI aCFs not only enhanced gene expression of ECM proteins as well as pro-angiogenic factors, which likely promote tissue repair, but also improved cardiac function in the acute phase after MI. These findings add substantial emphasis on HIF-1 signalling in aCFs as promising therapeutic target to promote cardiac healing and ameliorate adverse cardiac outcome after MI.

Abbreviations

aCF	activated cardiac fibroblast
BAY	BAY 60-6582
CAD	coronary artery disease
cDNA	complementary DNA
CF	cardiac fibroblast
CILP	cartilage intermediate layer protein
CM	cardiomyocyte
COL1A1	collagen type 1 alpha 1 chain
Ct	cycle threshold
CTGF	connective tissue growth factor
CTHRC1	collagen triple helix repeat containing 1
cTn	cardiac troponin
CXCL14	CXC motif chemokine ligand 14
DAMP	danger associated molecular patterns
DDR2	discoidine receptor 2
DFO	deferoxamine
DMOG	dimethyloxaloylglycine
dpMI	days post myocardial infarction
ECG	electrocardiogram
ECM	extracellular matrix
EDV	end-diastolic volume
EF	ejection fraction
EMT	epithelial-to-mesenchymal transition
EndoMT	endothelial-to-mesenchymal transition
ESV	end-systolic volume
F-Act	fibroblast-activated
F-Cyc	fibroblast-cycling
FGF	fibroblast growth factor
FIH-1	factor inhibiting HIF
FN1	fibronectin
FOV	field of view
F-SH	fibroblast-sca1 high
F-SL	fibroblast-sca1 low
FSP1	fibroblast specific protein 1

F-WntX	fibroblast-Wnt expressing
GEM	gel beads in emulsion
GO	gene ontology
GOI	gene of interest
HIF-1α	hypoxia inducible factor 1 alpha
HRE	hypoxia response element
i.p.	intraperitoneal
IC	immune cell
IGF1	insulin-like growth factor 1
IgFLASH	IntraGate fast low angle shot
IL-1	interleukin-1
KO	knockout
LAD	left anterior descending artery
LANUV	state office for nature, environment and consumer protection
LOX	lysyl oxidase
LPS	lipopolysaccharide
MI	myocardial infarction, myocardial infarction
MMP	matrix metalloproteinases
MRI	magnetic resonance imaging
MYDGF	myeloid derived growth factor
MYO	myofibroblast
NF	nuclear factor
NGS	normal goat serum, next generation sequencing
OCR	oxygen consumption rate
PDGFRα	platelet derived growth factor receptor alpha
PHD	prolyl-4-hydroxylase
POSTN	periostin
pPCI	primary percutaneous coronary intervention
pVHL	E3 ubiquitin ligase Von Hippel-Lindau
qRT-PCR	quantitative real-time PCR
ROS	reactive oxygen species
scRNAseq	single cell RNA sequencing
SV	stroke volume
TCF21	transcription factor 21
TGF	transforming growth factor
THBS1	thrombospondin-1
THY1	thymocyte 1

TIMP	tissue inhibitor of MMPs
TLR	toll-like receptor
Tregs	regulatory T-cells
UMI	unique molecular identifier
VEGF	vascular endothelial growth factor
WIF1	Wnt inhibitory factor 1
ZETT	central facility for animal research and scientific animal welfare
α-SMA	alpha smooth muscle actin

Contents

1 Introduction

1.1 Myocardial infarction (MI)

The leading cause of death worldwide is represented by ischemic heart disease including myocardial infarction (MI): between 1990 and 2019 deaths by ischemic heart disease increased from 6.1 million to 9.14 million[1]. The pathological definition of MI is myocardial cell death caused by a prolonged ischemic event[2]. In animal models the apoptosis-associated cardiomyocyte (CM) cell death after induced MI can be biochemically detected within 10 min[3]. In contrast, it can take hours until myocyte necrosis after MI is detectable in humans e.g. by post-mortem examination[3].

In the healthy heart the right and left coronary arteries supply the myocardium with sufficient oxygen[4]. In case of a MI, the oxygen supply of the myocardium via the coronary artery is interrupted resulting in an ischemic area[5]. The oxygen deficiency in the affected area leads to necrosis of CMs which results in a significant loss of contractile function of the heart[6].

Since different triggers can initiate MI, it was classified into five types of infarcts depending on differences in pathology, clinics and prognosis to define the appropriate treatment strategy[2]. Within the different types of MI, type I and II are the most common ones[7]. Type I is characterised by an atherothrombotic coronary artery disease (CAD) with a rupture or erosion of an atherosclerotic plaque[2]. Plaque rupture, which is the main cause of acute MI, or plaque erosion occur either with or without an occlusive thrombus[8,9]. Type II is not caused by an atherosclerotic plaque but by a mismatch between oxygen supply and demand in the myocardium[7]. This oxygen imbalance is mostly caused by a reduction of the vessel diameter due to atherosclerosis, vasoconstriction or a non-atherosclerotic dissection of the coronary artery[2,10].

In the clinics, several biomarkers are used to diagnose myocardial injury. Especially cardiac troponin (cTn) is used with its regulatory proteins troponin I and T which are mainly expressed in the heart[11,12]. Due to myocardial damage both proteins are released to the blood stream and serve as the preferred biomarker in the serum of

CAD patients with MI[13]. A myocardial injury is identified as acute MI when the injury is associated with ischemia and a rising cTn level[11,12,14,15]. However, it is known that the increase of the cTn values can also arise in absence of a myocardial injury[16,17]. False positive results for cTn value increases can be caused by fibrin clots[18] or heterophile antibodies[19] and thus might lead to an incorrect treatment strategy.

The main treatment after identifying an acute MI is myocardial reperfusion to reoxygenate tissue area downstream of the blocked coronary artery. Due to early myocardial reperfusion, tissue damage is reduced and consequently the survival rate of patients is improved[20]. Early reperfusion limits injury and this strategy has been improved in recent years by using primary percutaneous coronary intervention (pPCI) or different ischaemic conditioning strategies[21,22]. Despite this strategy, there is tissue loss mainly due to loss of CMs and the deposition of extracellular matrix (ECM) due to the activation of cardiac fibroblasts (CFs). This results in cardiac fibrosis that occurs post MI and is defined as cardiac remodelling[23]. The consequences of the cardiac remodelling include the alteration of cardiac structure and the irreversible reduction of cardiac function[24].

To be able to counteract these detrimental consequences, cardiac remodelling and especially its underlying molecular mechanisms have to be further studied to identify new therapeutic approaches. Since the activation of CFs and their deposition of ECM is one of the key processes of cardiac fibrosis post MI[25], it is important to further investigate the molecular mechanisms and signalling pathways initiated by activated cardiac fibroblasts (aCFs).

1.2 Role of CFs in cardiac repair and remodelling post MI

Ischemia during MI induces a massive CM death due to necrosis and apoptosis. In the adult mammalian heart, with its barely existing regenerative capacity, CFs form a collagen rich scar in the infarcted area during the healing process[26]. Cardiac tissue repair and remodelling is divided into three overlapping phases after MI which are precisely orchestrated[23]: inflammation (3 hours – 3 days), proliferation (3 days – 14 days), and scar maturation (14 days – 2 months)[27] (Figure 1). The times given here apply to the mouse heart.

The inflammatory phase is initiated immediately after MI and defined by intense inflammation and infiltration of immune cells (IC)[28]. As consequence of ischemia, danger-associated molecular patterns (DAMPs) are released by necrotic and stressed or injured cells. Additionally, components of the damaged ECM can serve as DAMPs that activate the innate immune system and serve as a warning system by triggering the inflammatory response[29,30]. The downstream signalling induced by DAMPs includes the activation of the complement pathway[31], toll-like receptor (TLR)-associated pathways and the nuclear factor (NF)-κB pathway[32]. The activation of these pathways, especially the NF-κB pathway, which also occurs in CFs, lead to the expression of pro-inflammatory genes including CXC and CC chemokines, inflammatory cytokines and cell adhesion molecules[33,34]. The expression of chemokines induces the recruitment of immune cells to the infarcted myocardial area and the immune cell survival can be pro-longed by the DAMP-signalling. CXC chemokines recruit neutrophils which infiltrate the infarcted heart as the first immune cell type, while CC chemokines are monocyte and $CD4^+$ T cell attractants[28,35,36]. Besides immune cells, also CFs play a crucial role in the inflammatory phase after MI. During 24-72h post MI CFs change from a homeostatic to an activated pro-inflammatory phenotype[37]. The phenotype change is due to stimulation by reactive oxygen species (ROS) and interleukin-1 (IL-1). IL-1 signalling in aCFs promotes also the expression of matrix metalloproteinases (MMPs)[38].

The proliferative phase is initiated by a change of the cardiac microenvironment due to the clearance of dead cells and debris by the recruited immune cells[23]. At this time point post MI neutrophil survival is no longer pro-longed by DAMPs and cytokines which is why neutrophiles undergo apoptosis[39,40]. The phagocytosis of apoptotic neutrophiles leads in macrophages to a phenotype change to M2 macrophages and induces the secretion of pro-fibrotic cytokines like transforming growth factor (TGF)-β as well as anti-inflammatory cytokines such as IL-10. The secretion of these cytokines promotes tissue repair while in parallel it inhibits inflammation.[41] Additionally, regulatory T cells (Tregs) infiltrate the infarcted heart during the proliferative phase to encourage wound healing and also resolve inflammation by producing IL-10, IL-13 and TGF-β[42]. The transformation of the pro-inflammatory aCF phenotype into myofibroblasts and the TGF-β-induced proliferation of aCFs, which become the most dominant cell type in the infarct area[34], play a major key role in the proliferation phase

post MI[43,44]. Transformation into myofibroblasts is induced among others by the loss of IL-1 signalling followed by the activation of α-smooth muscle actin (α-SMA) expression which is characteristic for myofibroblasts[34,43]. The myofibroblasts expressing contractile proteins infiltrate into the infarct area and secrete large amounts of matrix proteins [45–47]. The migration to the infarct area may be controlled by growth factors such as TGF-β and fibroblast growth factors (FGFs)[48]. The secretion of tissue inhibitors of MMPs (TIMPs) inhibits MMPs to ensure that newly synthesised collagens are not degraded[49]. Additionally, the proliferative aCFs and also myofibroblasts secrete pro-fibrotic and angiogenic factors. While the earlier proliferative aCFs express pro-fibrotic and pro-angiogenic factors like vascular endothelial growth factor (VEGF), myofibroblasts show the opposite profile and express anti-angiogenic factors like CXC motif chemokine ligand 14 (CXCL14) and thrombospondin-1 (THBS1)[50]. However, to date, the main focus of past studies has been on the matrix proteins expressed by CF. The expression of angiogenic, fibrotic and other paracrine factors need to be further investigated. The proliferative phase ends with forming a collagen-based matrix and with that introducing scar maturation[34].

Maturation is the last phase of cardiac remodelling and is characterised by ECM accumulation, which is mainly contributed by aCFs, and scar formation[51]. The number of myofibroblasts decreases[52] and the phenotype of the aCFs changes from myofibroblasts to matrifibrocytes by disassembling the stress fibers[53]. Matrifibrocytes secrete collagen-crosslinking enzymes such as lysyl oxidases (LOX) which are stabilising the scar[54]. In parallel the remaining reparative cells such as ICs and also aCFs are deactivated and undergo apoptosis[23,27,52].

The deposition of ECM by myofibroblasts during the cardiac remodelling builds the collagen-rich scar and prevents the infarcted heart from a ventricular rupture[27,55,56]. However, a fibrosis stiffening the myocardium could cause heart failure through the negative impact on heart function.

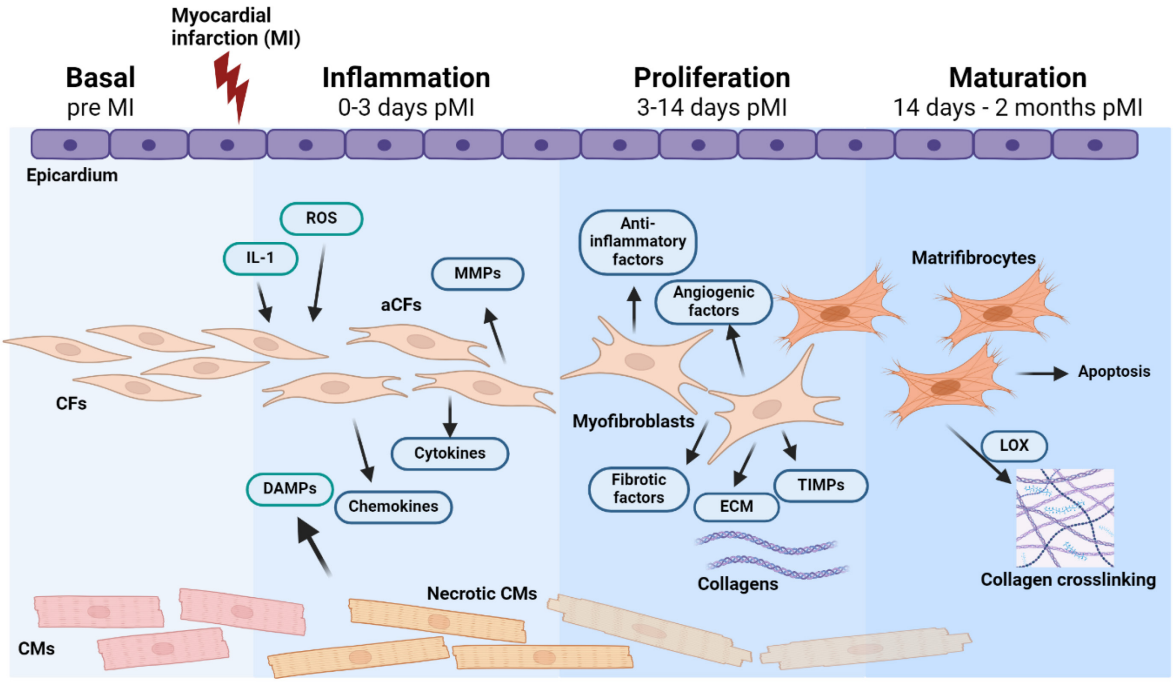

Figure 1: Role of cardiac fibroblasts (CFs) in the different phases of cardiac remodelling post MI (figure modified after Humeres *et al.*, 2019[27])

After MI the injured myocardium undergos remodelling which is devided in three overlapping phases: inflammation (0-3 days pMI), proliferation (3-14 days pMI) and maturation (14 days - 2 months pMI). During ischemia cardiomyocytes get necrotic and release damage-associated molecular patterns (DAMPs) which activate the innate immune system and inducing the inflammatory phase by recruiting leukocytes. Inflammation induced ROS and IL-1 stimulate resident CFs and promote their change into activated cardiac fibroblasts (aCFs) with a pro-inflammatory phenotype. These aCFs secrete pro-inflammatory cytokines and chemokines as well as matrix metalloproteinases (MMPs). The clearance of dead cells and debris by immune cells and the associated change in the cardiac microenvironment together with proliferating CFs initiate the proliferative phase of cardiac remodelling. The secretion of pro-fibrotic and anti-inflammatory cytokines by immune cells promotes tissue repair. In the following pro-inflammatory aCFs convert into myofibroblasts which are the main source of ECM and additionally express anti-inflammatory, angiogenic and fibrotic factors as well as tissue inhibitors of MMPs (TIMPs). At the end of the proliferative phase collagen-rich matrix is produced initiating scar maturation. The amount of myofibroblasts strongly decreases as they convert to matrifibrocytes or undergo apoptosis. Matrifibrocytes secrete the cross-linking enzyme lysyl oxidases (LOX) which is responsible for stabilisation and maturation of the collagenous scar. (Figure was created with © 2024 BioRender)

1.3 The regenerative potential of CFs

The limited regenerative capacity of the adult mammalian heart is one reason why cardiovascular disease is still the leading cause of death worldwide[1]. Due to MI, at least 25% of left ventricular CMs are irreversibly wiped out within hours[57]. In contrast to some lower vertebrates[58] and mammals in the early neonatal period[59], the adult mammalian heart lacks the capacity to renew CMs in the injured heart to restore heart function. To investigate a possible regenerative response of the adult mammalian heart to enhance cardiac function post MI, researchers within the last decades have focused on cell-based therapies, especially stem cells[60]. Besides initial promising results using stem cell therapy[61], numerous clinical studies did not show consistent beneficial effects[62]. As a consequence more recent research on heart regeneration focused on the modulation of existing differentiated cells such as CFs, CMs and ECs in the adult mammalian heart[63].

Due to their high number in the myocardium post MI, especially in the border and infarct zone, aCFs represent a promising cell population for regenerative therapy approaches[63]. CFs have been shown to have the potential to be reprogrammed to differentiate into CMs[64–66]. The reprogramming was done with several substance cocktails including transcription factors[65,67] or miRNAs[68,69]. However, the tested therapy approaches on the CF differential potential to reprogram into CMs were not successful. Another aspect is the beneficial influence of aCF-secreted paracrine factors on wound healing processes, repair and cardiac remodelling post MI which could also lead to heart function-improving therapy approaches[66,70]. For example the by CFs secreted paracrine factor insulin-like growth factor 1 (IGF1) has been discovered to play a cardioprotective role in myocardial hypertrophy[66]. Another paracrine factor found to be expressed by CFs[71] was myeloid-derived growth factor (MYDGF) and is known to have cardioprotective effects[72]. To identify possible therapeutical targets deeper insights into the molecular processes and important signalling pathways in aCFs post MI are warranted.

1.4 Heterogeneity of CFs

CFs are mesenchymal cells which originate from two main sources (Figure 2), the pro-epicardial organ as the major source with cells undergoing epithelial-to-mesenchymal transition (EMT) and the endocardium from which cells undergo endothelial-to-mesenchymal transition (EndoMT) and contribute to cardiac valves[73,74]. Additionally, a minor number of CFs origins from the neural crest by undergoing EndoMT[75]. Around 85% of CFs located in the adult myocardium have an epicardial origin[74].

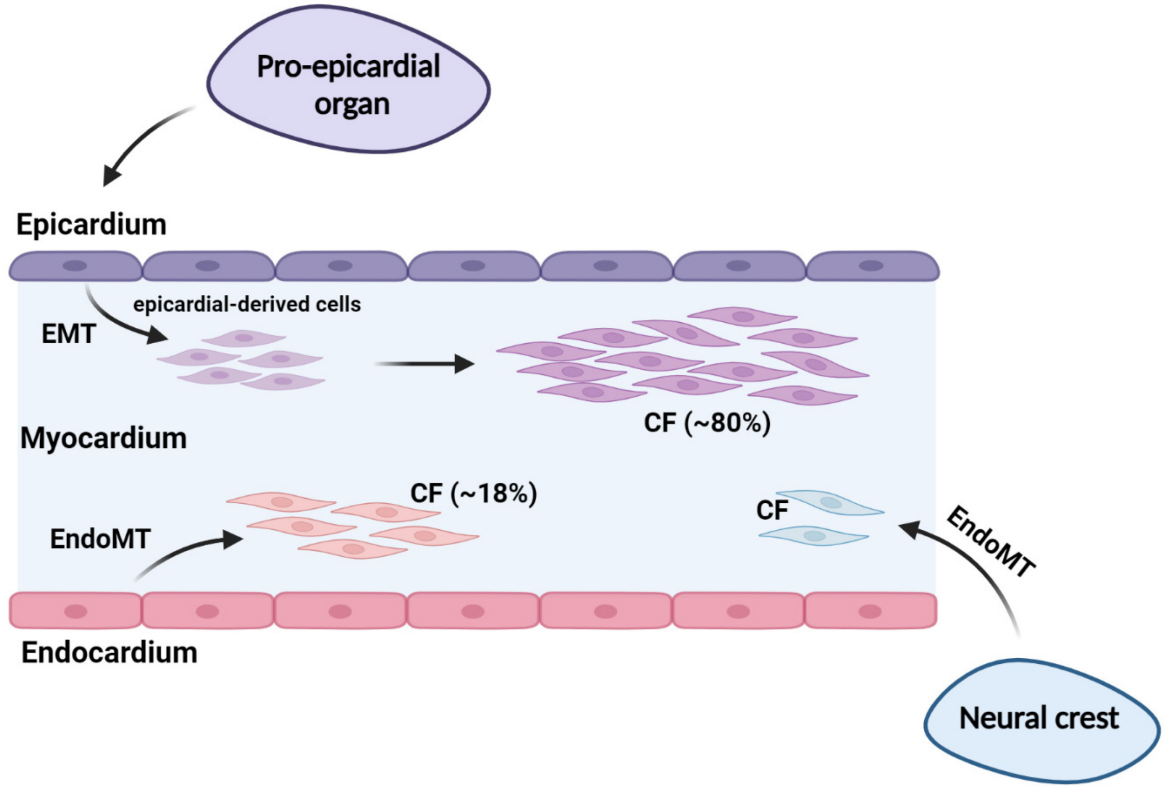

Figure 2: Generation of CFs during embryogenesis (figure modified after Doppler et al. 2017[76])
During embryogenic developement of the heart CFs originate from two major sources: the pro-epicardial organ and the endocardium. The epicardium derives from the pro-epicardial organ and epicardial cells undergo epithelial-to-mesenchymal transition (EMT) forming epicardium-derived cells which further differentiate into CFs. The CF population deriving from the pro-epicardial organ represents with approximately 80% the largest proportion of CFs. The second major origin of CFs with around 18% is the endocardium from which cells undergo endothelial-to-mesenchymal transition (EndoMT) to form CFs. Additionally, a third very minor source of CF development is the neural crest. Cells from this progenitor population can also undergo EndoMT and form CFs. (Figure was created with © 2024 BioRender)

The cell morphology of CFs is flat and spindle-shaped[77]. In early publications CFs were thought to represent the major non-myocyte cell type in the heart[78]. New investigations using an improved flow cytometry protocol showed that the proportion of CF within nonmyocytes was below 20% and ECs displayed the largest cell proportion of all nonmyocytes with about 60%[79]. In a healthy heart resident CFs are found throughout the whole cardiac tissue and are surround CMs.[80] CFs highly express connexins are connected to CMs via gap junctional channels to modulate the electrophysiological CM properties[81]. Thus, CFs form a highly complex 3-D network within the surrounding tissue[82,83]. During their resident state CFs constantly maintain homeostasis in the whole cardiac environment by communicating within a range of electrical, chemical and mechanical signals with the surrounding cardiac tissue and preserving the basal ECM turnover[51,84]. For example, the secretion of cytokines, MMPs and growth factors by CFs maintains the balance of synthesising and degrading components of the connective tissue[80]. With these processes CFs are assisting the CMs to maintain the normal contractile function of the heart[51]. Resident CFs are mostly quiescent cells involved in the maintenance of myocardial structure but also have biochemical, mechanical and electrical charcteristics[80].

Due to the heterogeneity of the CFs is hard to identify CFs by expression of only one marker gene. Multiple markers were found to be characteristic for resident CFs like discoidine receptor 2 (DDR2)[83], thymocyte 1 (THY1)[74], transcription factor 21 (TCF21)[85], fibroblast specific protein 1 (FSP1)[86] and platelet derived growth factor receptor alpha (PDGFRα)[87]. All these marker genes are individually no specific CF markers, because they are also expressed in other cell types besides fibroblasts[77].

Upon cardiac injury, for example after MI described above (1.1), CFs differentiate into different activated phenotypes (1.2, Figure 1) and play a major role in cardiac repair and remodelling. Marker genes of the aCFs differ from the markers of resident CFs but are also different between the aCF phenotypes. One of the key markers for aCFs is αSMA (*Acta2*) which is expressed after MI at high levels in myofibroblasts and is not found in resident CFs[88,89]. Another aCF marker appearing post MI is periostin (POSTN, *Postn*). POSTN is expressed in CFs during development but somehow disappears and is not expressed in resident CFs in the adult heart before reappearing post injury[90]. Farbehi *et al.*[91] showed that aCFs are also characteristic for an upregulated expression

of collagen type 1 alpha 1 chain (COL1A1, *Col1a1*), collagen triple helix repeat containing 1 (CTHRC1, *Cthrc1*) and fibronectin (FN1, *Fn1*).

All in all, the identification either of CFs or aCFs with one specific cell marker is not possible. It is therefore necessary to use several of these markers to reliably identify the different phenotypes of CFs.

As shown in Figure 2, CFs can have different developmental origins[76]. Early studies demonstrated that fibroblasts differ in several aspects like in their size, their gene and protein expression profile as well as in their proliferative activity[92–94]. Although it is known that CFs and aCFs both play a crucial role in cardiac remodelling, their different phenotypes are poorly understood and have to be further studied[27]. A recent lineage tracing single cell RNA sequencing (scRNAseq) study identified 11 CF/aCF subpopulations, comparing cells from sham-operated mouse hearts and cells from mouse hearts 3 and 7 days post MI (dpMI)[91]. This study by Farbehi *et al.*[91] showed that the proportion of the subpopulations extensively changed between the three conditions. The different subpopulations were characterised and defined based on their transcriptional profile. Among the different cell populations Farbehi *et al.*[91] identified two resident fibroblast populations, Fibroblast-*Sca1*^{high} (F-SH) and Fibroblast-*Sca1*^{low} (F-SL). While CFs from F-SH highly expressed *Pdgfra* and *Ly6a* (*Sca1*), are comparable to S^+P^+ [95] cells and are characterised by expressing genes involved in cell adhesion processes, the F-SL population expressed much lower *Sca1* levels and the gene expression profile indicated that these cells play a role in signalling and signal transduction. The most characteristic CF populations in an activated state described by Farbehi *et al.*[91] are Fibroblast-*Wnt* expressing (F-WntX), Fibroblast-activated (F-Act), Fibroblast-cycling (F-Cyc) and Myofibroblast (MYO). F-WntX, F-Act and F-Cyc appear at the early timepoint 3 dpMI and were mostly diminished at 7 dpMI while in contrast the MYO population appeared at day 7 pMI as a large population. The F-WntX population mainly expressed genes associated with the Wnt-signalling pathway, especially Wnt inhibitory factor 1 (WIF1, *Wif1*) which is essential for cardiac repair and an antagonist of the *connective tissue growth factor* (CTGF) signalling. This population is due to its transcriptional profile thought to be anti-Wnt, anti-CTGF and anti-TGF-ß signalling. Another population expressing genes to inhibit TGF-ß signalling is F-Act by expressing the TGF-β inhibitor *cartilage intermediate layer protein* (CILP, *Cilp*). F-Act also highly expressed *Postn* and was described as a pre-MYO population.

The cell cycle signature of the gene expression profile from F-Cyc CFs together with the high levels of *Postn* and *Acta2* expression indicate that these CFs are highly proliferative. All of these three populations mostly diminish with the appearance of the MYO population at 7 dpMI. This population expressed high levels of collagens, *Postn* and *Acta2* as well as *Fn1* and *Cthrc1* indicating to play a key role in wound healing and cell migration.

Comparable results of CFs/aCFs from mouse hearts 5 dpMI and sham surgery with regard to the different subpopulations and their transcriptional profile have been recently reported by our group[71]. Various paracrine factors described as cardioprotective were identified in this analysis. Both studies revealed a heterogeneous gene expression of paracrine factors, cytokines, chemokines as well as ECM-associated genes comparing CF and aCF populations but also within the different subpopulations of aCFs.

As mentioned above, the problem to detect all aCFs is due to the lack of cell type specific marker genes. Although several marker genes have been described for aCF, they catch either only a subpopulation of aCF or are also expressed in other cell types[63].

1.5 Hypoxic signalling

Under physiological oxygen conditions, oxygen which is delivered to the lung binds to circulating haemoglobin and the oxygenated blood is pumped to the periphery by action of the heart. The delivery of oxygenated blood maintains organ and cell function enabling continuous oxidative phosphorylation to take place.[96] In case of an oxygen-limiting event such as a MI, the affected area of the heart remains hypoxic/ischemic until the tissue is reperfused/reoxygenated. Hypoxia induces the stabilisation of the hypoxia-inducible factor 1α (HIF-1α) subunit leading to the activation of hypoxia-associated signalling pathways[97].

Under normoxic conditions the HIF-1α protein is continuously degraded (Figure 3). The proteasomal degradation is introduced by the hydroxylation of two specific HIF-1α proline residues (proline 402 and 564) by action of the oxygen-dependent prolyl-4-hydroxylases (PHDs)[98]. The E3 ubiquitin ligase Von Hippel-Lindau (pVHL) binds to the hydroxylated HIF-1α[99]. The polyubiquitination leads to the degradation of the protein.

Additionally, a second oxygen-dependent mechanism inhibits the transcriptional function of any HIF-1α which escaped the PHD and pVHL mediated degradation. This mechanism is characterised by the hydroxylation of an asparagine residue of HIF-1α due to the factor inhibiting HIF (FIH-1)[100]. The hydroxylation of the asparagine residue in the N-terminal activation domain interferes with recruiting the transcriptional co-activator p300 leading to the inhibition of transcriptional function[101].

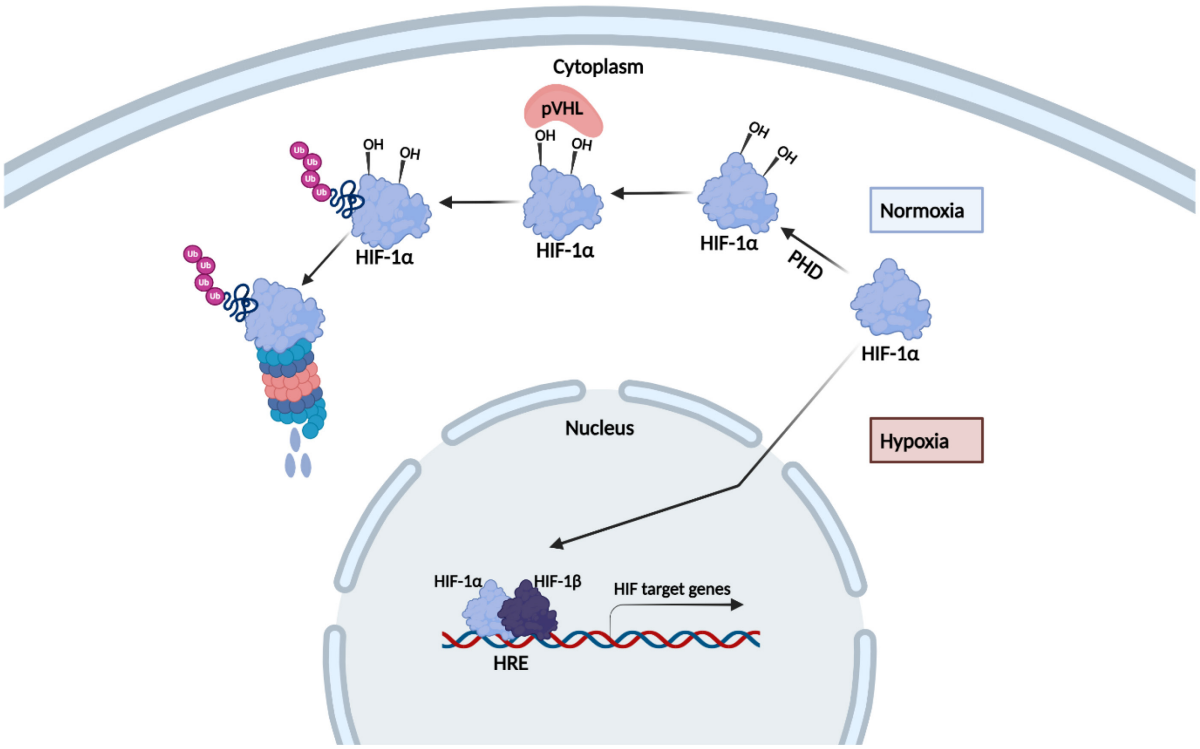

Figure 3: Regulation of HIF-1α during normoxia and hypoxia by proline hydroxylation (figure modified after Lee *et al.* 2019[96])

During normoxia HIF-1α is hydroxylated by prolyl-4-hydroxylases (PHDs) and polyubiquitinated by the E3 ubiquitin ligase Von Hippel-Lindau (pVHL). The polyubiquitination of the hydroxylated HIF-1α protein leads to its proteosomal degradation. During hypoxia the PHD are inhibited due to lack of oxygen. HIF-1α translocates into the nucleus and forms a transcription factor complex with the HIF-1β subunit. The complex binds to the DNA sequence of the hypoxia response element (HRE) inducing the expression of HIF target genes. (Figure was created with © 2024 BioRender).

Triggered by hypoxia, oxygen deficiency inhibits PHD and FIH-1 leading to the stabilisation of the HIF-1α subunit. Thereafter, HIF-1α translocates to the nucleus and forms a transcription factor complex with HIF-1β. The heterodimeric complex binds to the hypoxia response element (HRE) inducing the expression of HIF target genes. The transcriptional gene regulation of several cascades mostly triggers an adaptive response as well as signalling for tissue protection[96].

Additionally, there is evidence that HIF-1 can also be induced and activated by non-hypoxic stimuli[102]. Studies have shown that even under normoxic conditions the stimulation of different cell types with growth factors[103,104], vasoactive hormones[103,105] and cytokines[106] leads to the activation of HIF-1α. In contrast to the hypoxic stabilisation of HIF-1α protein, the non-hypoxic induction is thought to increase HIF-1α protein translation but not inhibit protein degradation[102]. Besides the increase in protein also mRNA transcription can be enhanced by action of vasoactive hormones and lipopolysaccharide (LPS) [102]. In addition to these findings, our group has reported that in CFs the activation of the adenosine receptor $A_{2B}R$ induced HIF-1α under normoxic conditions which was of the same magnitude as under hypoxia [107]. Still another way to stabilise HIF-1α without oxygen deficiency is to genetically modify the *Hif1a* sequence: an exchange of prolines at positions 402 and 564 to alanine has the consequence that the mutated HIF-1α escapes the recognition of the pVHL and therefore is not further degraded which leads to protein stabilisation of HIF-1αdPA[108].

1.5.1 Targets of HIF-1α signalling

HIF-1α is described as the master regulator of oxygen homeostasis and known to play a crucial role in the adaption of cells to oxygen deficiency[109]. HIF-1α signalling induces the expression of numerous target genes involved in the adaption to hypoxia[110]. One crucial cell protective effect induced by HIF-signalling is the metabolic switch of cells towards glycolysis during the lack of oxygen. Therefore, HIF-1α upregulates the transcriptional expression of glycolytic genes[111]. In an attempt to restore the oxygen supply, HIF signalling additionally induces the expression of pro-angiogenic genes like *Vegf*[112] to promote angiogenesis. Moreover, it has been shown that HIF-signalling also targets collagens and other ECM molecules confirming a role in ECM remodelling processes[113,114].

1.5.2 The cardioprotective potential of HIF-1α

HIF-1α-induced signalling pathways are crucial for cardiovascular biology[115,116]. These pathways have an extensive influence on mechanisms involved in endogenous cardioprotection[117]. In the so called “myocardial preconditioning” the myocardium is exposed alternately to short periods of ischemia and short bursts of reperfusion to

protect the heart from acute MI[118]. Since ischemic preconditioning is beneficial for cardiac outcome post MI, it was shown that one mechanism activated by this treatment is the HIF transcription complex envolving the expression of HIF target genes[119–123]. As a result of these findings, various strategies were developed to enhance and stabilise HIF in the heart to improve cardiac outcome after MI. On the one hand, studies used the global treatment with chemical reagents like dimethyloxalylglycine (DMOG)[122,124,125], deferoxamine (DFO)[126] or cobalt chloride[127] to inhibit PHDs and therefore stabilise HIF. The outcome of all three treatments was a reduction of infarct size. On the other hand, several genetic strategies to enhance, stabilise or deplete HIF have been studied in the last years. Genetical downregulation or the knockout of PHDs have been suggested to be beneficial for the improvement of cardiac function as well as the reduction of infarct size post MI[117]. Constitutively active HIF-1α which was cardiac-specific also resulted in a reduced infarct size together with an improvement in cardiac function 4 weeks post MI[128]. Additionally, Cai et al. showed, by using a global HIF-1α knockout (KO), that HIF-1α is required for ischemia pre-conditioning induced ROS production as well as for the cardiac protection against injury caused by ischemia[121]. Other studies also focussed on cell-specific accumulation of HIF. Cardiomyocyte-specific knock out of PHD2 protects from acute MI[129], whereas the cardiomyocyte-specific overexpression of PHD3 does not alter cardiac function but increases infarct size[130]. An endothelial-specific KO of PHD2/3 stabilised HIF in cardiac endothelial cells of neonatal and adult mice resulted in stimulated cardiomyocyte proliferation and improved cardiac function post MI[131]. In addition it should be mentioned that in all studies in which HIF was stabilised by manipulation of the PHDs or the VHL protein, HIF stabilisation is also possible by exchanging the prolines at sites 402 and 564[108]. HIF proteins with this proline exchange cannot be targeted and degraded by PHDs leading to a HIF protein stabilisation[108]. However, there are studies in which CM-specific HIF stabilisation had negative effects on the heart. Moslehi *et al.*[132] described that a CM-specific inactivation of PHD2 and PHD3 and therefore a long-term stabilisation of HIF-1α resulted in dilated cardiomyopathy. Also, CM-specific deletion of the VHL protein caused severe heart failure in mice[133]. Besides CM- and EC- specific HIF regulation, HIF-1α deletion was also studied in Pdgfra^{+} CFs. Janbandhu *et al.*[97] demonstrated that the deletion of HIF-1α in resident CFs of healthy hearts decreased the expression of HIF target genes and increased the amount of mesenchymal progenitor cells. Following sham injury, CF

activation in mice with HIF-1α deletion increased without proliferative activity. Post MI the HIF-1α deficiency in Pdgfra^{+} CFs had extensive consequences such as a high increase in CF proliferation followed by excessive scar formation and contractile dysfunction[97].

Aside from the two CM-specific PHD and VHL knockout studies, all previous studies showed that HIF-1α has the potential to be cardioprotective. In addition, these studies provided strong evidence that HIF signalling is a key regulator in CFs, but this has not been investigated so far.

1.6 Aim of the study

Given that CFs are pivotal mediators of post-MI cardiac remodelling and that HIF signalling is essential for the adequate cellular response to ischemic events, the overriding question of this study was to investigate how HIF signalling controls the cellular activity of CFs. Especially, the expression of ECM and paracrine factors by CFs post MI were from high interest, because they might represent promising targets for the development of new therapeutic approaches in the future. Due to the crosstalk between CFs and surrounding cardiac cell types[134], the manipulation of the HIF-controlled secretion of paracrine factors by CFs might not only target CFs itself, but also cardiac cell types including ECs and ICs which receive signals from CFs.

Thus, the aim of this study was to characterise and explore HIF signalling in both CFs and MI-induced aCFs to define potential differences in their response. Three different approaches were implemented to achieve this goal:

1. The *in vitro* exploration of the HIF-mediated switch towards glycolysis in CFs and aCFs after normoxic HIF-1α induction by chemical activation of the adenosine receptor $A_{2B}R$ (see 1.5) using the A_{2B} agonist BAY60-6583. The chosen normoxic conditions enabled us to investigate the cellular effects of A_{2B} stimulation on both oxygen consumption and glycolysis by measuring the extracellular oxygen and proton flux (Seahorse platform). Additionally, the effects of the A_{2B} agonist BAY60-6583 may be of special interest, since this compound can be administered systemically and therefore might be an option for future therapy approaches to promote HIF-1α induction.

2. The *in vitro* characterisation of CF and aCF gene expression in response to hypoxic HIF-1α induction by quantitative real-time polymerase chain reaction (qRT-PCR). With this approach it is possible to investigate the effects of canonical HIF induction (see 1.5.1) in CFs and MI-induced aCFs and thereby identify potential differences in their molecular response to oxygen deprivation. The focus was on HIF-induced changes in expression of tissue remodelling and repair-associated genes, including fibrotic and angiogenic genes, and paracrine factors like cytokines and chemokines.

3. The analysis of the effects of HIF-1α stabilisation on gene expression in CFs and aCFs without the activation of additional pathways by native stimuli. In contrast to HIF-1α induction by hypoxia or other signals such as $A_{2B}R$ activation, this approach allows to explore the effects of HIF-1α accumulation without influencing other pathways concomitantly triggered by the stimuli.

    a. In an *in vitro* attempt, CFs and aCFs are to be transfected with a HIF-1αdPA plasmid (see 1.5). Since CFs and aCFs as primary cells may be hard to transfect, the transfection efficiency was controlled by including the sequence of EGFP as fluorescent reporter within the plasmid.

    b. In an *in vivo* attempt, a conditional transgenic mouse line ($Postn^{CreERT2}$*Gt(ROSA)26Sor*$^{tm3(HIF1A*)Kael}$) is used, in which after CreERT2 induction by tamoxifen MI-activated POSTN-positive aCFs express HIF-1αdPA *in vivo*. Gene expression was analysed by scRNAseq, which simultaneously allows to explore the effects on CF heterogeneity. Furthermore, cardiac function parameters after MI are assessed by magnetic resonance imaging (MRI).

2 Materials

2.1 Equipment and devices

Table 1: Used equipment and devices.

Device	Type designation	Manufacturer
Analytical balance	PA214	Ohaus Europe (Greifensee, Switzerland)
Autoclave	LabStar 150	Zirbus technology GmbH (Bad Grund, Germany)
Camera systems	F-View Soft Imaging System	Olympus (Tokyo, Japan)
	AxioCam ICm1	Zeiss (Oberkochen, Germany)
Centrifuges	5424R	Eppendorf (Hamburg, Germany)
	Allegra X-30R	Beckman Coulter (Brea, USA)
	Megafuge 16R	Thermo Fisher Scientific (Waltham, USA)
	Megafuge ST Plus Series	Thermo Fisher Scientific (Waltham, USA)
Chromium single-cell gene expression system		10X Genomics (Pleasanton, USA)
Cryostat	Leica CM1520	Leica Biosystems (Nussloch, Germany)
Data acquisition hardware device	PowerLab/16SP	ADInstruments (Spechbach, Germany)
Drying cabinet	UN30	Memmert (Büchenbach, Germany)
Electronic pipette	E1-ClipTip	Thermo Fisher Scientific (Waltham, USA)
Flow cytometer	BD FACSCanto II	Becton Dickinson (Franklin Lakes, USA)
Fluorescence microscopes	BX61	Olympus (Tokyo, Japan)
	Axio Vert.A1	Zeiss (Oberkochen, Germany)
Heating circulator bath	DC1-B3	Thermo Haake (Karlsruhe, Germany)
Heating bath	WB5	P-D Industriegesellschaft mbH (Dresden, Germany)
Incubator	Heracell 150i	Thermo Fisher Scientific (Waltham, USA)

Langendorff equipment		Physiology workshop, University Duesseldorf
Magnet	Mojosort Magnet	BioLegend (San Diego, USA)
Magnet system	Magnet System 400’89 Ascend	Bruker Switzerland AG (Fällanden, Switzerland)
Micro forceps	MICRO FCPS 20 MM 115 MM	Aesculap (Tuttlingen, Germany)
Micro scissors	Vannas Scissors, curved, 85 mm	Aesculap (Tuttlingen, Germany)
	Vannas Scissors, curved, 160 mm	Aesculap (Tuttlingen, Germany)
	Vannas Scissors, straight, 85 mm	Aesculap (Tuttlingen, Germany)
Nanodrop	NanoDrop 2000	Thermo Fisher Scientific (Waltham, USA)
Neubauer counting chamber	Neubauer counting chamber 0.100 mm depth, 0.0025 mm^2	neoLab Migge GmbH (Heidelberg, Germany)
NMR microimaging system	Mini 0.5	Bruker (Rheinstetten, Germany)
NMR resonator coil	25 mm *birdcage*	Bruker (Rheinstetten, Germany)
NMR spectrometer	9.4 Tesla Bruker Avance III Wide Bore	Bruker (Rheinstetten, Germany)
Nucleofector	4D-Nucleofector	Lonza Group AG (Basel, Switzerland)
PCR System	Mastercycler X50s	Eppendorf (Hamburg, Germany)
Peristaltic pump	Minipuls 3	Gilson, Inc. (Middleton, USA)
Pipets	Research	Eppendorf (Hamburg, Germany)
Plate reader	FLUOstar OPTIMA	BMG Labtech (Ortenberg, Germany)
Plate reader	Infinite M200 Pro	Tecan Trading AG (Männedorf, Switzerland)
Plate shaker	MTS 2/4	IKA Werke (Staufen, Germany)
Real-Time PCR system	StepOne Plus	Applied Biosystems (Waltham, USA)
Extracellular flux technology	Seahorse XFe96	Agilent Technologies (Santa Clara, USA)
Stereo microscope	Leica MZ6	Leica Biosystems (Nussloch, Germany)
Sterile bench	Scanlaf Mars Pro Cytosafe Class 2	Labogene (Lynge, Denmark)
Small animal blood flow meter	T160	Transonic Systems Inc. (New York, USA)

Spectrophotometer	NanoDrop 2000	Thermo Fisher Scientific (Waltham, USA)
Tweezers	Tweezers straight pointed, 130 mm	Roth (Karlsruhe, Germany)
Ultrasonic bath	Sonorex RK 100 H	Bandelin (Berlin, Germany)
Vacuum pumping unit	PC 3004 VARIO	Vacuubrand GmbH (Wertheim, Germany)
Vortexer	Vortex-Genie 2	neoLab (Heidelberg, Germany)

2.2 Expendable materials

Table 2: Used expendable materials.

Material	Manufacturer
0.5 ml insulin syringe	Becton Dickinson (Franklin Lakes, USA)
6-Well plate TC	Greiner Bio One (Kremsmunster, Austria)
12-Well plate TC	Greiner Bio One (Kremsmunster, Austria)
24-Well plate TC	Greiner Bio One (Kremsmunster, Austria)
96-Well plate TC	Greiner Bio One (Kremsmunster, Austria)
20 ml syringe	Braun (Melsungen, Germany)
Cell culture flask T25, T75	Greiner Bio One (Kremsmunster, Austria)
Cell scraper	Roth (Karlsruhe, Germany)
Cell strainer40 µm	Greiner Bio One (Kremsmunster, Austria)
Cell strainer 100 µm	Greiner Bio One (Kremsmunster, Austria)
Coverslips	Roth (Karlsruhe, Germany)
Customised TaqMan Array Cards, 364 Well	Thermo Fisher Scientific (Waltham, USA)
5 ml round-bottom tubes	Becton Dickinson (Franklin Lakes, USA)
Centrifugation tubes 15 ml, 50 ml	Greiner Bio One (Kremsmunster, Austria)
ImmEdge Hydrophobic Barrier PAP Pen	BIOZOL Diagnostica Vertrieb GmbH (Eching, Germany)
MicroAmp Fast 96-Well Reaction Plate	Life Technologies (Carlsbad, USA)

Microscope slides 76 mm x 26 mm x 1mm	Engelbrecht Medizin und Labortechnik GmbH (Edermünde, Germany)
PCR reaction tube 0.2 ml	Greiner Bio One (Kremsmunster, Austria)
PCR plate, 96-Well, 0.2 ml	STARLAB International GmbH (Hamburg, Germany)
Pipet tips 10 µl, 200 µl, 1000 µl	Greiner Bio One (Kremsmunster, Austria)
Reaction tube low retention 1.5 ml, 2 ml	Eppendorf (Hamburg, Germany)
Scalpel No. 10	Feather Safety Razor Co. (Osaka, Japan)
Seahorse FluxPak mini	Agilent Technologies (Santa Clara, USA)
Stripets 5 ml, 10 ml, 25 ml, 50 ml	Greiner Bio One (Kremsmunster, Austria)
Syringe filter 0.22 µm	Becton Dickinson (Franklin Lakes, USA)

2.3 Buffer

Table 3: Used buffers and the compositions.

Buffer	Components	Manufacturer
Cell lysis buffer	RLT Plus 1 % Beta-mercaptoethanol	
Immunofluorescence blocking buffer	PBS 0.2 % Saponin 5 % NGS 1:50 IgG mouse	
Cell sorting buffer	PBS 5 mM EDTA 0.5 % BSA	
Phosphate buffered saline (PBS)	137 mM NaCl 10 mM NaH_2PO_4 2.7 mM KCl 1.8 mM KH_2PO_4 pH 7.2	Roth (Karlsruhe, Germany)
RLT Plus	/	Qiagen (Hilden, Germany)
XF Calibrant	/	Agilent Technologies (Santa Clara, USA)

2.4 Media

Table 4: Used media and their composition.

Media	Components	Manufacturer
DMEM high glucose	4.5 g/l Glucose Sodium pyruvate 3.7 g/l $NaHCO_3$	PAN Biotech GmbH (Aidenbach, Germany)
Cell culture medium	DMEM high glucose 20 % dialyzed, heat-inactivated FBS 1 % Penicillin/streptomycin 1 % Glutamax	
OPTI-MEM reduced serum medium	HEPES 2.4 g/l Sodium bicarbonat L-Glutamine	Thermo Fisher Scientific (Waltham, USA)
Seahorse medium	XF DMEM medium pH 7.4 1 mM Pyruvate 2 mM Glutamine 10 mM Glucose	
XF DMEM medium pH 7.4	/	Agilent Technologies (Santa Clara, USA)

2.5 Chemicals

Table 5: Used chemicals.

Chemical	Manufacturer
BAY-606583	Tocris Bioscience (Bristol, United Kingdom)
Beta-mercaptoethanol	Sigma-Aldrich (St. Louis, USA)
Bovine serum albumin (BSA)	Thermo Fisher Scientific (Waltham, USA)
Collagenase Type II	Worthington Biochemical Corporation (Lakewood, USA)
Dimethyl sulfoxide (DMSO)	Sigma-Aldrich (St. Louis, USA)
Ethanol	Thermo Fisher Scientific (Waltham, USA)
Fetal bovine serum, dialysed (FBS)	Thermo Fisher Scientific (Waltham, USA)
Fixable Viability Dye eFluor 780	eBioscience (Frankfurt am Main, Germany)
Gadovist	Bayer (Leverkusen, Germany)
Glucose, 1.0 M solution	Agilent Technologies (Santa Clara, USA)

Glutamax	Thermo Fisher Scientific (Waltham, USA)
Glutamine, 200 mM solution	Agilent Technologies (Santa Clara, USA)
Heparin sodium 25000 I.E./5 ml	B. Braun Melsungen AG (Melsungen, Germany)
IgG anti mouse	R&D Systems (Minneapolis, USA)
Isoflurane	Actavis GmbH (Wien, Austria)
KP-CryoCompound	ImmunoLogic (Duiven, Netherlands)
Lipofectamine 3000	Thermo Fisher Scientific (Waltham, USA)
Methanol	Roth (Karlsruhe, Germany)
Nail polish	Essie (New York, USA)
Normal goat serum (NGS)	Thermo Fisher Scientific (Waltham, USA)
Paraformaldehyde (PFA), 4 %	Labochem international (Athens, Greece)
Penicillin/streptomycin, 10000 U/ml	PAN Biotech GmbH (Aidenbach, Germany)
ProLong Gold antifade reagent with DAPI	Thermo Fisher Scientific (Waltham, USA)
2-Propanol	Roth (Karlsruhe, Germany)
Pyruvate, 100 mM solution	Agilent Technologies (Santa Clara, USA)
Saponin	Merck (Darmstadt, Germany)
Streptavidin nanobeads, Mojosort	BioLegend (SanDiego, USA)
TaqMan Fast Advanced Master Mix	Thermo Fisher Scientific (Waltham, USA)
TaqMan Gene Expression Master Mix	Thermo Fisher Scientific (Waltham, USA)
Trypan blue stain, 0.4 %	Thermo Fisher Scientific (Waltham, USA)
Trypsin-EDTA, 0.05 %	Thermo Fisher Scientific (Waltham, USA)

2.6 Kits

Table 6: Used Kits.

Kit	Manufacturer
Chromium Next GEM Single Cell 3' Reagent Kits v3.1	10X Genomics (Pleasanton, USA)
High-Capacity cDNA Reverse Transcription Kit	Thermo Fisher Scientific (Waltham, USA)
P1 Primary Cell 4D-Nucleofector X Kit L	Lonza (Basel, Switzerland)
Primary Cell Optimization 4D-Nucleofector X Kit	Lonza (Basel, Switzerland)
RNeasy Plus Micro Kit	Qiagen (Hilden, Germany)
Seahorse XF Glycolytic Rate Assay Kit	Agilent Technologies (Santa Clara, USA)

2.7 Antibodies

2.7.1 Primary antibodies

Table 7: Primary antibodies used for immunofluorescence and flow cytometry.

Specificity	Clone	Host	Dilution	Manufacturer
CD31	monoclonal	rat	1:100	BD Bioscience (Franklin Lakes, USA)
CD45	monoclonal	rat	1:400	BD Bioscience (Franklin Lakes, USA)
Mouse anti HA	monoclonal	mouse	1:100	Thermo Fisher Scientific (Waltham, USA)
Mouse anti HIF-1α	monoclonal	mouse	1:100	Thermo Fisher Scientific (Waltham, USA)
Rat anti HA	monoclonal	rat	1:100	Novus Biologicals (Nordenstadt, Germany)
Rabbit anti HIF-1α	monoclonal	rabbit	1:100	Abcam (Cambridge, UK)
Rabbit anti POSTN	polyclonal	rabbit	1:100	OriGene (Rockville, USA)

2.7.2 Secondary antibodies

Table 8: Secondary antibodies used for immunofluorescence.

Specificity	Fluorochrome	Clone	Host	Dilution	Manufacturer
Goat anti mouse IgG	AF 488	polyclonal	goat	1:200/ 1:1000	Thermo Fisher Scientific (Waltham, USA)
Goat anti mouse IgG	AF 594	polyclonal	goat	1:200/ 1:1000	Thermo Fisher Scientific (Waltham, USA)
Goat anti rabbit IgG	AF 488	polyclonal	goat	1:200/ 1:1000	Thermo Fisher Scientific (Waltham, USA)
Goat anti rabbit IgG	AF 594	polyclonal	goat	1:200/ 1:1000	Thermo Fisher Scientific (Waltham, USA)
Goat anti rat IgG	AF 594	polyclonal	goat	1:200/ 1:1000	Thermo Fisher Scientific (Waltham, USA)

2.8 TaqMan Assays

Quantitative real-time PCR (qRT-PCR) was performed with a customised TaqMan Array Card in the 96-Well format using *TaqMan Gene Expression Assays* from Thermo Fisher Scientific (Waltham, USA). The Assays contain a primer pair and a fluorescence-labelled probe.

Table 9: TaqMan Gene Expression Assays used for qRT-PCR.

Gene product	Gene code	Assay-ID
Hypoxia inducable factor 1, alpha subunit	Hif-1α	Mm00468869_m1

Table 10: TaqMan Gene Expression Assays used for the Array Cards.

Gene product	Gene code	Assay-ID
Chemokine (C-C motif) ligand 2	*Ccl2*	Mm00441242_m1
Chemokine (C-X-C motif) ligand 12	*Cxcl12*	Mm00445553_m1
Fibroblast growth factor 1	*Fgf1*	Mm00438906_m1
Fibroblast growth factor 2	*Fgf2*	Mm01285715_m1

Fibroblast growth factor 9	*Fgf9*	Mm00442795_m1
Fibroblast growth factor 11	*Fgf11*	Mm00679875_m1
Insulin-like growth factor 1	*Igf1*	Mm00439560_m1
Insulin-like growth factor 2	*Igf2*	Mm00439564_m1
Insulin-like growth factor binding protein 1	*Igfbp1*	Mm00515154_m1
Insulin-like growth factor binding protein 2	*Igfbp2*	Mm00492632_m1
Insulin-like growth factor binding protein 3	*Igfbp3*	Mm01187817_m1
Insulin-like growth factor binding protein 4	*Igfbp4*	Mm00494922_m1
Interleukin 6	*Il6*	Mm00446190_m1
Jagged 1	*Jag1*	Mm00496902_m1
Myeloid-derived growth factor	*Mydgf*	Mm00840829_m1
Platelet-derived growth factor A	*Pdgfa*	Mm01205760_m1
Platelet-derived growth factor C	*Pdgfc*	Mm00480205_m1
Platelet-derived growth factor D	*Pdgfd*	Mm00546829_m1
Transforming growth factor beta 1	*Tgfb1*	Mm01178820_m1
Transforming growth factor beta 2	*Tgfb2*	Mm00436955_m1
Transforming growth factor beta 3	*Tgfb3*	Mm00436960_m1
Vascular endothelial growth factor A	*Vegfa*	Mm00437306_m1
Vascular endothelial growth factor C	*Vegfc*	Mm00437310_m1
Wilms tumor 1 homologe	*Wt1*	Mm01337048_m1
Chemokine (C-X-C motif) receptor 4	*Cxcr4*	Mm01996749_s1
Adenosine A2b receptor	*Adora2b*	Mm00839292_m1
Ectonucleoside triphosphate diphosphohydrolase 1	*Cd39*	Mm00515447_m1
5‘ nucleotidase, ecto	*Cd73*	Mm00501910_m1
Wingless-type MMTV integration site family 4	*Wnt4*	Mm01194003_m1
Angiopoietin 1	*Angpt1*	Mm00456503_m1
Tumor necrosis factor	*Tnfa*	Mm00443258_m1
Endothelin 1	*Edn1*	Mm00438659_m1
Chemokine (C-X-C motif) ligand 2	*Cxcl2*	Mm00436450_m1
Chemokine (C-X-C motif) ligand 3	*Cxcl3*	Mm01701838_m1
Connetive tissue growth factor	*Ccn2*	Mm01192933_g1

Collagen triple helix repeat-containing 1	*Cthrc1*	Mm01163611_m1
Collagene, type 1, alpha1	*Col1a1*	Mm00801666_g1
Collagene, type 3, alpha1	*Col3a1*	Mm00802300_m1
Collagene, type 5, alpha1	*Col5a1*	Mm00489299_m1
Tenascin C	*Tn-c*	Mm00495662_m1
Periostin	*Postn*	Mm01284919_m1
Serine peptidase inhibitor, clade E, member 1	*Serpine1*	Mm00435858_m1
Alpha smooth muscle actin	*Acta2*	Mm00725412_s1
Fibronectin	*Fn*	Mm01256744_m1
Cysteine rich protein 61	*Ccn1*	Mm00487498_m1
Lysyl oxidase	*Lox*	Mm00495386_m1
Thrombospondin 1	*Tsp1*	Mm00449032_g1
Secreted acidic cysteine rich glycoprotein	*Sparc*	Mm05915229_s1
Interleukin 33	*Il33*	Mm00505403_m1
Tissue inhibitor of metalloproteinase 3	*Timp3*	Mm00441826_m1
Mesoderm-specific transcript	*Mest*	Mm00485003_m1
Tissue inhibitor of metalloproteinase 1	*Timp1*	Mm01341361_m1
Adrenomedullin	*Adm*	Mm00437438_g1
Clusterin	*Clu*	Mm01197002_m1
WNT1-inducible signaling pathway protein 2	*Ccn5*	Mm00497471_m1
Rap guanine nucleotide exchange factor 3	*Epac1*	Mm00522941_m1
Glucose transporter 1	*Glut1*	Mm00441480_m1
Glucose transporter 3	*Glut3*	Mm00441483_m1
Glyceraldehyde-3-phosphate dehydrogenase	*Gapdh*	Mm99999915_g1
Enolase 1	*Eno1*	Mm01619597_g1
Hexokinase 1	*Hk1*	Mm00439344_m1
Lactate dehydrogenase A	*Ldh1*	Mm01612132_g1
Glucose phosphate isomerase 1	*Gpi1*	Mm01962484_u1
Phosphofructokinase, muscle	*Pfkm*	Mm01309576_m1
Aldolase A	*Aldoa*	Mm00833172_g1
Triosephosphate isomerase 1	*Tpi1*	Mm00833691_g1
Phosphoglycerate kinase 1	*Pgk1*	Mm00435617_m1
Phosphoglycerate mutase 1	*Pgam1*	Mm02526975_g1
Pyruvate kinase, muscle	*Pkm*	Mm00834102_gH
Aldolase C	*Aldoc*	Mm01298116_g1
FXYD domain-containing ion transport regulator 1	*Plm*	Mm00444674_m1
Glucose transporter 4	*Glut4*	Mm00436615_m1
Endoglin	*Eng*	Mm00468252_m1
Leptin	*Lep*	Mm00434759_m1

Nitric oxide synthase 2, inducible	*Nos2*	Mm00440502_m1
Heme oxygenase 1	*Hmox1*	Mm00516005_m1
Erythropoietin	*Epo*	Mm01202755_m1
Proprotein convertase subtilisin/kexin type 6	*Pcsk6*	Mm01319135_m1
Solute carrier family 29, member 1	*Slc29a1*	Mm01270577_m1
Adenosine A1 receptor	*Adora1*	Mm01308023_m1
Adenosine A2a receptor	*Adora2a*	Mm00802075_m1
Adenosine A3 receptor	*Adora3*	Mm00802076_m1
Netrin 1	*Ntn1*	Mm00500896_m1
Chemokine (C-C motif) ligand 3	*Ccl3*	Mm00441259_g1
Interleukin 1b	*Il1b*	Mm00434228_m1
Purinergic receptor P2X, 7	*P2rx7*	Mm01199500_m1
Pannexin 1	*Panx1*	Mm00450900_m1
Purinergic receptor P2Y, 2	*P2ry2*	Mm02619978_s1
Egl-9 family hypoxia-inducible factor 3	*Phd3*	Mm00472200_m1
Apelin	*Apln*	Mm00443562_m1
Ribosomal protein P0, large	*Rplp0*	Mm00725448_s1
Chemokine (C-X-C motif) ligand 10	*Cxcl10*	Mm00445235_m1
Chemokine (C-X-C motif) ligand 1	*Cxcl1*	Mm04207460_m1
Chemokine (C-C motif) ligand 7	*Ccl7*	Mm00443113_m1
Chemokine (C-X3-C motif) ligand 1	*Cx3cl1*	Mm00436454_m1

2.9 Plasmids

Table 11: Plasmids used for transfections.

Plasmid	Manufacturer
HA-HIF1alpha P402/P564-pcDNA3	Addgene
pcDNA3.1(+) IRES GFP	Addgene

2.10 Software

Table 12: Software used for different analysis.

Software	Manufacturer
Design & Analysis Software 2.6.0	Thermo Fisher Scientific (Waltham, USA)
ImageJ/Fiji 1.53s	Rasband, W.S., ImageJ, U.S. National Institutes of Health (Bethesda, USA)
Inkscape 1.3.2	Freedom Conservancy (New York, USA)
Office 365	Microsoft (Redmond, USA)
Prism 8	GraphPad Software Inc. (La Jolla, USA)
Wave 2.6.1	Agilent Technologies (Santa Clara, USA)

3 Methods

3.1 Animals

All laboratory animals used in experiments (8-12 weeks old transgenic mice, see 3.1.2) were bred and kept at the central facility for animal research and scientific animal welfare (ZETT) of the Heinrich Heine University Duesseldorf. Standard chow and water were supplied *ad libitum*. All animal experiments were compliant with animal welfare regulations and have been approved by the state office for nature, environment and consumer protection (LANUV) of North Rhine-Westphalia, Germany (81-02.04.2020-A321).

3.1.1 Wildtype mice

C57Bl/6J wildtype mice for organ harvesting were purchased from Janvier (Le Genest Isle, France) and were kept in the ZETT before sacrificing.

3.1.2 Postn^{CreERT2}Gt(ROSA)26Sor$^{tm3(HIF1A*)Kael}$ mice

For the analysis of the role of HIF-1α in cardiac fibroblasts, a mouse was generated which expresses a stable HIF-1α protein in POSTN positive activated cardiac fibroblasts. The mouse strain contains an inducible Cre/loxP recombination system. For this purpose a transgenic Postn$^{CreERT2\ BAC(+/-)}$/J mouse strain (PostnCre) (Jackson Laboratory, Bar Harbor, USA) expressing the CreERT2 recombinase under the control of a *Postn* promotor was mated with the transgenic mouse strain B6.129S6(C)-Gt(ROSA)26Sor$^{tm3(HIF1A*)Kael}$ (stock no: 009673, Jackson Laboratory, Bar Harbor, USA) containing a mutated HIF1-α sequence (Hif-1α P402A P564A) with a stop codon flanked by floxP sides in front of its position. The CreERT2 recombinase contains an estrogen receptor which prevents the entry of the recombinase into the nucleus in the absence of tamoxifen. Descendants the *Postn*^{CreERT2}*Gt(ROSA)26Sor*$^{tm3(HIF1A*)Kael}$ (Postn Hif-1αdPA) mice carry the CreERT2 recombinase sequence together with the loxP-flanked stop codon before the mutated Hif-1α sequence. The injection of tamoxifen leads to a split off of the estrogen receptor, inducing Cre recombinase activity CreERT2-expressing, *Postn*-expressing cells. By entering the nucleus, the Cre recombinase cuts out the stop codon, inducing the expression of the mutated HIF1-α

gene. The HIF1-α P402A P564A mutation leads to the stabilisation of HIF1-α protein, because proline was substituted by an alanine at two binding sites of the prolyl-4-hydroxylase 3 which inhibits its binding ability. The activity of the CreERT2 recombinase was induced by intraperitoneal injection of 200 µl tamoxifen (2 mg/ml in sesame oil) 1 day before, at the day of and 1, 2 and 3 days after the induction of MI according to a published protocol[135].

3.2 Induction of MI (ischemia/reperfusion)

Buprenorphine (0.1 mg/kg, injection volume: 45 µl at 0.3 mg/ml buprenorphine) was administered subcutaneously 30 minutes before surgery for pain relief. For induction of ischemia, the animals were anaesthetised (1.5% isoflurane (after flooding of 2-3 vol%) in ambient medical air (80% N2, 20% O2). Mice were intubated to artificially ventilate them during surgery with a respiratory rate of 150 breaths per minute. To maintain body temperature of the mice the surgery was performed on a heating panel. Additionally, electrodes of an electrocardiogram (ECG) were attached to the paws to monitor the heartbeat during surgery. After opening the chest, the left anterior descending artery (LAD) was ligated for 50 min by using an 8-0 polypropylene thread. Ischemia was monitored by checking the ECG for ST-segment elevation. The ligation of the LAD was dissolved afterwards and reperfusion was induced. Successful reperfusion was verified by a normalised ST-segment and red coloration of the infarcted area. The chest was closed by suturing and the suture was disinfected.

The surgery of mice was kindly performed by Zhaoping Ding, MD.

3.3 Magnetic resonance imaging (MRI)

MRI is a non-invasive imaging technique to illustrate organs and tissues *in vivo*. In this work an ^{1}H atomic nucleus was used and each individual nucleus has a frequency of 400.21 MHz. Hydrogen nuclei possess a magnetic dipole moment due to which the nuclei align in an external magnetic field and assume two different energetic states. While imaging organs and tissues with a natural amount of protons, multiple nuclear dipole moments are recorded. For energetic reasons more nuclei are in a parallel orientation resulting in net magnetisation at the axis of the outer magnetic field. In the beginning of the measurements, energy is supplied in form of a short radio frequency

pulse followed by excitation of the nuclei. Due to the fact that the radio pulse is perpendicular to the external magnetic field, the vector of the net magnetisation is tilted from the direction of the main field. The strength and duration of the excitation pulse determines the degree of deflection and influences the intensity of the measured MR signal. After the radio waves are switched off, the excited nuclei and the magnetisation vector return to the initial state through rotational movements. In the following a measurable voltage is induced in the receiver coil, which provides the MR signal.

The 9.4 Tesla Bruker Avance III Wide Bore NMR spectrometer (Bruker, Rheinstetten, Germany) was used for MRI measurements. Furthermore, the microimaging system Mini 0.5 was applied in combination with a 25 mm birdcage resonator coil (Bruker, Rheinstetten, Germany). The control of the Bruker Avance^{III} console connected to the magnet was done by means of a linux computer using the ParaVision 360 3.2 software. Spatially resolved measurements were done with a water-cooled microimaging system with actively shielded gradient, an inner diameter of 40 mm and a gradient strength of 1.5 Tesla/m.

3.3.1 Measurement of cardiac function

To investigate the influence of Hif-1α stabilisation in aCFs on cardiac function, magnetic resonance imaging (MRI) was used to assess cardiac parameters (heart volume, ejection fraction as well as end diastolic and end systolic volume) before and after MI.

Initially, mice were anesthetised with 1.5 Vol% isoflurane (flooding 2.5 Vol%) in water-saturated air with a gas flow of 50 ml/min via a respiratory mask. The anesthetised mouse was placed in the probe head with a special designed animal handling system. By means of a circulation thermostat (set to 37 °C) coupled to the circulation system, the body temperature of the test animals was maintained. To monitor the heart rate, both front paws and the left hind paw were attached to ECG electrodes. In addition, a pressure sensor was placed on the animal’s back to record the respiration rate. Both signals were detected and processed via the Small Animal Monitoring and Gating System (SA Instruments, Inc., New York, USA). This system was also used to avoid respiratory and cardiac motion artifacts by triggering the acquisition on the exhalation phase and the QRS complex.

To localize the heart, an overview image and an orthogonal scan were used. In the following, 6-8 short axis sections were recorded along a long axis scan through the apex. The scans were performed with a respiration-triggered imaging frequency IntraGate Fast Low Angle Shot (IgFLASH) which was developed by Bruker Biospins. Within one heart cycle 16 pictures were recorded with a Field Of View (FOV) 3x3 cm^2 and a matrix size of 256x256 to determine diastole and systole.

3.3.2 Visualizing the infarct area via MRI

Due to MI, parts of the myocardium are undersupplied with oxygen. By injecting mice with the extracellular contrast agent gadolinium, the extent of the damaged myocardium (infarct area) can be determined by MRI. Gadolinium possesses seven unpaired electrons with intrinsic rotation which builds a magnetic moment. The magnetic dipole is 1000 times higher than the one of the protons. Due to the effect of an external magnetic field, surrounding protons also have a faster relaxation, which shortens the T1 time and leads to an increased signal intensity. Especially the imaging frequency IgFLASH is suitable to illustrate the contrast agent via MRI. The gadolinium measurements were performed while measuring cardiac function as described in 3.3.1 one day after MI. Gadolinium (Gadovist, Bayer, Leverkusen, Germany) was injected intraperitoneally (2 mmol/kg bodyweight in 200 µl saline solution).

3.3.3 Determination of functional parameters

The analysis of the MRI measurements was done using the ParaVision 360 3.2 software (Bruker, Rheinstetten, Germany). To determine the ventricular lumen of the left ventricle, the endocardium contours were marked in the end-diastole and -systole with the ROI (Region of Interest) tool of the software. By multiplying all areas which have a layer thickness of 1 mm the volumes of the individual short-axis sections were calculated. The summation of all layers results in the end-diastolic (EDV) and end-systolic volume (ESV). The following parameters were determined from this:

Stroke volume (SV): Amount of blood pumped out of the heart with every heartbeat.

SV (µl) = EDV -ESV

Ejection fraction (EF): Percentage of the SV in relation to the whole amount of blood in the heart chamber.

EF (%) = SV/EDV

3.4 Cell isolation of CF

30 units of heparin were injected intraperitoneal 10 min before the mice were sacrificed by cerebral dislocation. The thorax was opened with a scissor and the heart was taken out and directly transferred to ice cold PBS. By using a binocular, the heart was dissected and lungs, oesophagus, thymus, trachea and adipose tissue were removed. A cannulation of the heart via the aorta was done using the Langendorff apparatus. To wash out the residual blood from the coronaries the heart was retrogradely perfused with prewarmed PBS for 3 min at 37 °C. Subsequently, the system was switched to digest the heart for 8 min at 37 °C via perfusion with 1000 U/ml collagenase type II (Worthington Biochemical Corporation, Lakewood, USA). After the digestion the heart was taken from the cannula and the aorta and heart ears were removed. The digested heart tissue was carefully pulled apart on a glass slide and transferred into 5 ml of cell culture medium to inactivate the collagenase activity with FBS. After resuspending the tissue in the medium the cell suspension was filtered through a 100 µm cell strainer and centrifuged for 1 min at 55 xg and 15°C to pellet the CMs. The supernatant was passed through a 40 µm cell strainer and centrifuged for 7 min at 300 xg and 15 °C to pellet the remaining cells including CFs. Cells were further processed as described in the following.

3.5 Cell sorting

3.5.1 Flow cytometric cell sorting

Flow cytometry is a common method to characterize cells and cell populations quantitatively. Cells can be labelled with fluorescent antibodies for the flow cytometric analysis. For this purpose, cells in single cell suspension have to pass a monochromatic laser beam individually in a linear sample stream, which allows the detection of the resulting scattered and fluorescent light from the cells. The detection of the forward and sideward scattered light allows the determination of size and

granularity of the cells. The fluorescent signal is used to characterise the cell suspension with regard to the expression of the protein under investigation. In addition, the intensity of the fluorescent signal is proportional to the amount of linked antibodies. In this work CFs transfected with a control GFP plasmid and the HA-Hif-1αdPA plasmid were analysed using flow cytometry with respect to the amount of cells with a GFP signal.

For different gene expression analysis described in 3.9 the flow cytometric cell sorting was performed by Katharina Raba from the Core Facility Flow Cytometry at the Heinrich Heine University of Duessedorf. In this work this method was performed to exclude ECs and ICs from the cell suspension by sorting for their specific surface marker CD31 and CD45. The remaining CFs and aCFs were further sorted with regard to the cell number, viability and the aCF-specific tdTomato signal.

After isolating the cells like described in 3.4 the cell pellet was suspended in 400 µl cell sorting buffer. For the analysis of transfected cells (3.6.33.6.4) the cell suspension was stained with DAPI and subsequently sorted for living cells with a GFP signal to determine transfection efficiency. To sort cells for further qRT-PCR (3.9.1) and scRNAseq (3.9.2) analysis the cell suspension was stained with antibodies against IC marker (CD45) and EC marker (CD31) and the live-death dye (Fixable Viability Dye eFluor 780) as described in Table 7. For scRNAseq CFs and aCFs were characterised and sorted as eFluor780^{+}/CD45^{-}/CD31^{-}. ICs were characterised and sorted as eFluor780^{+}/CD45^{+}/CD31^{-}. For the gene expression analysis by using the TaqMan Array Cards CFs were sorted as eFluor780^{+}/CD45^{-}/CD31^{-}/tdTomato^{-} and aCFs as eFluor780^{+}/CD45^{-}/CD31^{-}/tdTomato^{+}.

3.5.2 Magnetic cell depletion

To purify CFs for cell culture experiments, CD31^{+} ECs and CD45^{+} ICs among the isolated primary cells from the digested heart tissue (described in 3.4) were magnetically depleted using MojoSort nanobeads and MojoSort magnet (BioLegend, San Diego, USA). According to the manufacture's protocol the cell pellet was resuspended with 200 µl MACS buffer and 20 µl biotin-conjugated anti-mouse CD31 antibodies (BioLegend, San Diego, USA) were added and gently mixed. The cell suspension was incubated for 15 min at 4 °C. Afterwards, 20 µl MojoSort mouse CD45

nanobeads (BioLegend, San Diego, USA) and MojoSort streptavidin nanobeads (BioLegend, San Diego, USA) were added and mixed gently followed by a 15 min incubation at 4 °C. The suspension was filled up with cell sorting buffer to a final volume of 3 ml and the tube containing the suspension was placed into the MojoSort magnet for 5 min at room temperature (RT). By tilting, the $CD31^-/CD45^-$ fraction was transferred to a 15 ml tube which was centrifuged for 5 min at 300 xg and RT. The supernatant was discarded and the pellet was resuspended in 1 ml cell culture media. The suspension was transferred to a well of a 6-Well plate prefilled with 3 ml warm cell culture medium. After the transferation, the tube was washed with 1 ml cell culture medium and this was also transferred to the well. Cells were incubated over night at 37 °C and 5% CO_2. On the following day cells were washed 3-6 times to remove remaining cell debris.

3.6 Cell culture

To avoid contamination due to microorganisms all cell culture experiments were performed under a sterile cell culture bench (LaboGene, Lillerod, Denmark) by using sterile glass- and plasticware. Cultivation of cells under normoxic conditions was done at 37 °C with a CO_2 content of 5 % and a humidity of nearly 95 %. For hypoxic treatment of cells an oxygen concentration of 1 % was used. Cultivation of cells was done in T25 or T75 cell culture flasks or in 6-, 24- or 96-Well plates (Greiner Bio-One, Essen, Germany).

3.6.1 Cultivation of cardiac fibroblasts

To reach the required number of cells for the *in vitro* experiments, CFs were cultivated. After the in 3.5.2 described magnetic depletion of ICs and ECs, the purified CFs were used for different experiments. Once cells reached a confluence of 90 % in the well of a 6-Well plate, cells were transferred into T25 cell culture flask. For that transferation cells were washed once with 3 ml of prewarmed PBS. After removing the PBS by using a vacuum pump, 300 µl of trypsin/EDTA were added to the cells and incubated for 5 min at 37 °C. To ensure that cells were detached, wells were checked under the microscope. Detached cells were taken up with 5 ml cell culture media and transferred to a T25 flask. If needed, the cells were grown to a confluency of 90% and then

detached as described above and transferred to a T75 flask in a final volume of 15 ml cell culture media.

3.6.2 Cell counting

To determine the number of living cells in a cell suspension the Neubauer cell counting chamber was used. Cells were diluted 1:2 with trypan blue stain (see 2.5) to distinguish between living and dead cells (nuclei of dead cells are stained blue by trypan blue). 10 µl of the suspension was pipetted to the Neubauer chamber and living cells were counted in 4 given squares. The cell number was determined using the following formula:

$$\frac{total\ number\ of\ cells}{4} * 10^4 \frac{1}{ml} * dilution\ factor = number\ of\ cells\ per\ ml$$

3.6.3 Chemical transfection of cardiac fibroblasts

To introduce DNA plasmids into cells the method of chemical transfection can be used. In this study lipofectamine 3000 was used to introduce a plasmid encoding Hif-1α P402A P564A into CFs (isolated from wildtype mice and cultivated as described in 3.4 and 3.6.1, respectively). The plasmid containing the Hif-1α P402A P564A (Figure 4) sequence was based on the pcDNA3.1 IRES GFP plasmid (Figure 5) which was used as the control plasmid. 100.000 cells/well were seeded into 6-Well plate the day before transfection. When cells were 70-90 % confluent the next day, the transfection was performed as described in the manufacturer's protocol. The transfected cells were checked for GFP signal under the microscope as well as by using flow cytometry 24, 48 and 72 h after transfection.

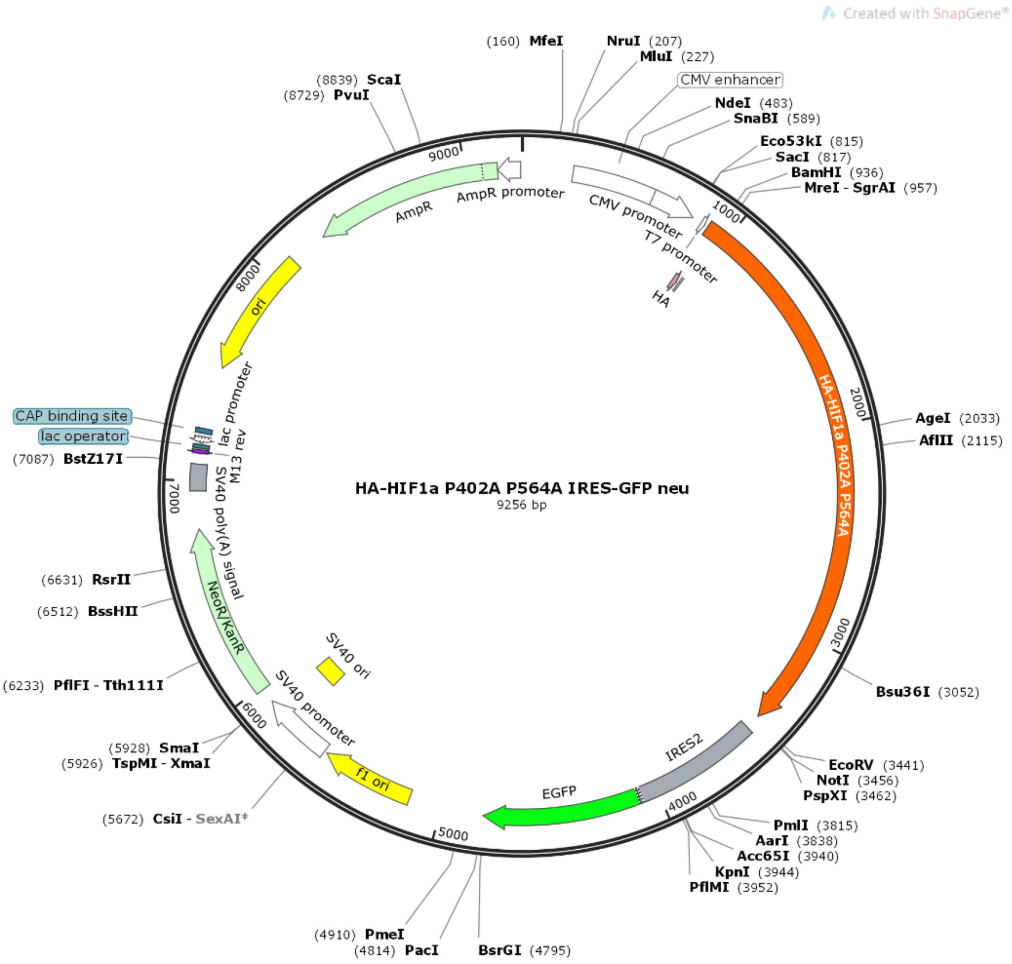

Figure 4: Plasmid card of the HA-Hif-1α P402A P564A IRES-GFP plasmid created with the SnapGene software.

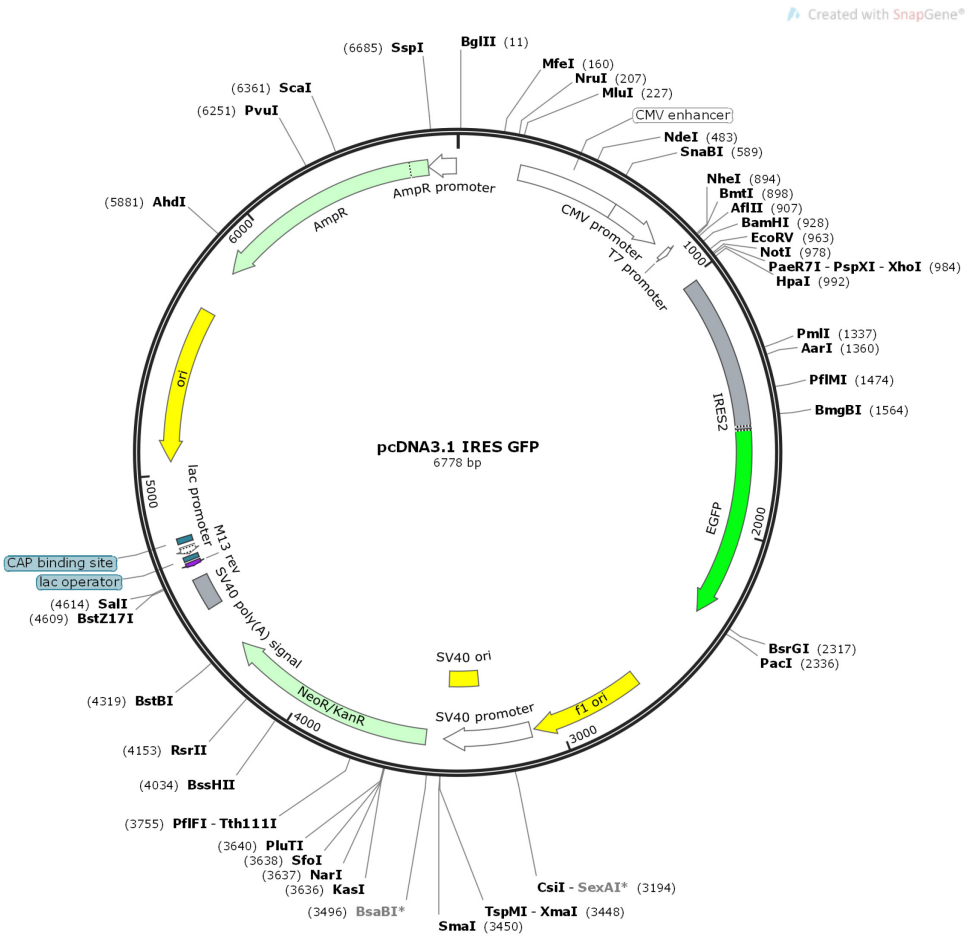

Figure 5: Plasmid card of the pcDNA3.1 IRES GFP plasmid created with the SnapGene software.

3.6.4 Transfection of cardiac fibroblasts by electroporation

Another method for introducing DNA plasmids into cells is electroporation. For this method the 4D-Nucleofector X Unit (Lonza, Basel, Switzerland) was used with a total amount of $1x10^6$ cells per electroporation in a 100 µl cuvette. To optimise the transfection of primary CFs, the Primary Cell Optimization 4D-Nucleofector X Kit from Lonza was used according to the manufacturer's protocol.

Cultivated CFs, isolated from wildtype mice, were electroporated with the HA-HIF1-α P402A P564A plasmid and a pcDNA3.1 control plasmid. For this, $1x10^6$ cells were trypsinised and pelleted by centrifugation for 10 min at 100 xg at RT and taken in suspension with 100 µl buffer from the kit. The suspension was directly transferred to the cuvette and electroporated by using the DS-137 program. To introduce a recovery step, the cells were incubated for 10 min at 37 °C afterwards in 400 µl RPMI medium.

Cells were plated in 6-Well cell culture plates filled with 3 ml prewarmed cell culture medium and incubated for 24, 48 and 72 h to check the best timepoint with the highest Hif-1α expression by counting the GFP^+ cells under the microscope.

3.7 Extracellular flux technology

CFs were seeded 24 h before performing extracellular oxygen and proton flux measurements with the Seahorse XFe96 (Agilent, Santa Cruz, USA). To figure out the best cell number of CFs for measurements, four different cell numbers ($5x10^3$, $1x10^4$, $2x10^4$ and $4x10^4$ cells) of CFs were seeded in a 96-Well Seahorse cell culture microplate 24 h before measuring the oxygen consumption rate (OCR) of the cells. Since the OCR of the $2x10^4$ cells reached the plateau of oxygen consumption which was concluded by the not significant higher OCR of $4x10^4$ cells it was decided that $1{,}5x10^3$ cells were the optimal amount of cells to be seeded.

To define the metabolic state of CFs and aCFs including basal glycolysis, proton efflux rate and compensatory glycolysis the glycolytic rate assay was performed according to the manufacturer's protocol with CFs from healthy hearts and aCFs from post-MI hearts, $1{,}5x10^3$ cells in 80 µl cell culture medium / well were seeded in the same 96-Well Seahorse cell culture microplate using an electronic multichannel pipet. The microplate was incubated for 1 h at room temperature to allow cells to settle down before overnight incubation at 37 °C. The Seahorse sensor was hydrogenated with 200 µl calibrant buffer overnight in an incubator without additional CO_2 supply. After overnight incubation, cells were checked for sufficient density (80-90 %). Cells were washed with 180 µl Seahorse medium. The wells were filled with 180 µl Seahorse medium and incubated for 1 h at 37 °C in the non-CO_2 incubator. The same procedure was done with CFs and aCFs, pre-treated with the $A_{2B}R$ agonist BAY-606583. For this, cells were seeded and treated with 10 µM BAY-60 for 24 h before starting the assay. BAY-606583 was also added to the Seahorse medium to ensure that it is also present during the assay.

During the incubation time the sensor was loaded with the Glycolytic Rate Assay Kit reagents:

Port A: 20 µl of 5 µM Rotenone plus Antimycin A, Port B: 22 µl of 500 mM 2-deoxy-D-glucose.

During the Assay the machine measured oxygen and pH levels with special sensors. The injection of rotenone and antimycin A from port A was done by the machine after the first three measurements. Three additional measurements were followed and 2-deoxy-D-glucose was injected from port B. Rotenone plus Antimycin A is inhibiting mitochondrial respiration which should lead to an increase in glycolysis. 2-deoxy-D-glucose is inhibiting hexokinases which then leads to a complete decrease in glycolysis.

To be able to normalise the results to cell numbers, a Hoechst 33342 staining was performed after the Seahorse measurements. A Hoechst 33342 solution of 1 mg/ml was prepared from the stock solution (20 mM, Thermo Fisher). The 1 mg/ml solution was diluted 1:10 in PBS and 27 µl of the dilution was added to each well of the 96-Well Seahorse microplate. The plate was shaken for 3 sec and incubated for 5 min in the darkness. Measurements were done with a Tecan plate reader at an excitation of 361 nm and an emission of 486 nm. The data was imported to the Wave software (2.10) and further processed with its normalisation tool with a normalisation unit of cells and the scale factor of 10^4.

3.8 Histology

To produce histological cryosections of healthy and infarcted mouse hearts, mice were sacrificed, hearts were harvested and immediately transferred to and washed in ice cold PBS. Hearts were then embedded in KP-Cryo Compound (Klinipath, Duiven, Netherland) and frozen in -40 °C isopentane for 10 min. Cryo-embedded mouse hearts were stored at -80 °C until usage. The hearts were cut into 8 µm slices at the cryostat (Leica Biosystems, Nussloch, Germany). Cutting was done from the apex to the basis of the heart. The slices were transferred to a glass slide and stored at -20 °C until immunostaining was performed.

3.8.1 Immunostaining

To prepare cultivated primary CFs for immunostaining, $2{,}5x10^3$ cells were seeded on coverslips placed in 24-Well plates and incubated overnight at 37 °C. To investigate HIF-1α levels induced by hypoxia, cells were treated for 6 h with 1% O_2 (hypoxic condition) and 20% O_2 (normoxic conditions). For fixation cells were washed with cold

PBS and 200 µl of ice-cold methanol were added and incubated for 5 min at 4 °C. Methanol was removed and the cells were washed with PBS. Coverslips were stored covered with PBS in 24-Well plates wrapped in parafilm at 4 °C until usage.

Immunostaining was performed on cultivated CFs on coverslips (fixated as described above) and cryosections of the heart. Cryosections were thawed, outlined with a hydrophobic barrier pen and fixated by incubation with 4% PFA for 15 min at RT. For permeabilisation, cell samples and cryosections were washed three times with 0.2% saponin in PBS. To avoid unspecific binding of secondary antibodies generated in goat, the cell samples were blocked with 500 µl 5% normal goat serum (NGS) in PBS/0.2% saponin for 1 h at RT. The cryosections were blocked with 150 µl immunofluorescence blocking buffer (see Table 3), for 1 h at RT, which included mouse IgG to additionally saturate potential binding sites for mouse primary antibodies in the cardiac tissue. Afterwards both, cell samples and cryosections, were incubated with 150 µl of PBS supplemented with 1% NGS, 0.2% saponin, and primary antibody at the desired concentration (see Table 7) overnight at 4 °C. To remove unbound antibodies, the samples were washed with 0.2% saponin in PBS three times for 5 min on the following day. Afterwards samples were incubated with 150 µl of PBS supplemented with 1% NGS, 0.2% saponin and secondary antibody at the desired concentration (see Table 8) for 2 h at RT. All following steps were performed in the dark. Samples were washed with 0.2% saponin in PBS two times for 5 min and one time with PBS only. The samples were mounted with ProLong Gold Antifade Reagent containing the nuclei staining DAPI. For cells on coverslips a drop of the reagent was placed on a glass slide and the coverslip was pressed with the cell site on it. For cryosections a drop of the reagent was put on the heart section and a fresh coverslip was pressed on it. The coverslips were outlined with nail polisher and dried for 30 min at 37 °C. Subsequently, cell samples were stored at 4 °C and heart section samples at -20 °C until inspection by fluorescence microscopy. The fluorescence microscope BX61 (Olympus, Tokyo) was used to take fluorescence images using different objectives (4x, 10x, 20x). Images were processed with ImageJ/Fiji 1.53s software.

3.9 Analysis of gene expression

3.9.1 Quantitative real-time polymerase chain reaction (qRT-PCR)

By means of qRT-PCR analysis the relative mRNA expression of a gene of interest (GOI) can be quantified and compared to a reference gene to explore the regulation of the mRNA expression of the GOI. Isolated mRNA is transcribed into complementary DNA (cDNA) by using reverse transcriptase. During the qRT-PCR specific cDNA fragments, defined by a forward and reverse primer, were amplified cyclically. Quantification of the amplification was achieved by fluorescent DNA probes (TaqMan assay) or intercalating dyes such as SYBR green.

In the TaqMan assay, which was used exclusively in this work, the two PCR primers hybridize at a specific section of the DNA. The probe carries a reporter dye at the 5' end and a quencher at the 3' end without producing any fluorescence signal. When the new 3'-strand is synthesised by the polymerase the probe is digested and dye and quencher are separated which leads to a fluorescence signal. The amplification of the cDNA is visualised by the emitted fluorescence signal which is directly proportional to the multiplication of the DNA. To detect the amount of cDNA the cycle threshold (Ct) was determined for every sample. The Ct value describes the number of cycles at which the accumulation of the amplified product is high enough to detect a fluorescent signal. Before this occurs, fluorescence remained only at background levels. If the Ct value of a reaction is high or low depends on the amount of templates present at the start of the amplification. Correspondingly with a high amount of cDNA at the beginning the amount of needed amplification cycles to get a fluorescent signal above background is low. In contrast a reaction with a low amount of cDNA needs more amplification cycles to reach a fluorescent signal above background remaining in a high Ct value.

3.9.1.1 RNA isolation and reverse transcription

RNA was isolated from CFs and aCFs from Postn-tdTomato mice 5 dpMI which were sorted for $tdTomato^+$ and $tdTomato^-$ according to 3.5.1 and further treated 6 h with 1% O_2 and 20% O_2. Additionally, RNA was isolated from healthy wildtype CFs and wildtype aCFs 5 dpMI which were treated for 24 h with and w/o 10 µM BAY-606583. RNA

isolation was done according to the manufacturers protocol using the RNeasy Microkit (Qiagen GmbH, Hilden, Germany).

The High-Capacity Reverse Transcription Kit (2.6) was used with 500 ng RNA per sample. All pipetting steps were performed on ice. RNA was diluted with RNAse- and nuclease-free water to a final concentration of 500 ng/10 µl. The reagent master mix was generated according to the pipetting scheme in Table 13. Per sample, 10 µl of the master mix were added to 10 µl of the template RNA. The reverse transcription reaction was performed according to the protocol in Table 14 using the Mastercycler X50s (Eppendorf, Hamburg, Germany). The cDNA samples were diluted 1:5 to a final concentration of 5 ng/µl. Samples were stored at -20 °C.

Table 13: Pipetting scheme for the master mix.

Reagent	Volume per sample
10x RT buffer	2 µl
25x dNTP mix	0.8 µl
10x RT random primers	2 µl
Nuclease-free water	4.2 µl
Reverse transcriptase	1 µl

Table 14: Cycle program for reverse transcription.

Cycle	Time	Temperature
1x	10 min	25 °C
1x	120 min	37 °C
1x	5 min	85 °C
1x	∞	4 °C

3.9.1.2 qRT-PCR using TaqMan gene expression assays (96-Well format)

Gene expression was quantified by using individual TaqMan assays with a cDNA start amount of 5 ng. The used TaqMan assays are listed in Table 10. Reagents for each PCR reaction were pipetted on ice as shown in Table 16, with technical duplicates of each sample. The StepOnePlus real-time PCR machine (Thermo Fisher Scientific, Waltham, USA) was used to perform qRT-PCR. The cycle program is described in Table 15. The results were analysed using the StepOnePlus software. The Ct value

was defined automatically by the software. The data normalisation to the housekeeping gene was done using the delta Ct method.

Table 15: Cycle program for the qRT-PCR

Cycle	Time	Temperature
1x	10 min	Heating up to 95 °C
40x	15 sec 1min	95 °C 60 °C
1x	∞	4 °C

Table 16: Pipetting scheme of the reagents for the PCR reaction

Reagent	Volume per sample
Takyon Master Mix (2x)	5 µl
TaqMan Gene Expression Assay (20x)	0.5 µl
ddH_2O	3.5 µl

3.9.1.3 qRT-PCR using TaqMan Array Cards (384 well format)

Gene expression of 95 different targets was measured in by using customised 384 well format TaqMan Array Cards, in which each well was prepared with dried-down TaqMan Assays listed in Table 10. The microfluidic cards contained eight fill reservoirs to load the sample together with the PCR reaction mix. Two samples were analysed per card, each with two technical replicates. cDNA samples were generated from isolated cardiac fibroblast RNA (see 3.9.1.1) using the High-Capacity cDNA Reverse Transcription Kit (Thermo Fisher Scientific, Waltham, USA) according to the manufacturer's protocol. For the PCR reaction the cards were prepared with a mix of 30 ng cDNA and TaqMan Fast Advanced Master Mix (Thermo Fisher Scientific, Waltham, USA) per fill reservoir. The qRT-PCR was set up and run according to the manufacturers protocol. The threshold for the Ct value was automatically set by the software for each GOI. Results were analysed with the Design & Analysis Software 2.6.0 (Thermo Fisher, Waltham, USA) (2.10) using the relative quantification (ΔΔCt) method.

3.9.2 Single-cell RNA sequencing (scRNAseq)

Using scRNAseq makes it possible to analyse the gene expression of every single cell in the used cell suspension. For this purpose, the cells are divided microfluidically into single cell suspensions and a next generation sequencing (NGS) cDNA library is created. For the creation of the library, small oil containing reaction vesicles, also called gel beads in emulsion (GEM), are built on a chip. Every GEM contains one single cell, reagents for the reverse transcriptase and barcoded oligonucleotides. Reverse transcription takes place within each GEM, so that the cDNA of the individual cell in the respective GEM is labelled with the same barcode. This barcode is used to track each individual cell. Furthermore, a second sequence called Unique Molecular Identifier (UMI) labels the cDNAs which originate from the same RNA molecule. The amplification of the whole labelled cDNA creates the NGS library which is subsequently sequenced.

In this work the scRNAseq, the data processing and the bioinformatical analysis was done by Dr. rer. nat. Tobias Lautwein from the BMFZ-Genomics and Transcriptomics Laboratory of the Heinrich Heine University Duesseldorf. The Chromium Next GEM Single Cell 3' Reagent Kit v3.1 was used in combination with the 10x system to perform the scRNAseq. Cell samples of healthy CFs and CFs/aCFs at 5 and 21 days post MI were isolated and sorted as described in 3.4 and 3.5.1.

3.9.2.1 Sample preparation and data analysis

The CFs and aCFs which were isolated with the Langendorff method (3.4) and flow cytometrically sorted (3.5.1) were counted in presence of trypan blue staining to check cell viability after the sorting procedure. Afterwards the cells were directly used to create the NGS cDNA library as described before (3.9.2) and the experimental protocol was performed according to the manufacturer. Depending on the cell output of living cells, 2000-20000 cells were used. Sequencing was performed according to the manufacturer's protocol by using the Hiseq 3000 Sequencing System (Illumina Inc., San Diego, USA). For CFs the average depth of sequencing amounted to ~70000 reads/cell. The processing of the sequencing raw data was done using the 10X Genomics CellRanger Software (V.4.1.1). Using the barcodes, the BCL-files resulting from the processing were assigned to the original CF samples. Subsequently, the files

were processed into fastq-files via the CellRanger *mkfastq* pipeline. The CellRanger *count* pipeline was used to count the UMIs and align the reads at the mm10 genome to generate a gene-barcode matrix.

3.9.2.2 Filtering and clustering of single-cell data sets

The following analysis was performed with the Seurat V4.1.1 R package[136]. To determine cell cluster and analyse gene expression the generated Feature Barcode Matrix was uploaded to the program. Cells with less than 200 detected genes, gene transcripts which were found in less than three cells and cells with a disproportionately high content (>20%) of mitochondrial genes were excluded by quality control from following analysis. Data was normalised by the SCTransform function. Biological replicates from each timepoint were integrated in one dataset. With help of the DoubletFinder (v.2.0.2) tool doublets were identified and excluded from the analysis. The cells were clustered by using the graph-based clustering approach of the R package Seurat v.3.0. Differentially gene expression between different cell clusters as well as the marker genes characterising each cluster were calculated with a two-sided Wilcoxon-Mann-Whitney-Test in the R package Seurat v.3.0. Heatmaps were generated with the GraphPad Prism 8 software. UMAP graphs and Dot plots were created with the interactive web application from the R package Shiny (v.1.7.4).

3.10 Statistics

GraphPad Prism 8 and Microsoft Excel 365 were used for statistical analysis. Results are displayed as mean values with standard deviations. The statistical tests used are stated in the individual figure legends. P values of < 0.05 were considered statistically significant.

4 Results

4.1 A_{2B}R-induced *Hif1a* gene expression and metabolic switch towards glycolysis in CFs

In previous studies of our group it was proposed that the normoxic A_{2B}R-induced HIF-1α plays a role in the HIF-1α-mediated cardioprotection[107]. Based on these findings the question arose, whether this mechanism of HIF-1α induction takes also place in aCFs from infarcted mouse hearts and if differences compared to CFs can be detected. Additionally, it was of interest by which mechanism normoxic HIF-1α induction may change the cellular energy metabolism in CFs and aCFs.

To investigate A_{2B}R-dependent effects on the gene expression level of *Hif1a* a qRT-PCR was performed. Using the A_{2B}R-selective agonist BAY 60-6583 (BAY) showed that A_{2B}R activation under normoxic conditions increased *Hif1a* gene expression in CFs from healthy mouse hearts and aCFs from mouse hearts 5 days after MI (Figure 6A). To analyse the metabolic consequences of an upregulation of *Hif-1α* gene expression in CFs and aCFs the glycolytic rate was assessed by the Seahorse XF Glycolytic Rate Assay from Agilent. This A_{2B}R-mediated HIF-1α activation was associated with a significant decrease in mitochondrial oxygen consumption in both cell types (Figure 6B). The normoxic A_{2B}R activation consistently induced a HIF-1α-associated metabolic switch towards glycolysis: Both, CFs and aCFs, showed a significant higher basal (Figure 6C) and compensatory glycolysis (Figure 6D) when A_{2B}R was activated compared to the controls. Additionally, the amount of extruded protons from the cells into the assay medium was increased in BAY-treated CFs and aCFs (Figure 6E). The results also indicate that without A_{2B}R activation the aCFs consumed significantly more oxygen (Figure 6B) and were in a higher glycolytic state than CFs (Figure 6C+E). Equally to *Hif1a* gene expression, the difference between CFs and aCFs in both oxygen consumption and glycolytic state was vanished after A_{2B}R activation.

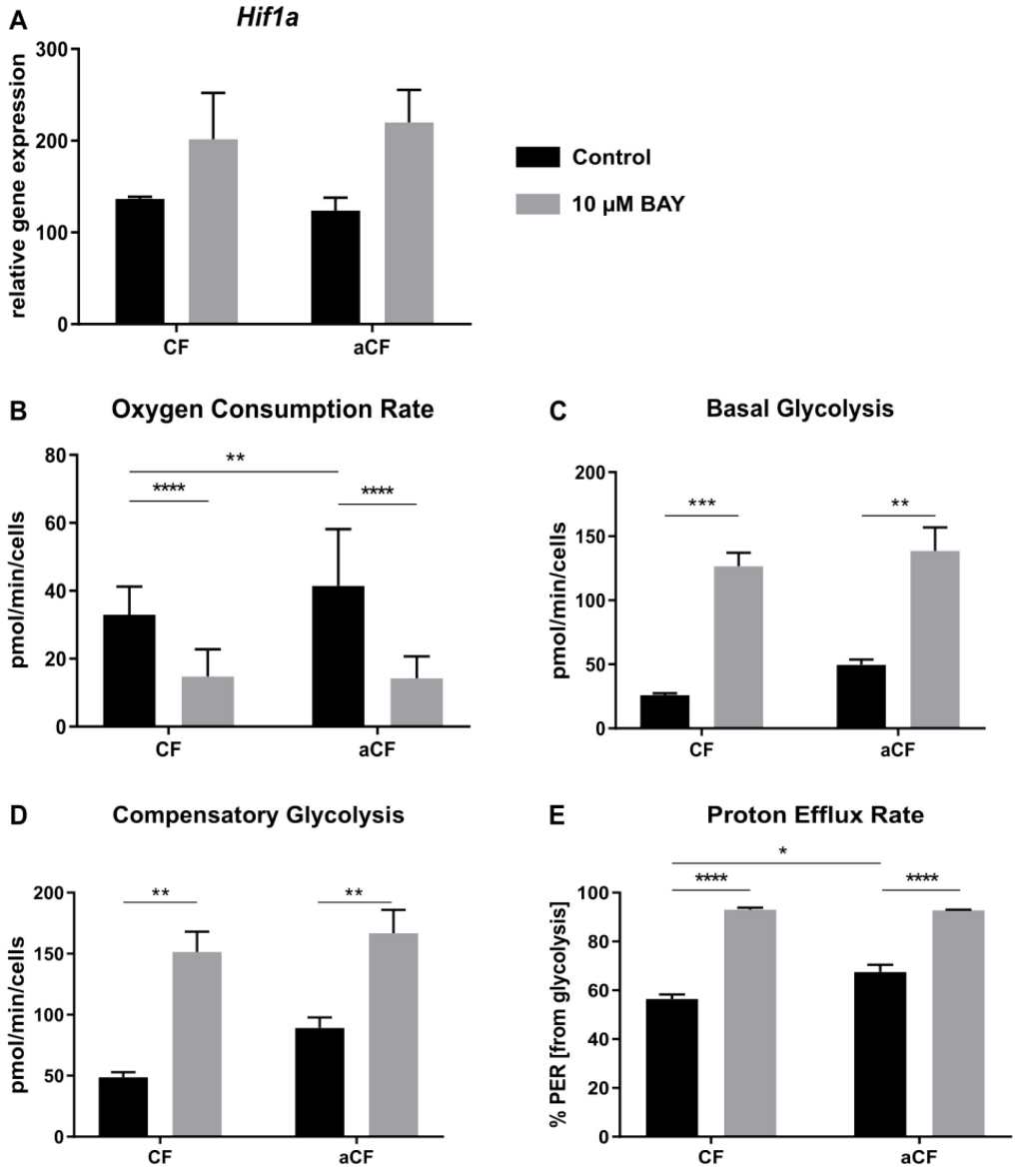

Figure 6: Effects of $A_{2B}R$ activation on HIF-1α expression and cellular energy metabolism in control CFs and post-MI aCFs.

A: Analysis of the relative gene expression of HIF-1α in untreated and 24 h BAY60-6583-treated CFs and aCFs by qRT-PCR (n=3). An ordinary one-way ANOVA and a Tukey's multiple comparison test was used for statistical analysis. No significance was detected. **B-E**: The metabolic state of untreated and 24 h BAY60-6583-treated CFs and aCFs was analysed by using the Agilent Seahorse Glycolytic Rate Assay. Bar charts show the oxygen consumption rate, basal glycolysis, proton efflux rate and the compensatory glycolysis of the cells (n=3 cell preparations each). Shown are mean values with standard deviations. An ordinary one-way ANOVA and a Tukey's multiple comparison test was used for statistical analysis (p-value: * < 0.05, ** < 0.01, *** < 0.001, **** < 0.0001).

4.2 Hypoxia-driven HIF-1α overexpression in non-activated CFs and infarct-activated aCFs

In 4.1 it was reported that the significant different rates of oxygen consumption in untreated CFs and aCFs were decreased to a comparable level by the A_{2B}R-dependent induction of *Hif1a* expression. Since it was known that under this specific setting HIF-1α induces metabolic changes in CFs and aCFs, the consequences of the hypoxia-induced HIF-1α upregulation in CFs and aCFs, especially what differences are detectable between the two cell types were investigated next. To this end, gene expression of a wide array of genes which are known to be associated with CFs, aCFs and HIF-1α were analysed. For this experimental setting CFs and aCFs were both isolated from the same $Postn^{CreERT2}ROSA^{tdTomato}$ mouse hearts 5 dpMI. In this mouse model $POSTN^+$ aCFs post MI express the orange fluorescent protein tdTomato by which they can be separated from the $POSTN^-$ CFs during the cell sorting. To avoid chemical side effects from BAY and achieve a higher HIF-1α protein level in CFs and aCFs, the cells were exposed to 1% O_2 (hypoxia) for 6 h. The impact of hypoxia on gene expression in CFs and aCFs from infarcted mouse hearts 5 dpMI was examined by qRT-PCR with customised TaqMan Array Cards. Cells were isolated from $Postn^{CreERT2}ROSA^{tdTomato}$ mouse hearts. In this mouse model the cre system was tamoxifen-induced 1 day before MI, at the infarct day as well as at day 1-3 dpMI. Due to the induction of the cre system, the tdTomato as the reporter for the activation marker POSTN was expressed in POSTN-positive cells of the mouse hearts. After isolation, cells were subsequently sorted on $eFluor780^+/CD31^-/CD45^-/tdTomato^+$ and $eFluor780^+/CD31^-/CD45^-/tdTomato^-$ using flow cytometry to exclude endothelial and immune cells and separate CFs from aCFs. Both cell preparations were incubated under 20% O_2 (normoxic) and 1% O_2 (hypoxic) conditions. After cell lysis, RNA was isolated and analysed. The customised TaqMan Array Cards contained primers and probes for transcripts of selected genes from different functional groups including fibrotic, metabolic and angiogenic genes as well as chemokines. The genes to be analysed were selected on basis of a description in the literature in context to CFs or/and HIF-1α signalling.

4.2.1 Hypoxia-induced HIF-1α expression in healthy CFs

In these experiments upregulation of HIF-1α protein expression in hypoxia-treated CFs was explored by immunostaining. CFs isolated from wildtype mice were grown on coverslips and treated for 6 h with 1% O_2 (hypoxia) or 20% O_2 (normoxia). Cells were fixed and stained with a HIF-1α primary antibody and an Alexa Fluor 594-conjugated secondary antibody. Normoxia-treated CFs only showed a few HIF-1α signals, while with the 6 h hypoxia treatment most of the nuclei were HIF-1α positive (Figure 7). Thus, hypoxia-induced HIF-1α expression was confirmed and the immunostaining was successfully established and further used for immunostaining of the heart cryosections in the following *in vivo* experiments.

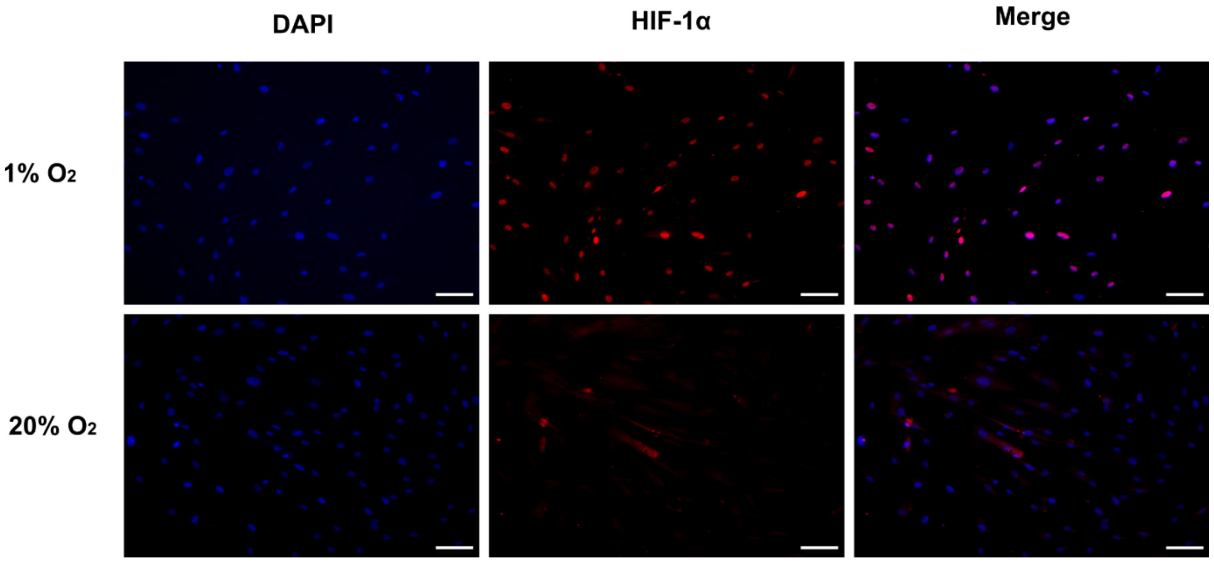

Figure 7: HIF-1α protein levels in wildtype CFs treated with 6h hypoxia and normoxia.
Representative images (n=3) of the immunostaining of wildtype CFs treated with 6 h 1% O_2 (hypoxia) and 20% O_2 (normoxia). CFs were isolated from wildtype mouse hearts. Cells were grown on coverslips and for 6 h exposed to hypoxia and normoxia. The immunostaining was performed with the HIF-1α primary antibody and the Alexa Fluor 594-conjugated secondary antibody. HIF-1α signals are shown in red. Nuclei were stained with DAPI (blue). Microscope images were taken with the 10x objective. Scale bars were set to 100 µm.

4.2.2 Hypoxia-induced changes in gene expression

As displayed in Figure 8A, in both CFs and aCFs most fibrotic genes showed a trend for a lower expression under hypoxic conditions. Expression of Tenascin C *(Tnc)* and Transforming growth factor beta-3 *(Tgfb3)* was significantly reduced in hypoxic CFs (Figure 8A, left panel). Among the metabolic genes, the genes encoding Phosphoglycerate mutase 1 (*Pgam1*), Phosphoglycerate kinase 1 (*Pgk1*) and Egl-3 Hypoxia Inducible Factor 3 (*Egln3*) were significantly upregulated in hypoxic aCFs compared to aCFs at 20% O_2 (Figure 8B, left panel). Expression of *Pgam1* was also significantly upregulated in hypoxic CFs (Figure 8B, right panel). The gene encoding Fibroblast growth factor 2 (*Fgf2*) was the only angiogenic gene with a significantly upregulated expression in aCFs (Figure 3C, left panel). Most of the selected angiogenic genes showed the tendency of a reduced expression under hypoxia (Figure 8C). Hypoxia did not significantly alter the gene expression of chemokines in CFs (Figure 8D). In aCFs expression of Interleukin 6 (*Il6*) and Fractalkine (*Cx3cl1*) were significantly downregulated under hypoxic conditions (Figure 8D, right panel). All in all, the analysis showed more significant effects on gene expression caused by hypoxia in aCFs than in CFs.

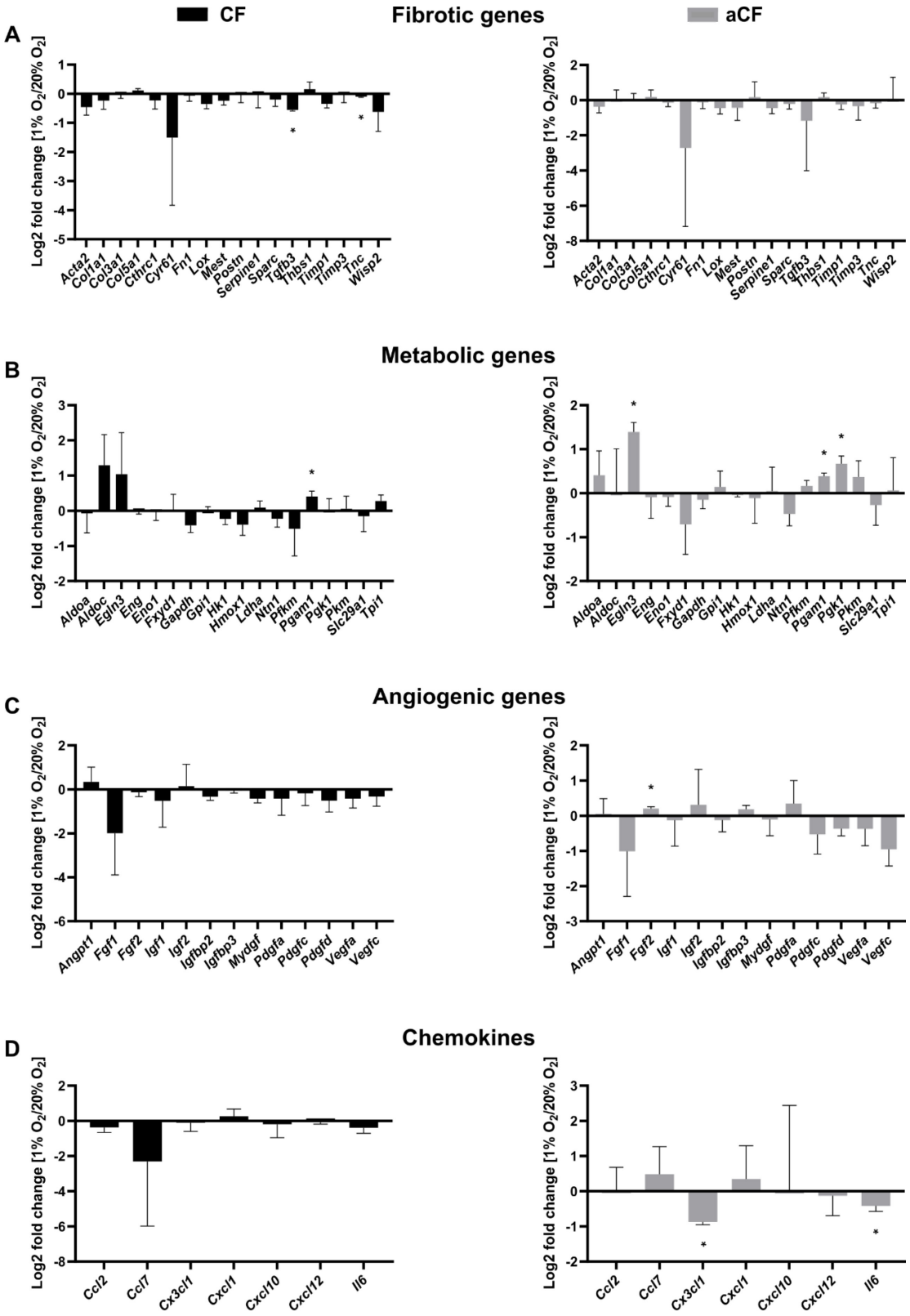

Figure 8: Hypoxia-induced changes of gene expression in CFs and aCFs.

CFs were isolated from Postn^{CreERT2}ROSA^{tdTomato} mice 5 dpMI. Tamoxifen was injected one day before and at day 0-3 pMI. Cells were sorted for tdTomato+ = aCF and tdTomato- = CF using flow cytometry. Cells were cultivated for 24 h and afterwards treated with 6 h hypoxia (1% O_2) and normoxia (20% O_2). RNA was isolated from the treated cells and gene expression was measured using a qRT-PCR with

Taqman Array Cards. Log2 fold change of gene expression levels from CFs (black, left panel) and aCFs (grey, right panel) under hypoxic (1% O_2) vs. normoxic (20% O_2) conditions. Selected genes were grouped in four functional groups: fibrotic, angiogenic, metabolic genes and chemokines (n=3 cell preparations each). Shown are mean values with standard deviations. Unpaired t-test was used for the statistical analysis (p-value: * < 0.05) (formal change following the comment by Prof. Dr Schrader: "Missing labelling A-D in the figure"*)*.

4.2.3 Changes in gene expression depending on the activation of CF

In addition to directly comparing hypoxia vs. normoxia treatment, the data obtained was also used to compare differences between aCFs vs. CFs. Figure 9 shows the differences in expression of fibrotic, metabolic and angiogenic genes and chemokines between aCFs and CFs under normoxic and hypoxic conditions.

In both oxygen conditions all selected fibrotic genes showed a trend to be upregulated in aCFs compared to CFs (Figure 9A). Collagen triple helix repeat-containing 1 (*Cthrc1*), known as a ligand of WNT signalling, and Thrombospondin 1 (*Thbs1*) were significantly higher expressed under hypoxic conditions. In addition, the activation of CFs did not show a clear trend to influence metabolic gene expression (Figure 9B). The gene encoding Heme oxygenase 1 (*Hmox1*) was the only metabolic gene whose expression was significantly downregulated in aCFs under hypoxia, while Lactate dehydrogenase A (*Ldha*) was significantly upregulated in gene expression. Conspicuously, all genes encoding glycolytic enzymes (*Gpi1*, *Pgam*, *Pkm*, *Ldha*, *Gapdh*, *Eno1*, *Hk1*, *Pfkm*, and *Pgk1*) showed a trend towards upregulation of gene expression in aCFs in comparison to CFs under both conditions (Figure 9B). Angiogenic gene expression showed most significant differences compared to the other functional groups (Figure 9C). Gene expression of Insulin-like growth factor-binding protein 2 (*Igfbp2*) and Platelet-derived growth factor C (*Pdgfc*) was significantly upregulated in aCFs in comparison to CFs under both oxygen conditions. Under normoxic conditions, also expression of Insulin-like growth factor 2 (*Igf2*) was significantly higher in aCFs. Expression of Insulin-like growth factor-binding protein 3 (*Igfbp3*), on the other hand, was significantly downregulated in aCF under both conditions, while a significant downregulation of Fibroblast growth factor 2 (*Fgf2*) gene expression was only visible under normoxic conditions. Analysis of gene expression for chemokines did not reveal any significant differences comparing aCFs to CFs under hypoxia and normoxia (Figure 9D).

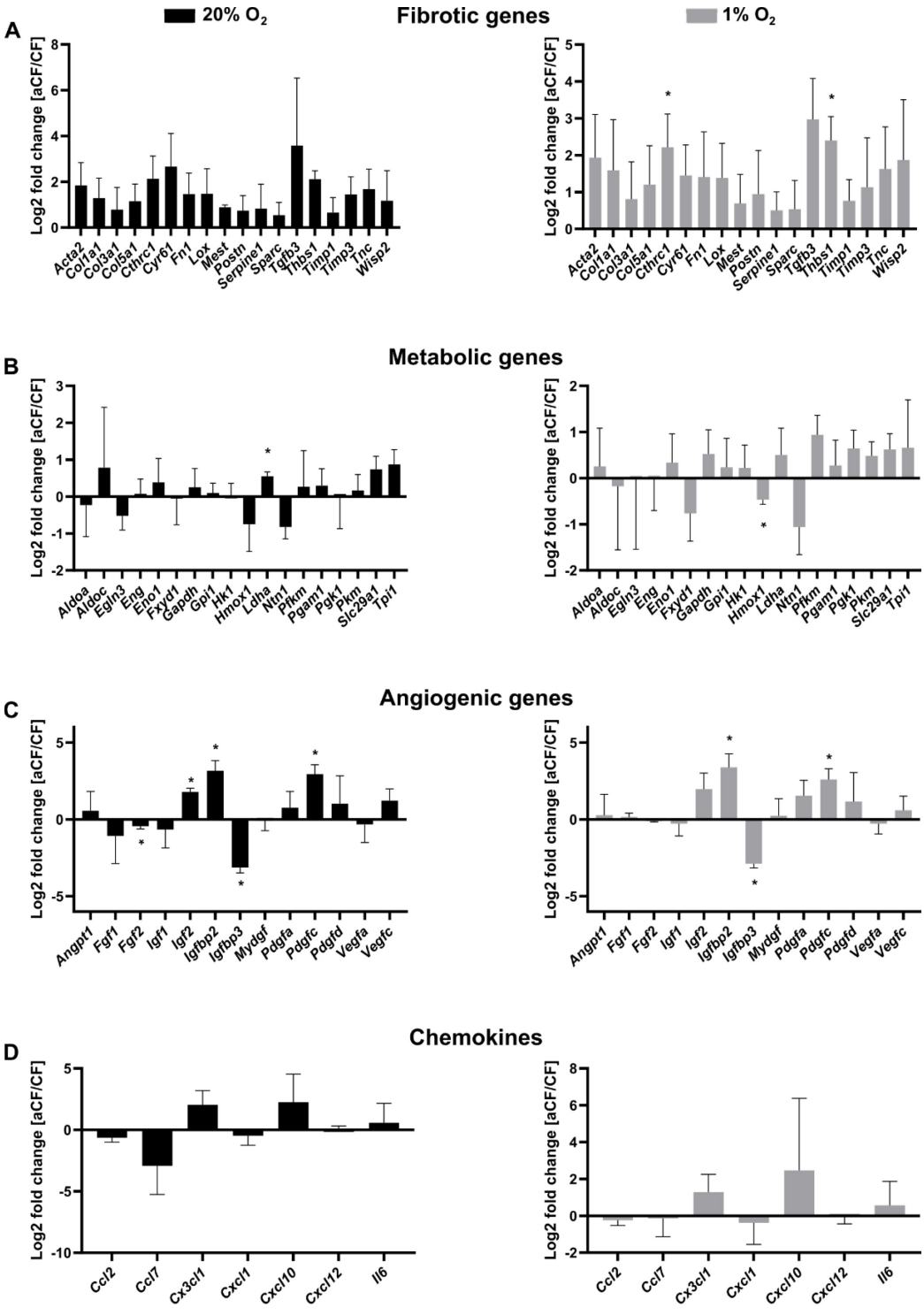

Figure 9: Hypoxia induced changes of gene expression in CFs and aCFs.

In this illustration, the same data from Figure 8 was used to directly compare aCFs and CFs and identify significant differences. The Log2 fold changes of gene expression levels from cells under hypoxic (1% O_2, grey, right panel) and normoxic (20% O_2, black, left panel) conditions comparing aCFs vs. CFs are displayed. Selected genes were grouped in four functional groups: fibrotic, angiogenic, metabolic genes and chemokines (n=3 cell preparations each). Shown are mean values with standard deviations. Unpaired t-test was used for the statistical analysis (p-value: * < 0.05) (formal change following the comment by Prof. Dr Schrader: “Missing labelling A-D in the figure”).

4.3 Transfection efficiency in CFs

The results of both preceding experiments to upregulate *Hif1a* on gene expression level, including the chemical $A_{2B}R$ induction via BAY60-6583 and the hypoxia treated cells, might have been influenced by possible side effects. To investigate the true influence of HIF-1α on metabolism and gene expression of CFs and identify possible side effects in the previous experiments, a plasmid for co-expression of *Hif1adPA* and GFP was produced for transfection. A pcDNA3.1-GFP plasmid was used as the control plasmid. The *Hif1adPA* sequence is characterised by a replacement of the proline by an alanine at positions 402 and 564. This exchange means that the PHDs can no longer label the HIF-1α protein for degradation. With a successful transfection the CFs should express a HIF-1αdPA protein which is stabilised without being degraded also under normal O_2 conditions. The co-expression of GFP by the same plasmid was used to visualize and quantify the transfection efficiency. CFs were isolated from wildtype mice, cultured and passaged 2 times before transfection protocols were performed. Chemical transfection with Lipofectamine 3000 (Thermo Fisher Scientific) as well as electroporation by using the Nucleofector 4D (Lonza) were tested for CF transfection.

4.3.1 Limited transfection efficiency in CFs by chemical transfection

To establish a transfection protocol to express stabilised HIF-1αdPA in wildtype CFs, chemical transfection with the transfection reagent Lipofectamine 3000 (Thermo Fisher Scientific) was first used. The reagent was chosen because it was proposed to result in a high transfection efficiency in primary and difficult-to-transfect cells.

To check transfection efficiency, cells were microscopically examined and documented 24 h and 48 h after transfection. In Figure 10A representative images of CFs transfected with the control plasmid are shown. While here single GFP-positive CFs were visible, CF transfected with the Hif-1αdPA-GFP plasmid did not display any GFP signal (data not shown).

For quantification of transfected cells, CFs were detached 48 h after transfection, stained with DAPI and analysed by flow cytometry with respect to a GFP signal in viable cells. In the CF sample transfected with the GFP-control plasmid, about 23,6% of the CFs were positive for GFP (Figure 10B). CFs which were transfected with the

Hif-1αdPA-GFP plasmid did not show GFP signal (0,1%) (Figure 10B). Also the transfection efficiency with the GFP-control plasmid was limited.

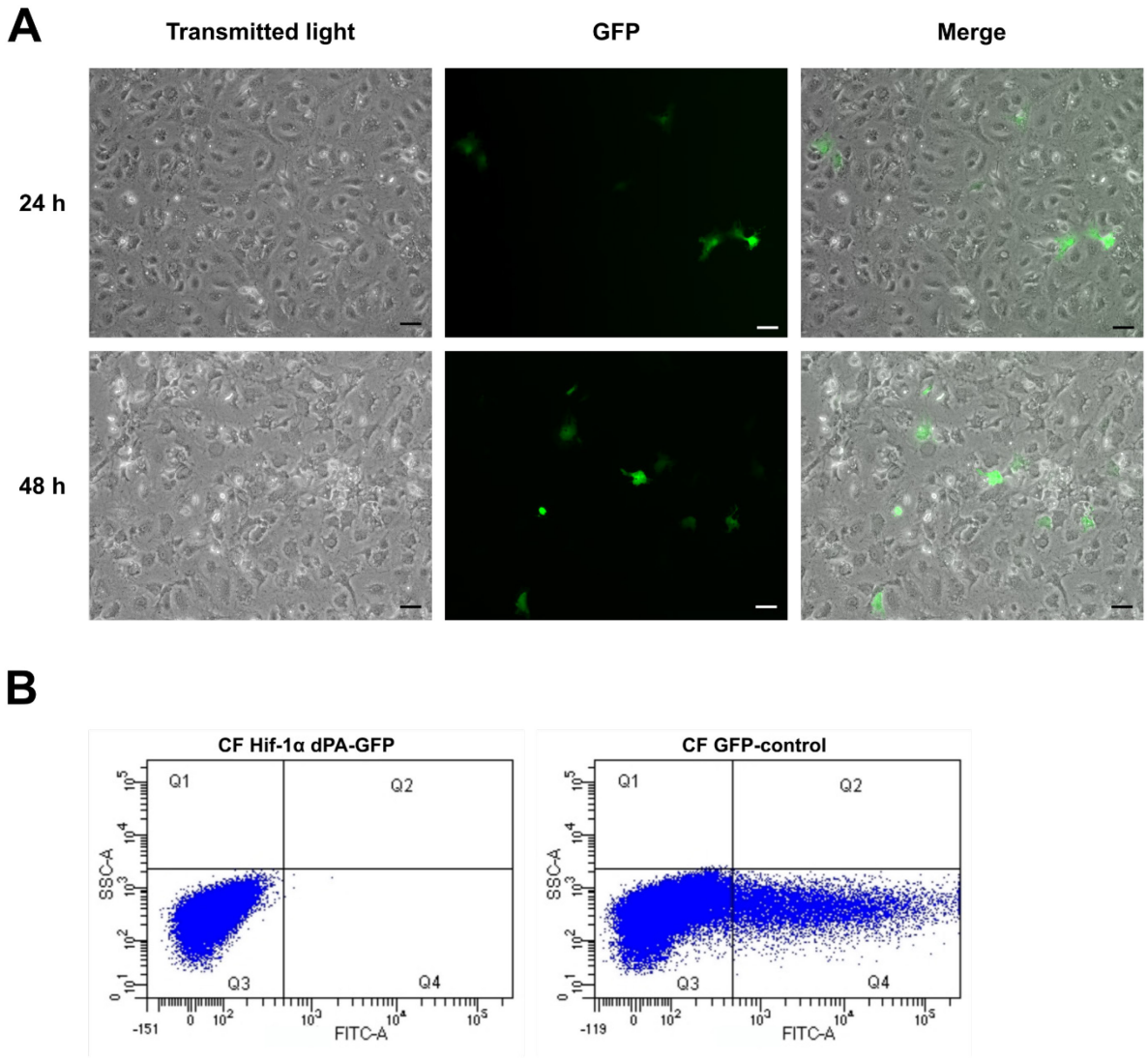

Figure 10: Transfection efficiency of Hif-1αdPA-GFP and GFP-control in CFs.
CFs were isolated from healthy wildtype mice and cultivated up to passage three before transfection. Cells were transfected with lipofectamine 3000 and images were taken 24 and 48 h after transfection. 48 h after transfection the CFs were analysed by flow cytometry. The gating was done on cell viability. **A:** Microscope images were taken with the 20x objective under transmitted light and in the GFP channel (green signal). Both conditions were merged in a third image (right panel). Representative images of n=3 experiments. Scale bars were set to 20 µm. **B:** Dotplots showing a representative flow cytometric analysis of CF transfection by lipofectamine 3000 48 h after transfection (n=1, technical replicates=3). Shown is a CF sample transfected with the Hif-1αdPA-GFP plasmid on the left as well as a CF sample transfected with the GFP-control plasmid on the right.

4.3.2 Limited transfection efficiency in CFs by electroporation

In another attempt, electroporation using the 4D-nucleofector (Lonza) was tested to transfect isolated CFs with the Hif-1αdPA-GFP plasmid. Again, the pcDNA3.1-GFP plasmid was used as the control. To find the most efficient electroporation protocol for primary CFs, the Primary Cell Optimization 4D-Nucleofector X Kit with the included GFP plasmid was used. Cells were cultivated for 48 h after electroporation, detached, stained with DAPI to discriminate dead cells, and analysed by flow cytometry for GFP expression.

As shown in Figure 11, Kit solution 1 achieved the highest transfection efficiencies as assessed by the percentage of GFP-positive cells in CFs compared to the other three solutions. Solution 2 was excluded from analysis, because most of the cells died after electroporation (data not shown). Comparing the different electroporation programs used with solution 1, the program G1 with a transfection efficiency of 74% was identified as the optimal program for primary CFs (Figure 6).

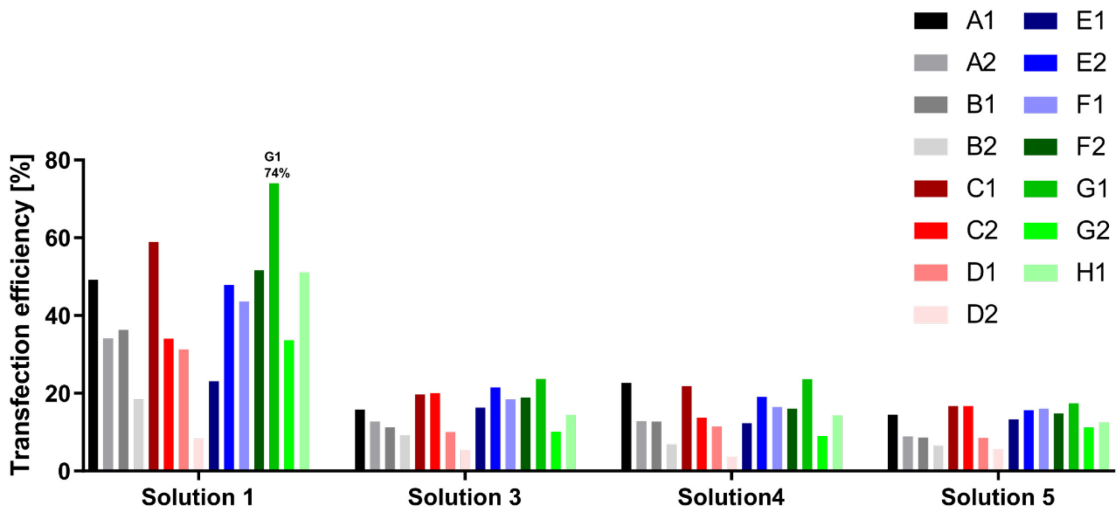

Figure 11: Transfection efficiency of different solutions and electroporation programs in CFs. CFs were isolated from healthy wildtype mice and cultivated up to passage three before electroporation. Cells were electroporated with four different solutions (1, 3, 4, 5) provided with the Primary Cell Optimization 4D-Nucleofector X Kit using the included GFP plasmid and electroporation programs A1-H1. The percentages of cells with a GFP signal were quantified via flow cytometry and are shown in the bar chart as measure of the transfection efficiencies (n=1 experiment).

Program G1 and solution 1 were then used to electroporate CFs with the Hif-1αdPA-GFP plasmid and the GFP-control plasmid. Cells were cultivated for 48 h after the transfection, microscopically examined at 24 and 48 h and subsequently analysed by flow cytometry. As negative control, non-transfected CFs were used.

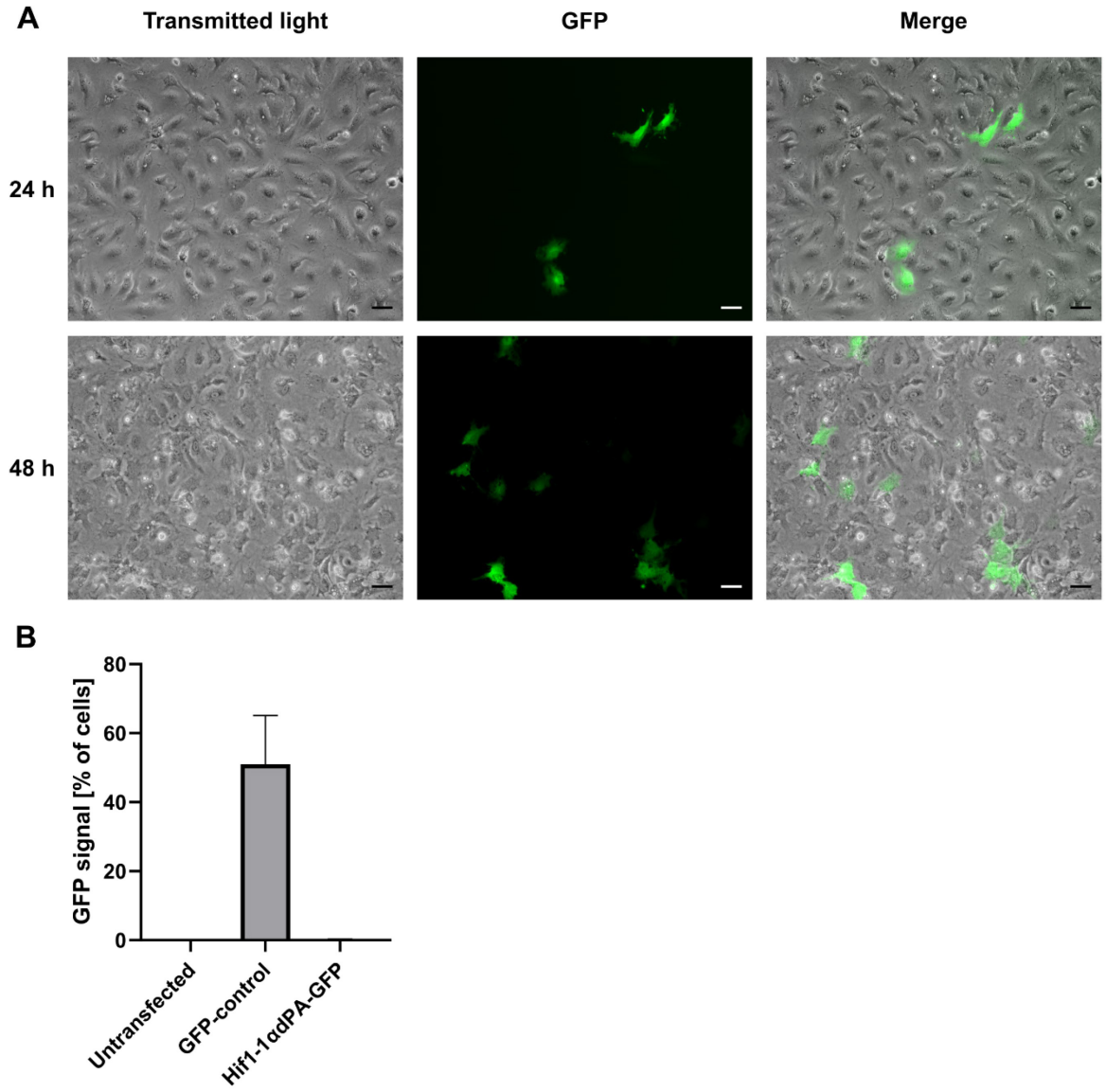

Figure 12: Electroporation efficiency of Hif-1αdPA-GFP and GFP-control in CFs.
Isolated CFs from wildtype mice were transfected with Hif-1αdPA-GFP and GFP-control plasmids using the 4D-Nucleofector. **A:** Representative transmitted light and fluorescence microscopy images 24 and 48 h after transfection (n=3). Scale bars were set to 20 µm. **B:** 48 h after electroporation, CFs were detached and the percentage of GFP-positive cells was quantified by flow cytometry. As negative control, untransfected cells were included. In the graph, means and standard deviations are displayed (n=3).

In the microscope images taken from the CFs transfected with the GFP-control plasmid, the GFP signal seemed to be slightly increased after 48 h compared to the images at 24 h after electroporation (Figure 12A). However, the CFs transfected with the Hif-1αdPA-GFP plasmid only showed a very low transfection efficiency of 0.3% (Figure 7B) and no positive cells were observed by microscopy (data not shown). As expected, non-transfected CFs did not show any GFP signal (Figure 12B), while 51% of CF in the sample transfected with the GFP-control plasmid were GFP-positive. Altogether, in primary CFs neither transfection of the Hif-1αdPA-GFP plasmid with Lipofectamine 3000 nor with electroporation did reach a transfection efficiency sufficient for functional analyses.

4.4 Impact of HIF-1αdPA stabilisation on fibroblast populations at different time points post MI

Since all previous experiments were performed with an *in vitro* HIF-1α upregulation in CFs, the aim of this experimental series was to additionally investigate effects due to a aCF-specific HIF-1α stabilisation after MI *in vivo*. For this purpose, a special mouse line (Postn-Hif-1αdPA) with a tamoxifen-inducible Postn-CreERT2-system was generated. The induction of the Cre-activity results in the expression of a mutated HIF-1α (HIF-1αdPA) with a HA-tag in *Postn*-expressing cells. *Hif-1αdPA* is characterised by an exchange of proline with alanine at positions 402 and 564 and the resulting protein cannot be degraded by the PHDs. The consequence is HIF-1αdPA stabilisation in *Postn*-expressing aCFs after MI. In the following experiments this mouse line was used to investigate possible positive effects of the HIF-1αdPA stabilisation in *Postn*-expressing CFs on regenerative processes in the mouse heart. To analyse differences in gene expression of crucial functional gene groups on single cell level, scRNAseq was performed with CFs and aCFs. This method not only provides insights into the gene expression of each individual cell, but also makes it possible to distinguish between different cell populations. Within the CF and aCF populations, it is also possible to subdivide into subpopulations. This enables a detailed analysis of all fibroblasts and also allows conclusions to be drawn about possible functions in the heart based on their gene profiles. An additional advantage of this method is that the cells do not need to be cultivated and can be analysed directly after isolation from the

heart. Furthermore, effects on cardiac function after MI were investigated using MRI measurements.

4.4.1 Localisation of *Hif-1α* expression in infarcted Postn-Hif-1αdPA mouse hearts

Due to the mutation in the *Postn*-driven *Hif1a* gene (*Hif-1αdPA)*, HIF-1αdPA-expression-induced Postn-Hif-1αdPA mouse hearts should contain HIF-1αdPA on protein level after MI. To confirm the induction of HIF-1αdPA-expression on protein level in Postn-Hif-1αdPA mouse hearts, immunostaining was performed. For this purpose, cryosections were generated at day 5 post-MI. Postn-Hif-1αdPA mouse hearts 5 dpMI without tamoxifen treatment served as negative control.

Cryosections of infarcted untreated Postn-Hif-1αdPA mouse hearts and hearts with induced HIF-1αdPA-expression were stained with two different antibody combinations to analyse HIF-1α accumulation on protein level. The first combination stained the extracellular matrix glycoprotein Tenascin C (TNC), which is known to be upregulated in the first 7 days after MI and deposited by CFs in the border zone[137,138], together with HIF-1α, which includes the staining of the endogenous HIF-1α as well as the HIF-1αdPA. Immunofluorescence images were taken with three different microscope objectives (4x, 20x and 40x) from the infarct/border zone of the left ventricle in the stained cryosections. Figure 13A shows images which were taken from Postn-Hif-1αdPA control mouse hearts. The TNC signal was clearly detectable in the infarct and border zone of both the control group (Figure 13A) and the group with induced HIF-1αdPA expression (Figure 13B). In none of the groups a specific HIF-1α signal was detectable, since observed signals of the secondary antibody were not located in the nucleus and were also visible without induction of HIF-1αdPA expression (Figure 13A). In line with this, control staining without primary antibody showed some unspecific binding of the Alexa Fluor 594 secondary antibody (data not shown).

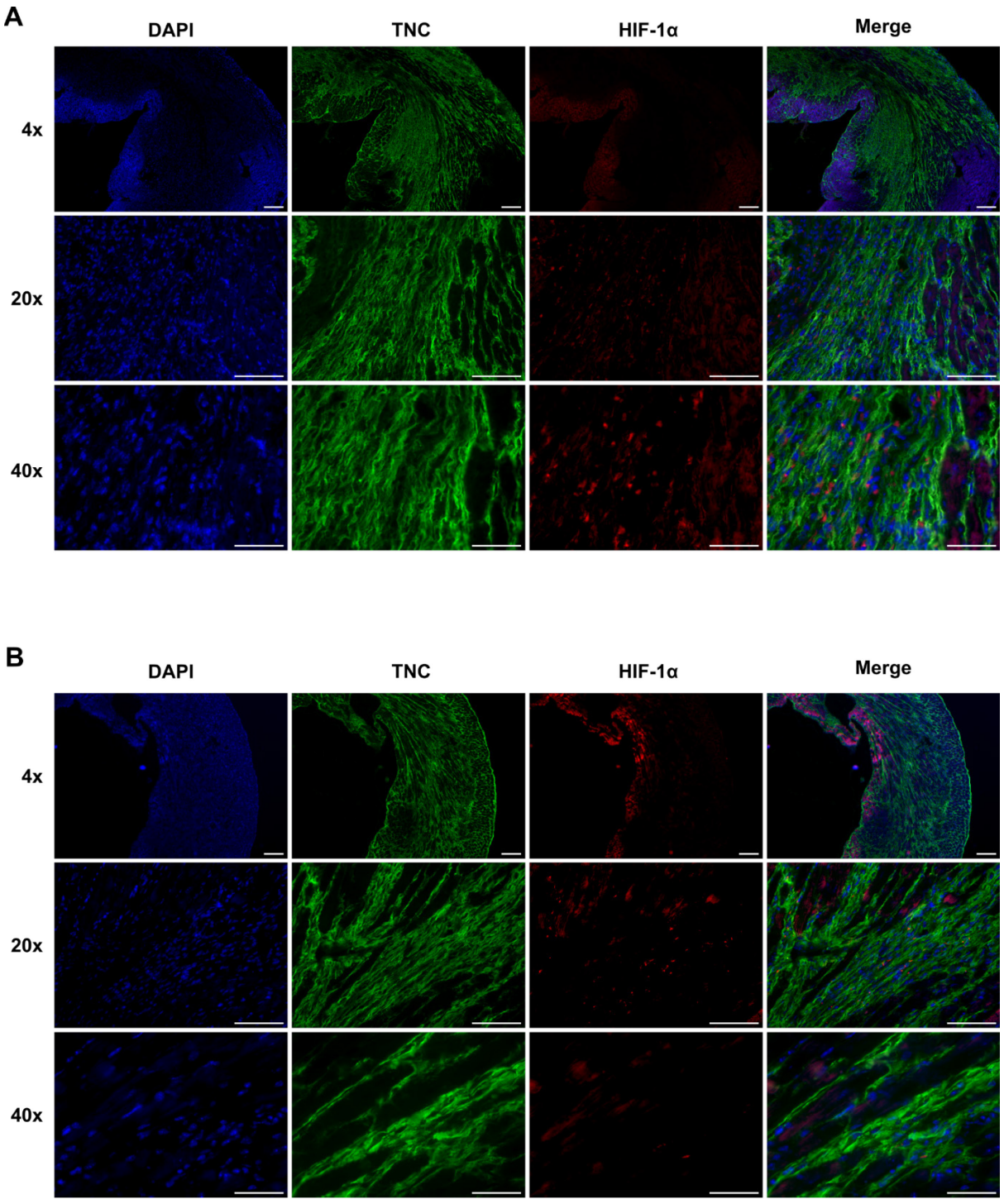

Figure 13: HIF-1α and TNC protein levels in untreated and tamoxifen-induced infarcted Postn-Hif-1αdPA mouse hearts 5 dpMI.

Hearts were taken from Postn-Hif-1αdPA mice with a *Postn*-driven CreERT2 expression after induction with tamoxifen (i.p. injections at -1, 0, 1, 2, 3 dpMI). The CreERT2 activity results in the expression of a stabilised HIF-1 αdPA protein. MI was induced with 50 min I/R and the hearts were harvested 5 dpMI. Cryosections were taken by horizontal cuts from the apex to the middle of the heart. Cryosections were stained with DAPI, primary antibodies for HIF-1α and TNC, and secondary antibodies conjugated to AF488 and AF594. Representative images (n=1 hearts, 3 sections/staining) of cryosections of Postn-

Hif-1αdPA mouse hearts 5 dpMI (**A**) without induction and (**B**) with induction of HIF-1αdPA expression by CreERT2 activity. Images were taken with three different objectives (4x, 20x and 40x) in the area of the left ventricular infarct/border zone. Nuclei were stained with DAPI (blue). Single images (TNC - green, HIF-1α - red) as well as merged images are displayed. Scale bars were set to 200 µm (4x objective), 100 µm (20x objective) and 50 µm (40x objective).

Since the used HIF-1α antibody was generated with an amino acid sequence of endogenous HIF-1α protein and therefore might be less effective in binding to mutated HIF-1αdPA, a second approach to detect HIF-1αdPA was performed, using an antibody targeting the HA-tag of HIF-1αdPA on cryosections of the same samples as above. To control its expression in POSTN-positive aCFs, a POSTN primary antibody was included in the staining protocol. POSTN signal was, as expected, detected in the infarct and border zone (Figure 14A+B). Since the control hearts should not contain any HA, the signals detected in the respective fluorescence channel were considered as background and unspecific binding signal from the secondary antibody. The immunofluorescence images from mouse hearts with induced HIF-1αdPA expression displayed in Figure 14B showed similar signals in all fluorescence channels as the controls without HIF-1αdPA expression in Figure 14A. Thus, in both immunostaining approaches it was not possible to visualise the tamoxifen-induced expression of HA-tagged HIF-1αdPA protein Postn-Hif-1αdPA mouse hearts. Since the developers of the Hif-1αdPA mouse strain reported that also with Western Blot HIF-1αdPA protein was only hardly detectable in cells with active Cre[108], the missing Hif-1αdPA-specific immunofluorescence signal might be due to only low Hif-1αdPA protein levels, precluding immunostaining but not functional analysis. Therefore, this project was continued by the analysis of the effects of HIF-1αdPA stabilisation on CFs/aCFs using single cell RNA sequencing (scRNAseq).

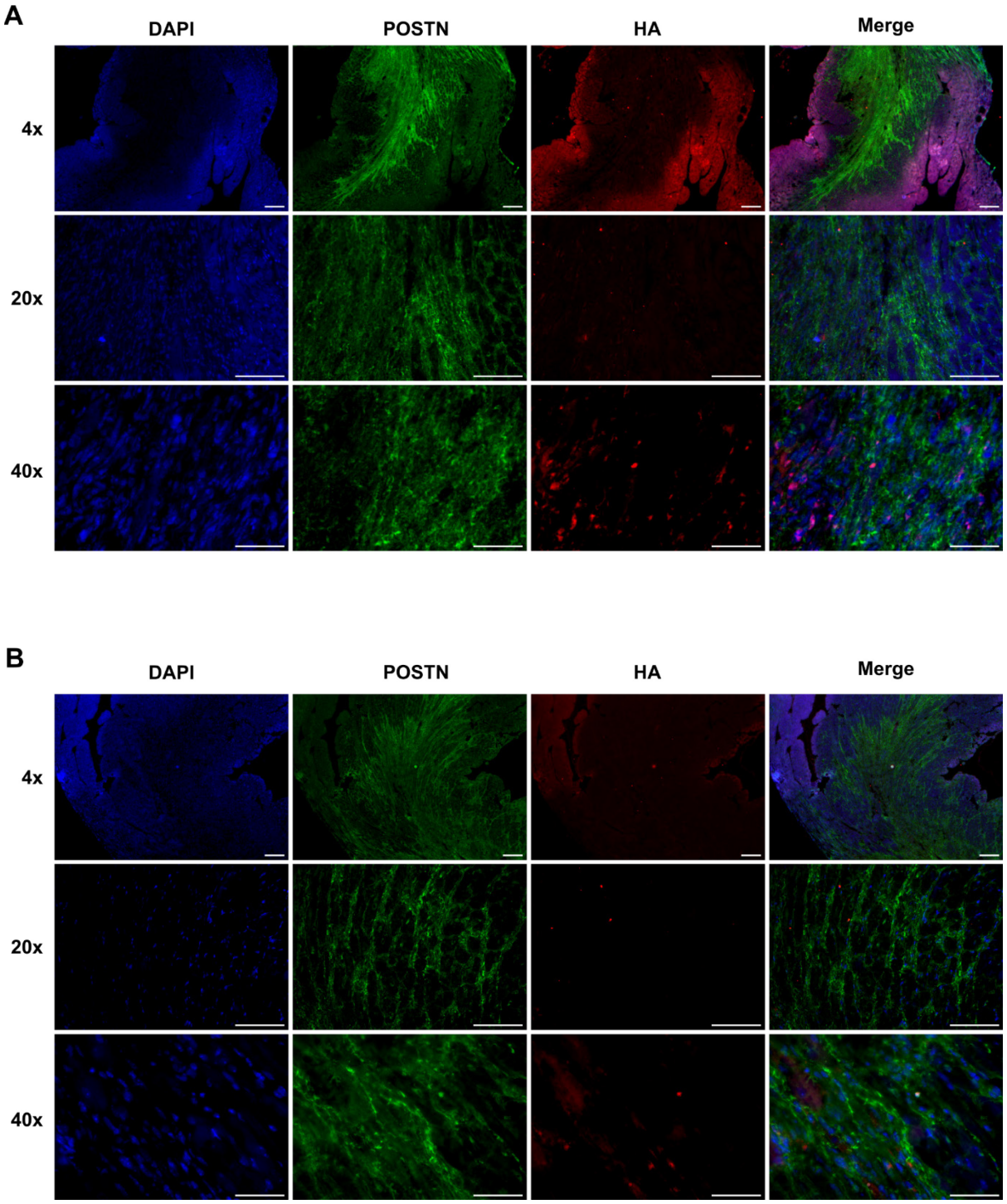

Figure 14: POSTN and HA protein levels in untreated and tamoxifen-induced infarcted Postn-Hif-1αdPA mouse hearts 5 dpMI.

Hearts were taken from Postn-Hif-1αdPA mice with a *Postn*-driven CreERT2 expression after induction with tamoxifen (i.p. injections at -1, 0, 1, 2, 3 dpMI). The CreERT2 activity results in the expression of a stabilised HIF-1 αdPA protein with an HA-tag. MI was induced with 50 min I/R and the hearts were harvested 5 dpMI. Cryosections were taken by horizontal cuts from the apex to the middle of the heart. Cryosections were stained with DAPI, primary antibodies for HA and POSTN, and secondary antibodies

conjugated to AF488 and AF594. Representative images (n=1 heart, 3 sections/staining) (**A**) without induction and (**B**) with induction of HIF-1αdPA expression by CreERT2 activity. Images taken with three different objectives (4x, 20x and 40x) in the area of the left ventricular infarct/border zone. Nuclei were stained with DAPI (blue). Single images (POSTN - green, HA - red) as well as merged images are displayed. Scale bars were set to 200 µm (4x objective), 100 µm (20x objective) and 50 µm (40x objective).

4.4.2 Time-dependent changes in CF populations with and without Hif-1αdPA expression after MI as analysed by scRNAseq.

To investigate differences at gene expression level and identify consequences of the stabilised HIF-1αdPA protein expression on selected functional gene groups like fibrosis-, proliferation- and angiogenesis-associated genes as well as the distribution of the different CF populations, CFs from Postn-Hif-1αdPA mice with induced HIF-1αdPA expression were isolated (3.4) 5 and 21 dpMI. CFs isolated from basal Postn-tdTomato mouse hearts as well as 5 and 21 dpMI served as comparison group without HIF-1αdPA expression. After flow cytometric sorting to exclude endothelial cells, immune cells, and dead cells (3.5.1), cells were applied to scRNAseq using the 10X Genomics Chromium System (3.9.2). For the basal heart samples, cell preparations of 3 hearts were pooled to achieve a sufficient CF cell count for the scRNAseq. Postn-Hif-1αdPA cell preparations of the post MI hearts (3 hearts / time point) were processed individually, since a sufficient CF count could be expected due to MI-induced CF proliferation. For the Postn-tdTomato samples post MI, cell preparations from 3 hearts were generated and sorted at 5 dpMI, but only one preparation could be successfully processed in the 10X system, probably due to clotting in the microfluidics chip. At 21 dpMI, Postn-tdTomato cell preparations from 3 hearts were pooled for scRNAseq. All sample data sets were analysed together in one bioinformatical analysis.

4.4.2.1 Classification of cell clusters in the heart

In the overall analysis, 19 different cell clusters were identified. To visualize the identified 19 cell clusters in the combined analysis, UMAP plots were created (Figure 15A-D). 14 of the 19 clusters were identified as CF clusters using the top 5 marker genes of each cluster (Figure 17), while the clusters 8 (epicardium), 13 (pericytes), 15 (endothelial cells), 16 (cardiomyocytes), 17 (macrophages), and 19 (glia cells) were

excluded from further analysis (see 4.4.2.2). Additionally, all CF clusters were grouped into two main groups, resident clusters and activated clusters, by analysing the expression levels of specific marker genes for both phenotypes and the proportion of expressing cells for each cluster. Cluster 0, 5 and 6 were classified as resident CF clusters, while all others were classified as activated CF clusters.

The UMAP plots in Figure 15B-D showed that the total count of cells differed between the time point of control hearts and the time points post MI, as was expected because of the different numbers of cells applied for scRNAseq (see 4.4.2). As mentioned above, for both time points after MI, CFs from two conditions, control and Hif-1αdPA-expressing, were analysed. The UMAP plots in Figure 15B-D also revealed differences in the proportion of cells at each time point contributing to the individual clusters, which are displayed in the bar chart in Figure 15E. This bar chart shows the relative percentage of cells in each cluster of the total cell count of the respective timepoint and condition: of CFs from control hearts the biggest proportion of cells was gathered in cluster 0, which was the largest cluster of the combined analysis. The majority of the cells from basal hearts were found in the resident CF clusters (0,5 and 6). In the samples from 5 dpMI, the proportion of cells contributing to resident clusters was profoundly lower than in the basal heart and the 21 dpMI samples. At the early time point after MI, the proportion of total cells was much higher in activated clusters, especially in cluster 2, 3, 4 and 10, compared to the samples from basal hearts and 21 dpMI (Figure 15E). In the 21 dpMI samples, the two largest cell proportions were assigned to the resident cluster 0 and the activated cluster 1. All in all, the proportions of the total cell count found in the individual clusters differed substantially between the samples from basal hearts, 5 dpMI, and 21 dpMI.

Comparing both conditions at individual time points after MI, it was visible that at 5 dpMI, a smaller proportion of cells from Postn-Hif-1αdPA mice allocated to the resident clusters in comparison to cells from Postn-tdTomato mice (Figure 15E). Only the activated cluster 9 showed a distinct higher cell proportion in CFs from Postn-Hif-1αdPA mice compared to the CFs from Postn-tdTomato mice 5 dpMI. On day 21 post MI, however, only in the resident clusters 0 and 6, the proportion of cells from Postn-Hif-1αdPA mice was considerably lower than from Postn-tdTomato mice. Comparing the cell proportions of Postn-Hif-1αdPA mice and Postn-tdTomato mice from the 21

dpMI samples the same trend was seen as it was observed above for 5 dpMI samples of both mouse lines.

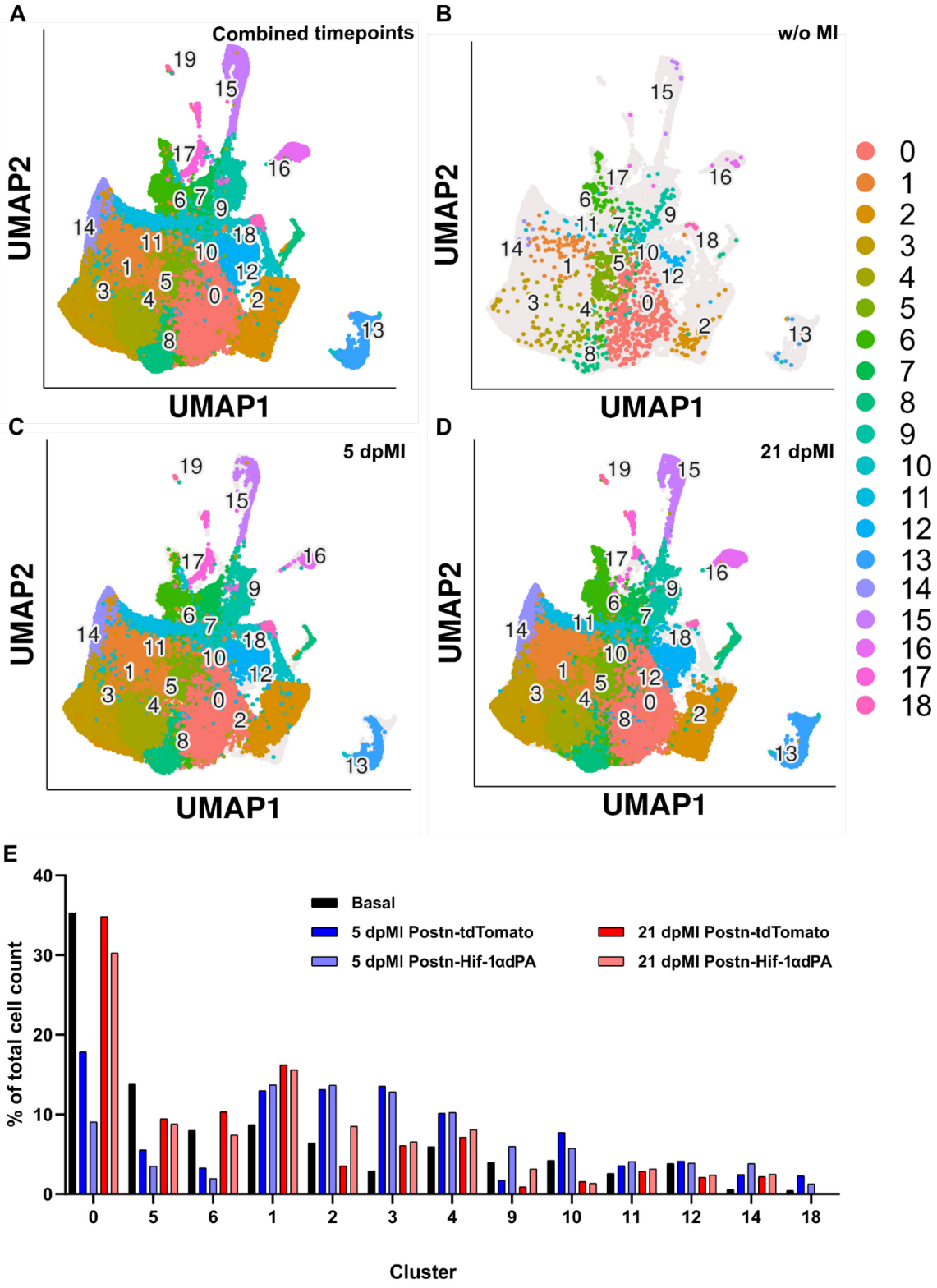

Figure 15: Clusters of the combined analysis of scRNAseq CF datasets w/o MI and 5 and 21 days after MI.

For scRNAseq, hearts were taken from Postn-Hif-1αdPA mice with a *Postn*-driven CreERT2 expression after induction of CreERT2 activity with tamoxifen (i.p. injections at -1, 0, 1, 2, 3 dpMI). The CreERT2 activity induced HIF-1αdPA expression in $POSTN^+$ CFs in these mice. Hearts taken from Postn-tdTomato mice with a *Postn*-driven CreERT2 expression after induction of CreERT2 activity with tamoxifen (i.p. injections at -1, 0, 1, 2, 3 dpMI) served as the control group. CreERT2 activity induces tdTomato expression in $POSTN^+$ CFs in these mice. CFs were isolated from basal control hearts (n=1 sample pooled from 3 hearts) and 5 and 21 dpMI from control (n=1 cell preparation and n=1 sample, pooled from 3 hearts, respectively) and HIF-1αdPA-induced hearts (n=3 and n=3 cell preparations, respectively). Isolated CFs were put into single cell suspensions and applied to the 10X Chromium System to further process the scRNAseq. The scRNAseq data sets of all samples were processed together in one bioinformatical analysis. After quality control filtering, transcriptional profiles of 1275 cells from basal Postn-tdTomato hearts, 5554 cells from Postn-tdTomato hearts 5 dpMI, 11337 cells from Postn-tdTomato hearts 21 dpMI as well as 29174 cells from Postn-Hif-1αdPA hearts 5 dpMI and 29420 cells from Postn-Hif-1αdPA hearts 21 dpMI were further analysed. A-D: UMAP plots of the CF datasets visualizing the identified CF clusters. Shown are all time points combined (A) or the individual data sets without (w/o) MI (B) and of days 5 (C) and 21 (D) after MI. Clusters were labeled according to size, starting with the largest one (cluster 0). The following non-CF clusters, as identified by expression of non-CF markers (see Figure 17), were excluded from further analysis: cluster 8 (epicardium), cluster 13 (SMC/pericytes), cluster 15 (ECs), cluster 16 (CMs), cluster 17 (macrophages), cluster 19 (glia cells). E: Bar chart showing differences in the proportion of cells at each time point contributing to the individual clusters. Clusters are grouped on basis of their transcription profile (Figure 16) in resident (0, 5, 6) and activated (1, 2, 3, 4, 9, 10, 11, 12, 14, 18) CF clusters.

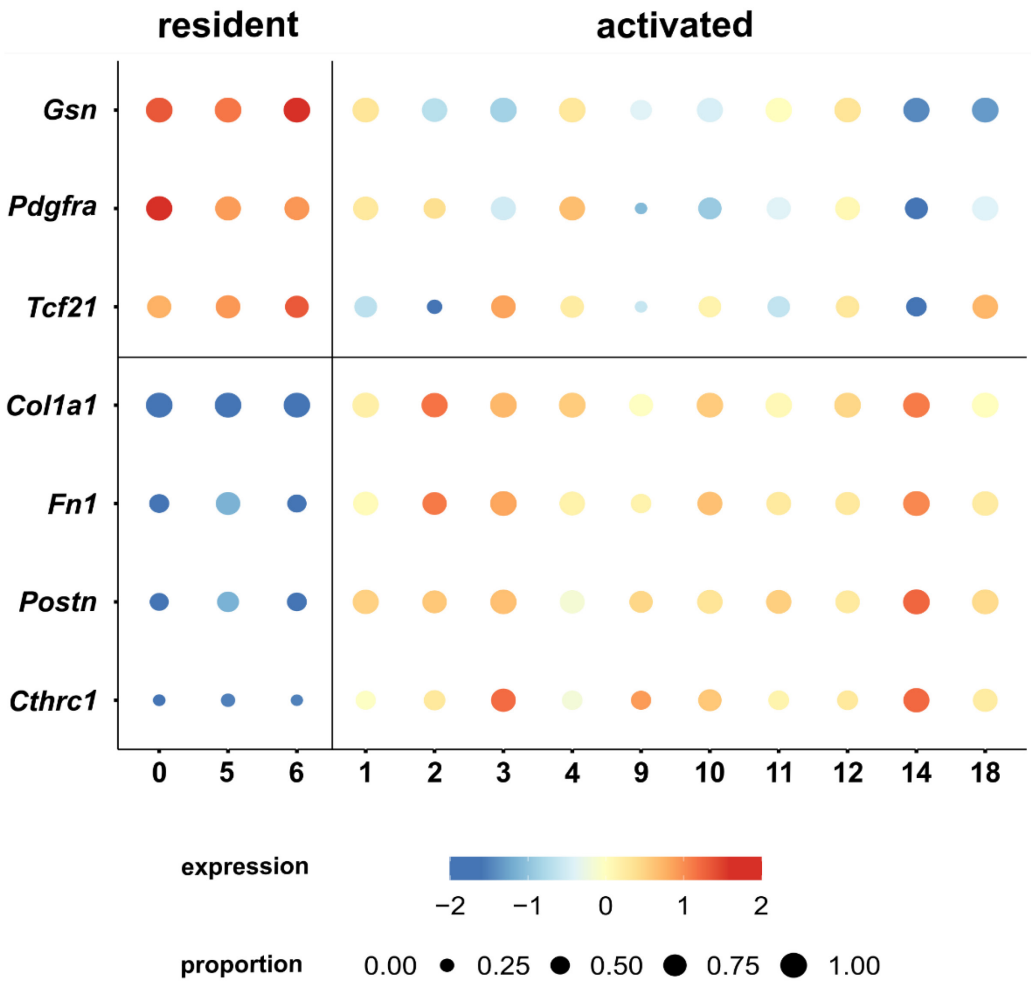

Figure 16: Expression of marker genes for resident and activated CFs.
The bubble plot shows the expression level of marker genes and the proportion of expressing cells for resident (*Gsn*, *Pdgfra* and *Tcf21*) and activated (*Col1a1*, *Fn1*, *Postn* and *Cthrc1*) CFs in each CF cluster.

4.4.2.2 Characterisation of cell clusters

To identify and characterise the CF clusters of the combined scRNAseq analysis according to their transcriptional profile, cluster marker genes were determined. Marker genes of a cluster were defined as the genes, which were significantly higher expressed in the respective cluster compared to all other clusters. During characterisation of the CF clusters, it was checked whether the cluster annotation according to the CF scRNAseq study of Farbehi *et al.*[91] could be applied. Additionally, all identified marker genes of each cluster were tested for significant enrichment of gene ontology (GO) annotations for biological processes by using the platform

GOrilla[139]. The expression of the top 5 marker genes and the top 3 enriched GO annotations within each CF cluster are visualised in Figure 17.

Cluster 0 was distinguished by expression of the typical resident fibroblast markers[140] *Ddr2*, *Tcf21* and *Pdgfra*. *Cxcl14*, *Smoc2*, *G0s2*, *Hsd11b1* and *Lpl,* all previously defined as marker genes for the resident fibroblast population F-SL (fibroblast: *Sca1*-low)[91], were among the top 10 marker genes. The search for the top 3 enriched GO annotations revealed “positive regulation of protein maturation”, “positive regulation of protein processing”, and “skeletal muscle cell differentiation”.

The top 10 marker genes of cluster 1 included *Cilp*, *Meox1*, *Col8a1,* and *Cst6,* which all have been assigned to the F-Act (fibroblast: activated)[91] population. *Postn* as marker gene for activated CFs[140] was also among the marker genes. No GO annotations were significantly enriched.

On the one hand cluster 2 showed *Fn1* as one of the top 10 marker genes and also expressed *Postn*, *Cilp*, *Cthrc1* and *Tnc* significantly higher, which are known as markers for an activated state of CFs[91]. On the other hand the top 10 marker genes also included the mitochondrial genes *mt-Atp6* and *mt-Co3,* which could be indication for apoptotic or lysing cells[141,142]. As top 3 GO annotations, “biological adhesion”, “cell adhesion”, and “developmental process” were found.

Cluster 3 was characterised by expression of *Sfrp2* and *Cthrc1*, which have been identified as myofibroblast marker genes, and expression of *Eln* and *Mfap4*, which are markers for the F-WntX population[91]. *Ccn5*, *Comp* and *Ecrg4* also belonged to the top 10 marker genes and are known as matrifibrocyte markers[52,143,144]. “Regulation of anatomical structure morphogenesis”, “regulation of developmental process” and “regulation of multicellular organismal development” were identified as the top 3 enriched GO annotations.

In cluster 4 the top 10 marker genes included *Ptn*, *Sfrp2*, *Comp*, and *Col3a1*, which are all associated with an activated state of CFs[143,145], and also the ECM gene *Fbln1*. Among the further marker genes beyond the top 10 were *Postn*, *Cilp*, *Cthrc1*, *Tnc* and *Fn1*, which are also activation and myofibroblast markers. The search for enriched GO annotations revealed “regulation of developmental process”, “regulation of multicellular organismal development” and “regulation of multicellular organismal process” as the top 3.

Cluster 5 was characterised by the presence of *Pi16*, *CD248*, *Gfpt2* and *Tmem100* in the top 10 marker genes, which have been assigned to the F-SH (fibroblast: *Sca1*-high) population[91]. Additionally, the resident fibroblast marker genes[140] *Ddr2* and *Tcf21* were significantly higher expressed. “UDP-N-acetylglucosamine metabolic process”, “nucleotide-sugar metabolic process” and “nucleotide-sugar biosynthetic process” were identified as the top 3 enriched GO annotations.

Among the top 10 marker genes of cluster 6 were *Apoe* and *Fgl2*, which are characteristic for the F-Trans population, *Myoc* and *Timp3*, characteristic for the F-WntX population, and the fibroblast marker gene *Gsn*. The search for enriched GO annotations revealed “negative regulation of lipid transport”, “regulation of membrane protein ectodomain proteolysis” and “negative regulation of secretion” as top 3.

Cluster 7 showed several mitochondrial or ribosomal genes among the top 10 marker genes, which might indicate dying cells[141,142]. The other marker genes included *Col1a1*, *Acta2*, *Col1a2*, *Cthrc1*, *Fn1*, *Ptn*, and *Ddah*, which are genes related to myofibroblasts[91,146]. The top 3 enriched GO annotations were “amide biosynthetic process”, “translation” and “peptide biosynthetic process”. Cluster 7 likely represented a cluster of dying cells and was excluded from downstream analysis.

Cluster 8 was identified as an epicardial cell cluster: *C3* and *Slit3*, which are known as epicardial signature genes[147] were included in the top 10 marker genes and various other epicardial genes, such as *Igfbp6*, *Efemp1* and *Ildr2*[147], were among the other marker genes of this cluster. “Regulation of multi-organism process”, “protein activation” and regulation of neuron death” were identified as the top 3 enriched GO annotations. These epicardial cells were excluded from further analysis.

No clear marker genes were found in the top 10 of cluster 9. Beyond the top 10, the cluster marker genes included aCF markers like *Postn*, *Acta2,* and *Tagln*, as well as the *Cthrc1*, *Ptn* and *Ddah1*, which are known as myofibroblast marker genes[91]. The top 3 GO annotations were found to be “mitochondrial respiratory chain complex assembly”, “mitochondrial respiratory chain complex I assembly” and “NADH dehydrogenase complex assembly”.

Cluster 10 resembled the proliferating fibroblast population F-Cyc (fibroblast: cycling)[91] in expression of the marker genes *Acta2*, *H2afz*, *Stmn1* and *Timp1*, which were among the top 10. The classification as a proliferation cluster is further supported by the

presence of the proliferation markers *Top2a* and *Mki67*[143] among the top 10 marker genes. The top 3 enriched GO annotations found for this cluster were “cell cycle”, “cell division”, and “mitotic cell cycle process”.

Cluster 11 showed genes in the top 10 markers which have been related to pro-apoptotic function like *Cdkn1a*, *Trp53inp1* and *Bax*[148–150]. Especially *Trp53inp1* is known to inhibit CF proliferation and transformation into myofibroblasts[149]. However, also markers associated with the F-Act population[91], like *Postn*, *Cilp*, *Meox1*, *Col8a1*, and *Cst6*, were included in the further marker genes beyond the top 10. The top 3 enriched GO annotations were “cellular response to DNA damage stimulus”, “signal transduction by p53 class mediator” and “intrinsic apoptotic signalling pathway by p53 class mediator”. Together these findings suggest, that also this cluster might be composed of cells of different previously identified CF populations.

In cluster 12 *Ifit1*, *Ifit3*, *Isg15*, *Iigp1* and *Rsad2* were included in the top 10 marker genes. These transcripts are characteristic for the F-IFNS (fibroblast: interferon stimulated) population.[91]. The search for enriched GO annotations returned the following top 3: “response to other organism”, “response to external biotic stimulus” and “response to biotic stimulus”.

In the top 10 marker genes for cluster 13 mainly pericyte- and smooth muscle cell-specific marker genes[151], like *Rgs5*, *Abcc9*, *Kcnj8*, *Vtn* and *Notch3*, were found. “Signal transduction”, “regulation of system process” and “G protein-coupled receptor signalling pathway” were found to be the top 3 enriched GO annotations. As non-fibroblast cluster, it was excluded from further analysis.

Cluster 14 was characterised by the marker genes *Thbs4*, which has been linked to matrifibrocytes, and *Cilp* and *Ddah1*, which have been associated with the F-Act population. The association to F-Act was underlined by the presence of *Postn*, *Acta2*, *Meox1* and *Col8a1* among the further marker genes. The remaining marker genes included a high number of genes encoding collagens and matrifibrocyte-associated genes. Additionally, myofibroblast-specific genes like *Cthrc1*, *Tnc*, and *Fn1* characterised this cluster. The search for enriched GO annotations revealed “regulation of lipid localisation”, “collagen fibril organisation” and “connective tissue development”.

Cluster 15 was distinguished by the endothelial cell-specific marker genes *Fabp4*, *Cd36* and *Gpihbp*[91]. The enriched GO annotations “angiogenesis”, “eye morphogenesis” and especially “lipid transport” found for this cluster underlined that this cluster consisted of endothelial cells. Cluster 15 was excluded from further analysis.

For Cluster 16 the top 10 marker genes showed with *Tnnt2*, *Mb*, *Myl2*, *Actc1*, and *Tnni3* predominantly marker genes for cardiomyocytes[143]. The top 3 enriched GO annotations “cardiac muscle contraction”, “striated muscle contraction” and “muscle contraction” which were found for this cluster confirm these findings. Thus, this cluster was also excluded from further analysis.

Cluster 17 was mostly characterised by marker genes specific for macrophages[91]: The top 10 included *Lyz2*, *Cd74*, *Ctss*, and *Lgals3*. This was underlined by the enriched GO annotations “immune response”, “immune system process” and “positive regulation of immune system process”.

Cluster 18 included the proliferation-associated genes *Top2a*, *H2afz*, *Stmn1*, and *Mki67* in the top 10 marker genes. Other proliferation-associated genes, such as *Racgab1*, *Ccnb2*, and *Cdk1*, were present among the further marker genes. Additionally, the activation marker genes *Acta2* and *Postn* belonged to the marker genes of this cluster. According to this proliferation-associated transcriptional profile cluster 18 was characterised as a F-Cyc population comparable to cluster 10. The search for enriched GO annotations returned the following top 3: “cell cycle process”, “mitotic cell cycle process”, and “cell division”.

For Cluster 19 the top 10 marker genes included *Kcna1* and *Plp1* which are characteristic for glia cells[152,153]. The search for enriched GO annotations revealed “cell-cell adhesion via plasma-membrane adhesion molecules”, “cellular potassium ion transport” and “potassium ion transmembrane transport”. Thus, this cluster was also excluded from further analysis.

A

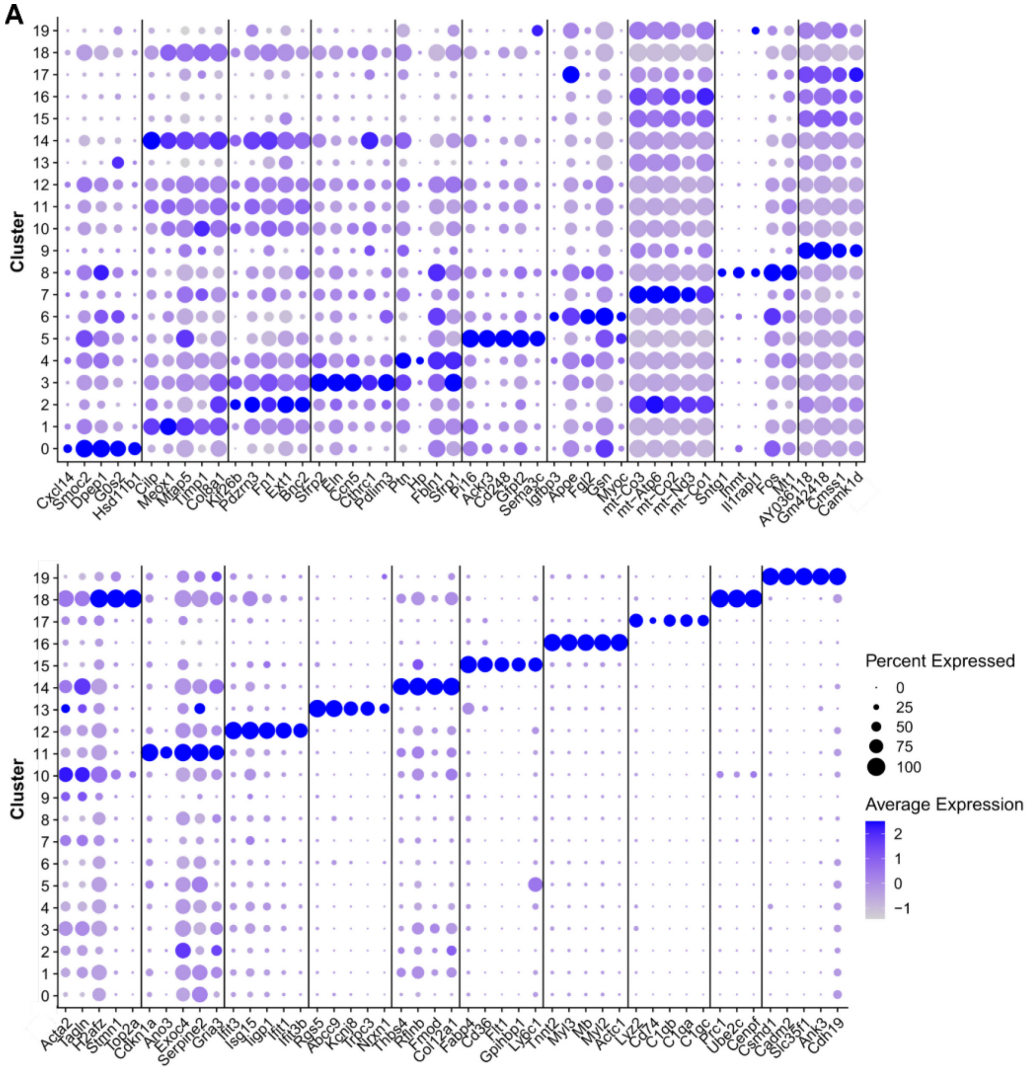

B

CF cluster	GO annotations (Top 3)	FDR q-value
0	positive regulation of protein maturation	1,00E+00
	positive regulation of protein processing	8.15E-1
	skeletal muscle cell differentiation	1,00E+00
1	/	/
2	biological adhesion	1.27E-5
	cell adhesion	6.34E-6
	developmental process	1.58E-3
3	regulation of anatomical structure morphogenesis	6.51E-2
	regulation of developmental process	3.97E-2
	regulation of multicellular organismal development	5.81E-2
4	regulation of developmental process	1.37E-5
	regulation of multicellular organismal development	5.68E-5
	regulation of multicellular organismal process	4.81E-5
5	UDP-N-acetylglucosamine metabolic process	6.83E-1
	nucleotide-sugar metabolic process	3.99E-1
	nucleotide-sugar biosynthetic process	6.83E-1
6	negative regulation of lipid transport	6.47E-1
	regulation of membrane protein ectodomain proteolysis	8.36E-1
	negative regulation of secretion	5.85E-1
7	amide biosynthetic process	2.19E-18
	translation	1.09E-18
	peptide biosynthetic process	7.29E-19
8	regulation of multi-organism process	1.66E-1
	protein activation cascade	1.1E-1
	regulation of neuron death	1.49E-1
9	mitochondrial respiratory chain complex assembly	1.01E-1
	mitochondrial respiratory chain complex I assembly	1.05E-1
	NADH dehydrogenase complex assembly	7.01E-2
10	cell cycle	3.13E-12
	cell division	1.05E-9
	mitotic cell cycle process	6.97E-8

CF cluster	GO annotations	FDR q-value
11	cellular response to DNA damage stimulus	5.37E-1
	signal transduction by p53 class mediator	3.29E-1
	intrinsic apoptotic signaling pathway by p53 class mediator	3.2E-1
12	response to other organism	1.25E-10
	response to external biotic stimulus	6.43E-11
	response to biotic stimulus	4.29E-11
13	signal transduction	3.85E-2
	regulation of system process	2.52E-2
	G protein-coupled receptor signaling pathway	4.93E-2
14	regulation of lipid localization	1.64E-1
	collagen fibril organization	4.08E-1
	connective tissue development	4.93E-1
15	angiogenesis	2.81E-2
	eye morphogenesis	1.16E-1
	lipid transport	9.03E-2
16	cardiac muscle contraction	2.52E-10
	striated muscle contraction	4.59E-9
	muscle contraction	4.72E-9
17	immune response	4.35E-9
	immune system process	3.17E-9
	positive regulation of immune system process	8.32E-7
18	cell cycle process	2.5E-32
	mitotic cell cycle process	5.86E-30
	cell division	6.55E-28
19	cell-cell adhesion via plasma-membrane adhesion molecules	7.6E-3
	cellular potassium ion transport	4.02E-1
	potassium ion transmembrane transport	2.68E-1

Figure 17: Top 5 marker genes and top 3 GO annotations of each cell cluster of the combined analysis of scRNAseq CF datasets w/o MI and 5 and 21 days after MI.
A: Dotplot showing the expression levels of the top 5 marker genes of each cluster. **B:** Table listing the top 3 enriched GO annotations of the marker genes of each cell cluster.

4.4.2.3 Correlation of *Hif1a* and *Postn* expression in CF clusters at different timepoints after MI

The combined scRNAseq data sets were also used to analyse the correlation of *Hif1α* and *Postn* expression in CFs from Postn-tdTomato mice (control group) and Postn-Hif-1αdPA mice with induced HIF-1αdPA expression. For each cluster, gene expression levels of *Postn* and *Hif1a* in CFs from uninjured hearts as well as 5 and 21 dpMI are displayed in Figure 18. In all clusters and at all timepoints the levels of gene expression of *Postn* were profoundly higher than the *Hif-1α* gene expression. In all resident (group I) and activated CF (group II) clusters *Postn* was most strongly expressed in cells from the 5 dpMI samples. It was least expressed in cells isolated from hearts under basal conditions before MI. There was a clear difference between CFs from control and HIF-1αdPA-expressing animals at 5 dpMI. CFs from Postn-Hif-1αdPA mice showed a higher *Postn* gene expression in all clusters. At day 21 post MI the gene expression levels of *Postn* were mostly comparable in control and HIF-1αdPA-expressing mice.

Also, the *Hif1a* gene expression levels showed a peak at 5 dpMI in most clusters (Figure 18). In the resident cell clusters, the *Hif1a* gene expression in cells from basal hearts was similar to cells from the post-MI samples. In the activated CF clusters, cells of the 5 dpMI samples showed the highest *Hif1a* expression. In all activated clusters (except for cluster 2) the cells of HIF-1αdPA-expressing mice 5 dpMI showed a significant higher *Hif1a* expression than the cells from the control 5 dpMI. In the majority of the activated CF clusters a trend for an increased *Hif1a* gene expression in CFs from Hif-1αdPA-expressing animals compared to control CF was visible. The differences between both conditions in *Hif1a* gene expression mostly disappeared at 21 dpMI, where the *Hif-1α* expression levels were nearly back to the basal value in CFs from basal hearts.

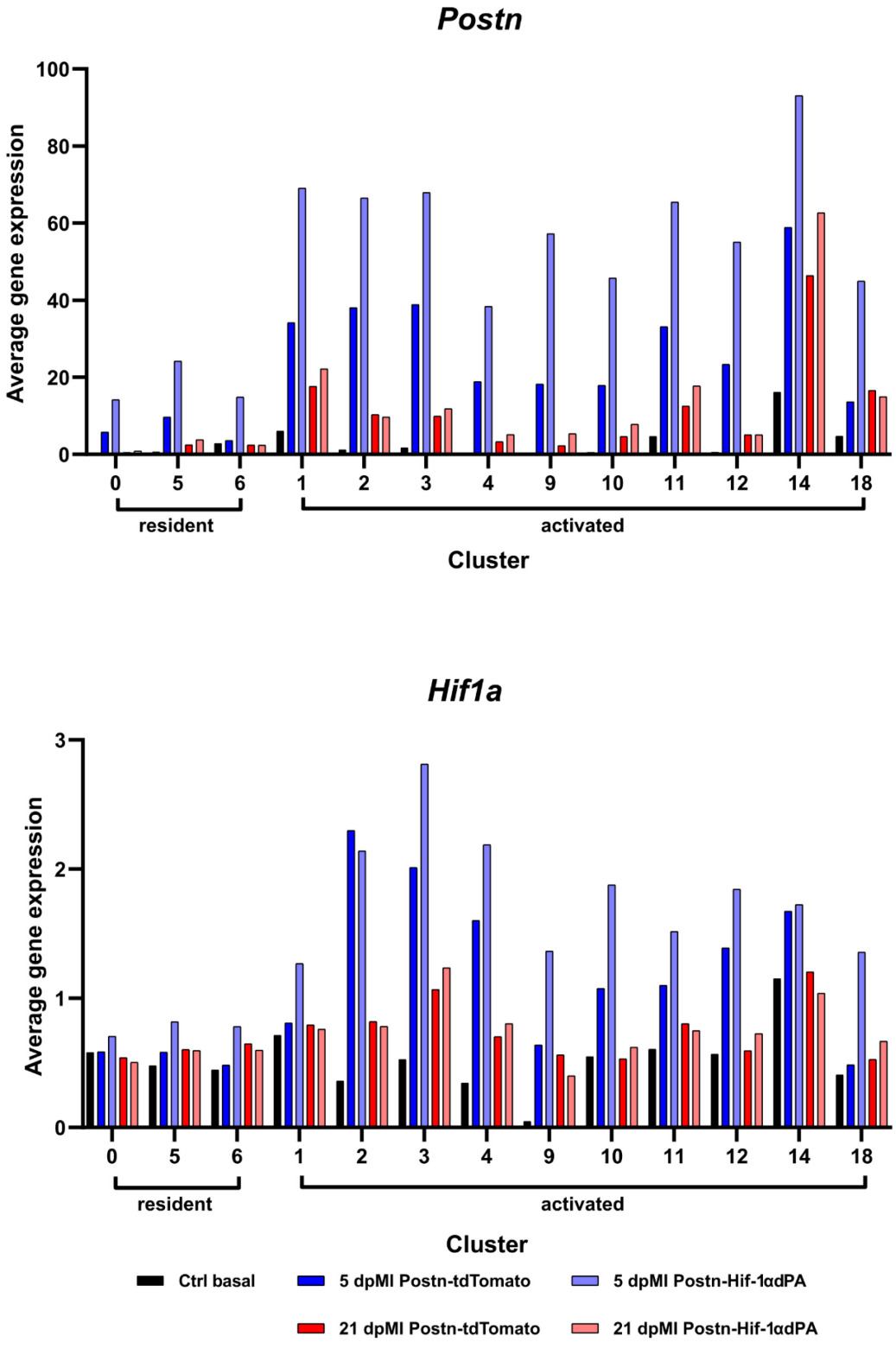

Figure 18: Changes in gene expression of *Hif1a* und *Postn* in the combined analysis of scRNAseq CF datasets w/o MI and 5 and 21 days after MI.

The gene expression was analysed in the same combined data set displayed in Figure 15. The bar charts show the average gene expression of *Postn* and *Hif1a* in every CF cluster, separated for cells

from the individual samples at different time points (without MI, 5 dpMI, 21 dpMI) and without (Postn-tdTomato mice) and with HIF-1αdPA expression (Postn-Hif-1αdPA mice). CF clusters are grouped into resident (group I) and activated (group II) CF clusters.

Altogether, a correlation between *Postn* and *Hif1a* expression can be seen especially in some of the activated clusters. The activated CF clusters 3, 4, 10 and 12 showed the same expression pattern of *Postn* and *Hif1a* during the time course and also comparing both mouse lines. In the activated clusters 9 and 11 a correlation can be drawn for the 5 dpMI timepoint between both gene expressions in both mouse lines. While the Postn expression in the resident clusters (0, 5 and 6) showed a peak at 5 dpMI, for *Hif1a* expression only a minimal effect was seen at 5 dpMI and only in the samples of Postn-Hif-1αdPA mice.

4.4.2.4 Time-dependent changes in the gene expression level

To investigate a time-dependent effect of MI in combination with the HIF-1αdPA stabilisation in $POSTN^+$ aCFs on the transcriptional profile in all identified CF clusters, gene expression levels of chemokines, fibrosis-, proliferation-, and angiogenesis-associated genes were analysed. Gene expression levels were compared between CFs of 5 and 21 dpMI samples from Postn-tdTomato mice and Postn-Hif-1αdPA mice and CFs from basal hearts. The clusters were grouped as mentioned above into resident (group I) and activated (group II) CF clusters.

Differences in expression levels of fibrosis-associated genes are displayed in Figure 19. At 5 dpMI most of the analysed pro-fibrotic genes were significantly upregulated especially in group II clusters in cells from both mouse lines. The upregulation of the pro-fibrotic genes seemed to be more intense in cells from Postn-Hif-1αdPA mice compared to cells from control animals, by means of higher log2 FC values and significant changes in more CF clusters. *Acta2*, *Cthrc1*, *Fn1*, *Lox,* and *Postn* showed the highest log2 FC values in gene expression among the activated CF clusters. Expression of genes encoding collagen chains as well as *Serpine1*, *Sparc*, and *Timp1* was upregulated in both cluster groups at 5 dpMI, mostly to the same extent. In CFs from Postn-tdTomato mice 5 dpMI, *Mmp2* was the only pro-fibrotic gene whose expression was downregulated in most of the activated clusters. In Postn-Hif-1αdPA mice, *Mmp2* was mostly downregulated in both of the cluster groups. Comparing both mouse lines, CFs from Postn-Hif-1αdPA mice showed the significant upregulation of

the expression of pro-fibrotic *Tgfb3* and *Thbs1* in more cell clusters. Interestingly, expression of anti-fibrotic genes was both up- and downregulated at 5 dpMI and showed also different patterns comparing both mouse lines. In Postn-tdTomato CFs, expression of *Airn* and *Timp3* was significantly downregulated in most of the clusters at 5 dpMI. In contrast, Hif-1αdPA-induced CFs showed upregulated *Airn* expression in the majority of clusters and less *Timp3* downregulation. With *Ccn5* the expression of an anti-fibrotic gene was significantly upregulated in CFs from both mouse lines at 5 dpMI. Taken together, in activated clusters the pro-fibrotic genes were higher upregulated compared to the resident clusters. Comparing the gene regulation of cells from Postn-tdTomato and Postn-Hif-1αdPA mice at 5 dpMI, a more intense upregulation in gene expression of fibrotic genes was detected with respect to higher log2 FC values and more clusters in which significant differences were detected.

At 21 dpMI the differences in fibrotic gene expression compared to basal heart CFs were not as big as they were at 5 dpMI (Figure 19, lower panels). The pro-fibrotic genes whose expression levels were highly upregulated at day 5 pMI had lower log2 FC values at 21 dpMI. Especially *Acta2*, the collagen genes and *Cthrc1*, which were some of the key genes with high log2 FC values at 5 dpMI, were not or only slightly upregulated in expression at 21 dpMI. *Mmp2* was upregulated in some clusters 21 dpMI, while 5 dpMI it was the only pro-fibrotic gene which expression was downregulated. The anti-fibrotic gene *Adm* was the only one without obvious differences in gene regulation compared to 5 dpMI. Interestingly, *Timp3* as an anti-fibrotic gene showed the opposite direction of its gene regulation in CFs from Postn-tdTomato mice 21 dpMI compared to 5 dpMI. Altogether, the comparison of the differences in gene expression between CFs from both timepoints after MI with the CFs from basal hearts revealed that there was a lot more fibrotic gene regulation at 5 dpMI than at the later timepoint of 21 dpMI.

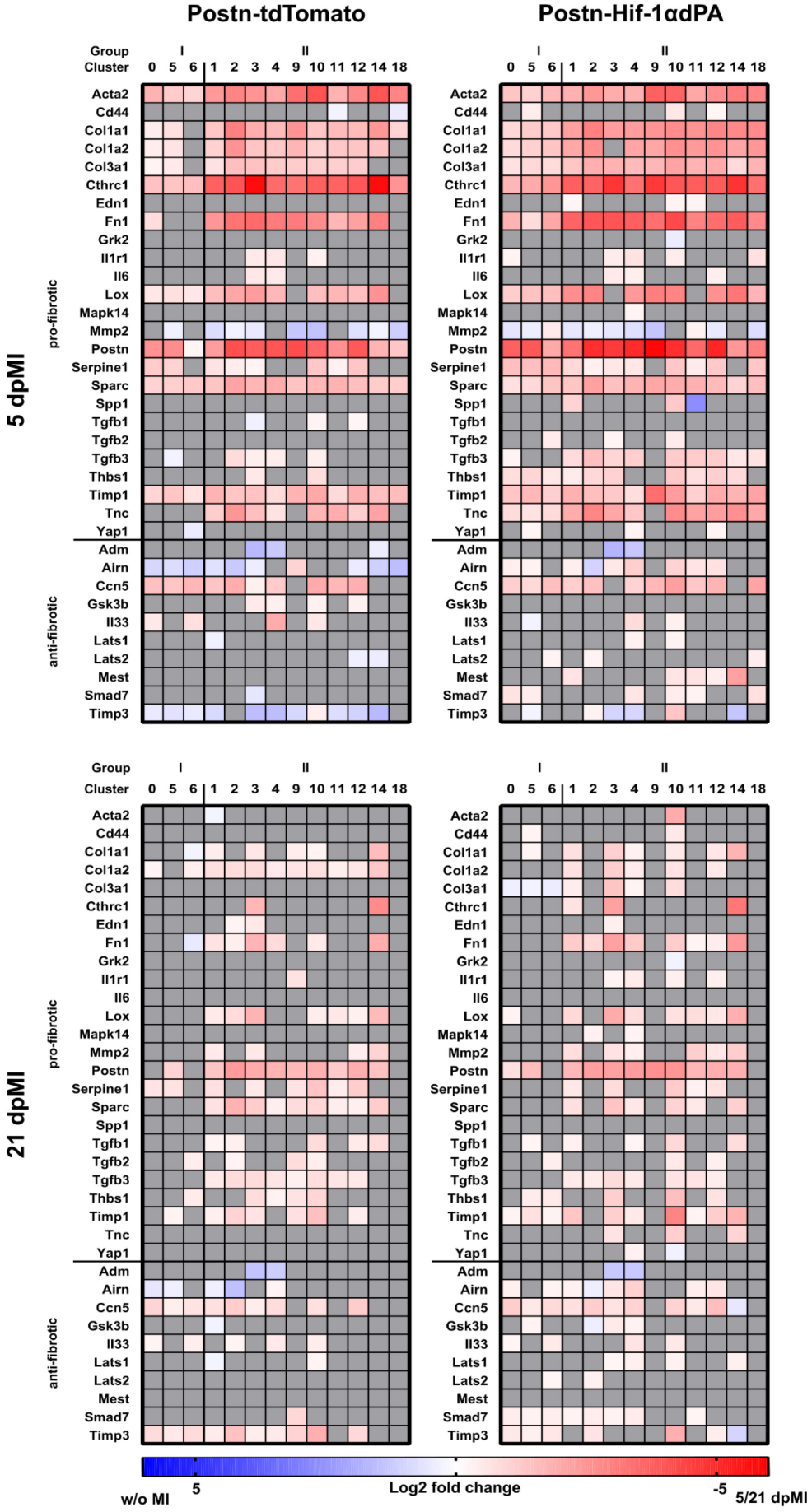
Postn-tdTomato
Postn-Hif-1αdPA
5 dpMI
21 dpMI
Group
Cluster
I
II
0 5 6 1 2 3 4 9 10 11 12 14 18
pro-fibrotic
anti-fibrotic
Acta2
Cd44
Col1a1
Col1a2
Col3a1
Cthrc1
Edn1
Fn1
Grk2
Il1r1
Il6
Lox
Mapk14
Mmp2
Postn
Serpine1
Sparc
Spp1
Tgfb1
Tgfb2
Tgfb3
Thbs1
Timp1
Tnc
Yap1
Adm
Airn
Ccn5
Gsk3b
Il33
Lats1
Lats2
Mest
Smad7
Timp3
w/o MI
5
Log2 fold change
-5
5/21 dpMI

Figure 19: Time-dependent changes in expression of fibrosis-associated genes in the combined analysis of scRNAseq CF data sets w/o MI and 5 and 21 days after MI.
The gene expression was analysed in the same combined data set displayed in Figure 15. The heatmaps show the differences in gene expression of pro- and anti-fibrotic genes in CFs comparing the basal timepoint (w/o MI) with 5 or 21 dpMI for each mouse line (Postn-tdTomato mice and Postn-Hif-1αdPA mice with HIF-1αdPA expression). CF clusters are grouped into resident (group I) and activated (group II) CF clusters. The differences in gene expression are displayed as log2 fold change (5 dpMI to w/o MI and 21 dpMI to w/o MI, respectively) and only significant differences are shown. Blue: higher gene expression in the cells of mice without MI. Red: higher gene expression at 5 or 21 dpMI. Grey: no significant differences in gene expression.

Furthermore, the time-dependent changes in expression of proliferation-associated genes were analysed in CFs from both mouse lines (Figure 20). In general, the expression of the selected proliferative genes was only slightly changed in comparison to the other analysed gene groups and again the effects displayed in the log2 FCs got less over time after MI comparing CFs from Postn-tdTomato and Postn-Hif-1αdPA mice at 5 dpMI and 21 dpMI in both resident and activated clusters in. In CFs from Postn-tdTomato mice at day 5 dpMI, *Nr4a1* and *Nr4a3* expression levels were significantly reduced in activated clusters. The expression levels of *Ranbp1* and *Tubb2a* were significantly upregulated in CFs from Postn-tdTomato mice at day 5 dpMI in both resident and activated clusters.

In CFs from the 21 dpMI samples less genes were significantly regulated compared to CFs from day 5 dpMI samples and significant log2 FCs were observed in less clusters (Figure 20, lower panel). This was seen in samples of Postn-tdTomato mice for *Ranbp1*. *Nr4a1* and *Nr4a3* were regulated in less clusters and into the opposite direction compared to CFs from 5 dpMI. *Atf3*, which was not significantly regulated at 5 dpMI, showed an increased gene expression in CFs from Postn-tdTomato mice at 21 dpMI in the resident clusters (Figure 20, lower left panel). Expression of *Tubb2a* was, in contrast to 5 dpMI, slightly but significantly downregulated at 21 dpMI.

The pattern of post-MI regulation of proliferation-associated genes in CFs from Postn-Hif-1αdPA mice differed from that in CFs from the control animals, but also did not show a lot significant changes compared to CFs from basal hearts (Figure 20, right panels). *Nr4a1* expression in the activated clusters was downregulated in CFs from the 5 dpMI sample (Figure 20, upper right panel), which was also observed in CFs from the control animals (see above). *Nr4a3* was differently regulated in the two cluster

groups. In all three resident clusters its expression was upregulated in CFs from Postn-Hif-1αdPA mice and in four of the activated clusters it was downregulated (Figure 20, upper right panel). In contrast to CFs from Postn-tdTomato mice, CFs from Postn-Hif-1αdPA mice at 5 dpMI expressed less *Rpl37* in resident clusters as well as in 8 activated clusters (Figure 20, upper right panel). The cluster showing the most significant changes in gene expression in CFs from Postn-Hif-1αdPA mice such as seen for angiogenic gene regulation, the F-Cyc cluster 10 (Figure 20, upper right panel).

At 21 dpMI most of the effects on expression of proliferation-associated genes detected in CFs from Postn-Hif-1αdPA mice at 5 dpMI was no longer detectable (Figure 20, lower right panel). For example, CFs in Cluster 10 did not show more significant changes compared to all other clusters as was observed for CFs from the 5 dpMI sample. Only the upregulation of *Nr4a3* in the resident CF clusters was stable over time. Interestingly, the downregulation of *Rpl37* expression in CFs from Postn-Hif-1αdPA mice at 21 dpMI was intensified compared to CFs from day 5 pMI.

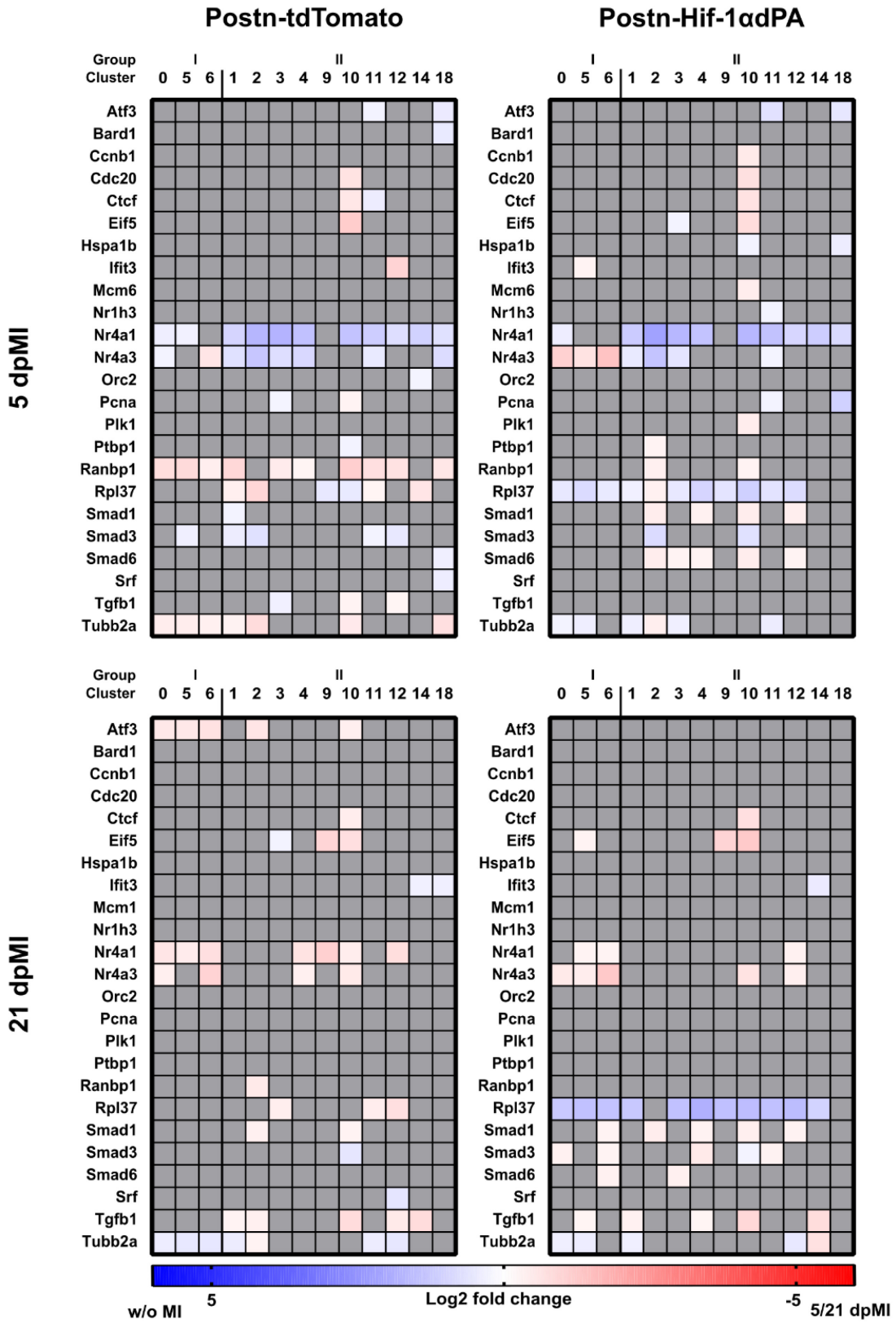
Postn-tdTomato
Postn-Hif-1αdPA
5 dpMI
21 dpMI
Group
Cluster
I
II
0 5 6 1 2 3 4 9 10 11 12 14 18
Atf3
Bard1
Ccnb1
Cdc20
Ctcf
Eif5
Hspa1b
Ifit3
Mcm6
Mcm1
Nr1h3
Nr4a1
Nr4a3
Orc2
Pcna
Plk1
Ptbp1
Ranbp1
Rpl37
Smad1
Smad3
Smad6
Srf
Tgfb1
Tubb2a
w/o MI
5
Log2 fold change
-5
5/21 dpMI

Figure 20: Time dependent changes in proliferation-associated gene expression in the combined analysis of scRNAseq CF datasets w/o MI and 5 and 21 days after MI.

The gene expression was analysed from the same combined data set as mentioned in Figure 15. The heatmaps show the differences in gene expression of proliferation-associated genes in CFs comparing the basal timepoint (w/o MI) with 5 or 21 dpMI for each mouse line (Postn-tdTomato mice and Postn-Hif-1αdPA mice with HIF-1αdPA expression). CF clusters are grouped into resident (group I) and activated (group II) CF clusters. The differences in gene expression are displayed as log2 fold change (5 dpMI to w/o MI and 21 dpMI to w/o MI, respectively) and only significant differences are shown. Blue: higher gene expression in the cells of mice without MI. Red: higher gene expression 5 or 21 dpMI. Grey: no significant differences in gene expression.

Since HIF-1α is known to also target angiogenic genes having an effect on cardiac regeneration[154], the scRNAseq data were checked for gene regulation of selected angiogenic genes. Differences in expression levels of angiogenic-associated genes are displayed in Figure 21. The most prototypical angiogenic genes *Vegfa* and *Vegfc* were only slightly affected. 5 dpMI the angiogenic gene regulation did not have a clear trend to up- or downregulation. In the CFs isolated from both mouse lines, the expression of the angiogenic genes *Col1a1*, *Mdk*, and *Ptn* were significantly upregulated in the activated clusters. In contrast, *Apoe*, *Fbln1* were significantly downregulated together with *Timp3,* which was already mentioned above, in CFs from Postn-tdTomato mice, more in activated clusters than in the resident clusters. While *Apoe* was the most downregulated gene in CFs from Postn-tdTomato mice at 5 dpMI, it was slightly upregulated in some clusters in CFs from Postn-Hif-1αdPA mice. In CFs from this mouse line the most downregulated expression at 5 dpMI was observed for *Angpt1*, which seemed not to be affected in cells from control animals. Like for fibrotic genes, the strongest effects on expression of angiogenic genes at 5 dpMI were seen in the activated clusters. In the CFs isolated from Postn-Hif-1αdPA mice, cluster 10 as a F-Cyc (proliferating CFs / CFs with an activated cell cycle) cluster showed significant changes in the majority of the selected angiogenic genes.

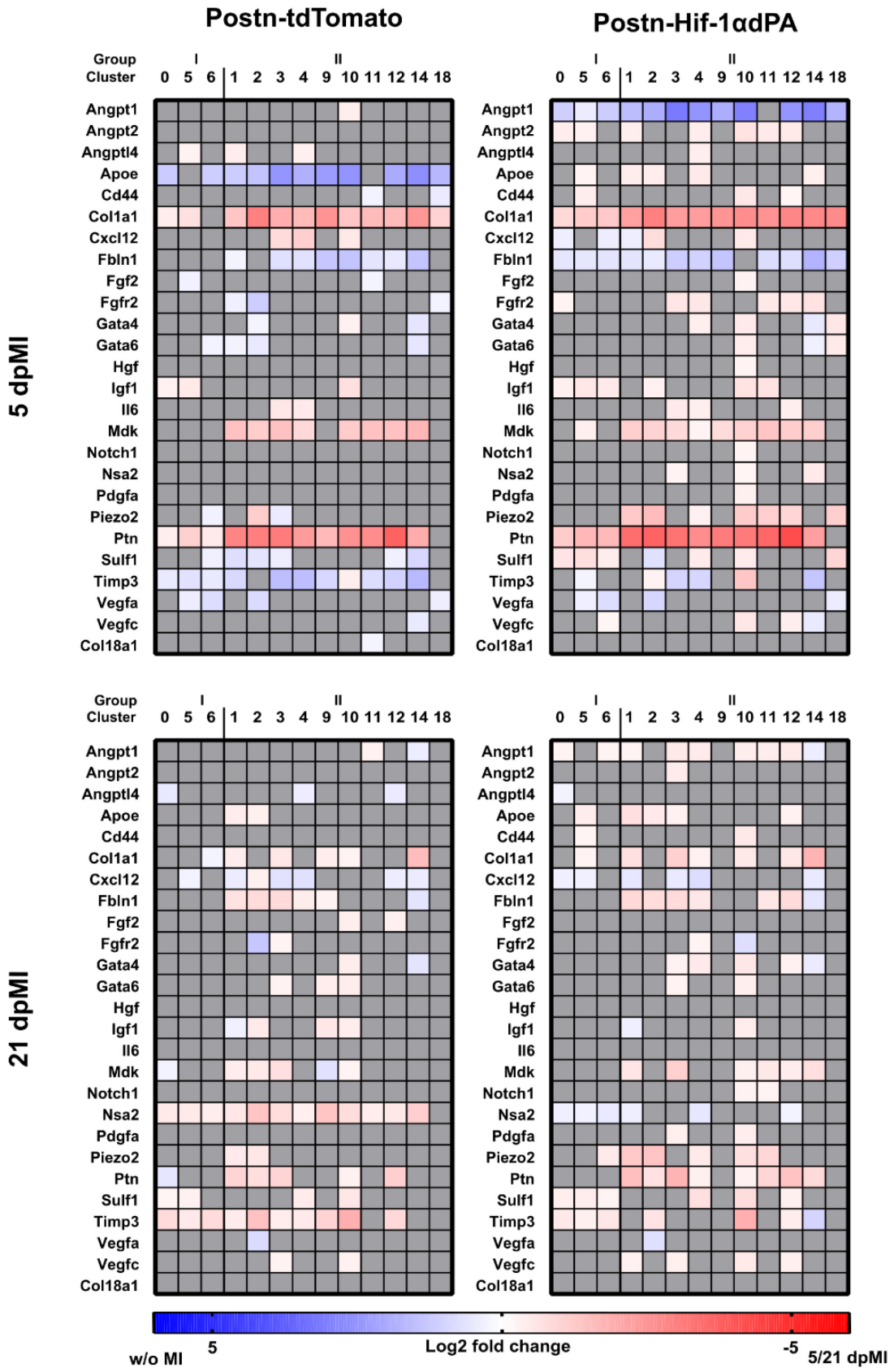
Postn-tdTomato
Postn-Hif-1αdPA
5 dpMI
21 dpMI
Group
Cluster
I
II
0 5 6 1 2 3 4 9 10 11 12 14 18
Angpt1
Angpt2
Angptl4
Apoe
Cd44
Col1a1
Cxcl12
Fbln1
Fgf2
Fgfr2
Gata4
Gata6
Hgf
Igf1
Il6
Mdk
Notch1
Nsa2
Pdgfa
Piezo2
Ptn
Sulf1
Timp3
Vegfa
Vegfc
Col18a1
w/o MI
5
Log2 fold change
-5
5/21 dpMI

Figure 21: Time-dependent changes in angiogenic gene expression in the combined analysis of scRNAseq CF datasets w/o MI and 5 and 21 days after MI.

The gene expression was analysed from the same combined data set as mentioned in Figure 15. The heatmaps show the differences in gene expression of angiogenic genes in CFs comparing the basal timepoint (w/o MI) with 5 or 21 dpMI for each mouse line (Postn-tdTomato mice and Postn-Hif-1αdPA mice with HIF-1αdPA expression). CF clusters are grouped into resident (group I) and activated (group II) CF clusters. The differences in gene expression are displayed as log2 fold change (5 dpMI to w/o MI and 21 dpMI to w/o MI, respectively) and only significant differences are shown. Blue: higher gene expression in the cells of mice without MI. Red: higher gene expression 5 or 21 dpMI. Grey: no significant differences in gene expression.

The time-dependent development of angiogenic gene expression showed the same pattern as the one of fibrotic genes: At 21 dpMI the log2 FC values were much lower and changes in gene regulation were found in less clusters compared to the time point 5 dpMI (Figure 21, lower panels). Interestingly, Tgf-beta-inducible nuclear protein 1 (*Nsa2*) known to regulate cell proliferation and cell cycle[155], was detected to be upregulated in CFs from Postn-tdTomato mice in all clusters (except for cluster 18) but slightly downregulated in the CFs of the Postn-Hif-1αdPA mice in all resident an 3 of the activated clusters at 21 dpMI. Only a few changes were found in its gene expression in cells from 5 dpMI samples.

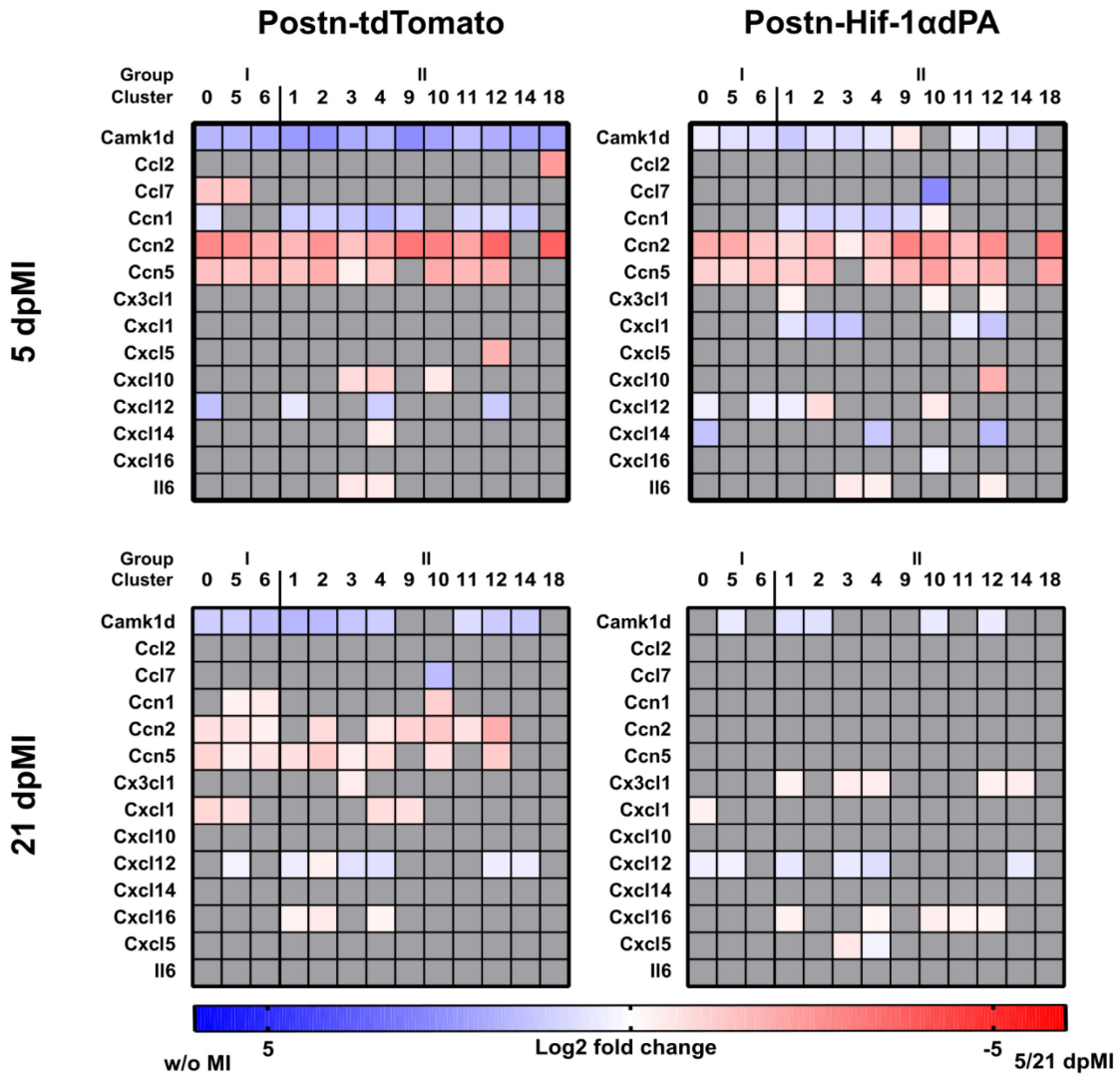

Figure 22: Time dependent changes in gene expression of chemokines and important signalling factors in the combined analysis of scRNAseq CF datasets w/o MI and 5 and 21 days after MI.

The gene expression was analysed from the same combined data set as mentioned in Figure 15. The heatmaps show the differences in gene expression of pro- and anti-fibrotic genes in CFs comparing the basal timepoint (w/o MI) with 5 or 21 dpMI for each mouse line (Postn-tdTomato mice and Postn-Hif-1αdPA mice with HIF-1αdPA expression). CF clusters are grouped into resident (group I) and activated (group II) CF clusters. The differences in gene expression are displayed as log2 fold change (5 dpMI to w/o MI and 21 dpMI to w/o MI, respectively) and only significant differences are shown. Blue: higher gene expression in the cells of mice without MI. Red: higher gene expression 5 or 21 dpMI. Grey: no significant differences in gene expression.

Finally, the differences in the expression of chemokines and other important signalling factors in CFs from both mouse lines was analysed and displayed in Figure 22. The pattern of significant gene expression changes was rather similar in CFs from both

mouse lines at 5 dpMI with respect to the amount of clusters with significant changes (Figure 22, upper panels). However, the log2 FC values differed between the CFs from both mouse lines. The gene regulation in CFs from Postn-tdTomato mice was stronger than in CFs from Postn-Hif-1αdPA mice. In CFs from both mouse lines, *Camk1d* and *Ccn1* showed a downregulated expression, while *Ccn2* and *Ccn5* were significantly upregulated. *Ccn1* was mostly downregulated in activated clusters. In CFs from HIF-1αdPA-expressing mice, expression of *Cxcl1* was significantly downregulated in five of the 10 activated clusters (Figure 22, upper right panel).

In CFs from control animals at 21 dpMI, the changes in chemokine expression decreased compared to the earlier timepoint. The downregulation of *Ccn1* expression observed in 5 dpMI CFs completely disappeared and changed to a slight upregulation in two of the resident CF clusters and one of the activated clusters (Figure 22, lower left panel). In CFs from Postn-Hif-1αdPA mice at 21 dpMI, there were almost no clear changes in gene expression of chemokines detectable (Figure 22, lower right panel).

In summary, gene expression levels in CFs from hearts 5 dpMI were more distinctly changed than in CFs from hearts 21 dpMI, where gene expression levels were nearly back to that of CFs from control hearts. CFs from HIF-1αdPA-expressing mice seemed to show a different pattern of gene expression regulation in comparison to CFs from the control group. To explore this in more detail, a separate analysis of the 5 dpMI samples was performed, directly comparing changes of gene expression in CFs from Postn-tdTomato mice and Postn-Hif-1αdPA mice.

4.4.3 HIF-1α-induced changes on gene expression in CF populations 5 days after MI

To directly compare gene expression levels in CFs from HIF-1αdPA-expressing Postn-Hif-1αdPA mice to CFs from Postn-tdTomato mice as control, only the data of the 5 dpMI scRNAseq samples from both mouse lines (see 4.4.2) were combined and processed in a separate bioinformatic analysis.

4.4.3.1 Classification of cell clusters

To visualize the identified 14 cell clusters in the combined analysis of the 5 dpMI samples of both mouse lines, UMAP-Plots were created (Figure 23A-C). 10 of 14

clusters were identified as CF clusters using the top 5 marker genes of each cluster (Figure 24). The remaining four clusters, cluster 10 (pericytes), cluster 12 (endothelial cells), cluster 13 (macrophages), and cluster 14 (epicardium), were excluded from further analysis (see 4.4.3.2). As stated above (4.4.2.1) the number of cells applied to scRNAseq differed between both mouse line samples (see 4.4.2.1), leading to different total cell counts in the data set (Figure 23A-C). The samples from both mouse lines showed also different cluster compositions (Figure 23A-C). To quantify this, the percentage of cells of the total sample cell count contributing to the individual clusters was calculated (Figure 23D). As described above (4.4.2.1), the CF clusters were grouped into resident CF clusters (cluster 1) and activated CF clusters (clusters 0, 2, 3, 4, 6, 7, 8, 9, 11). Interestingly, some of the clusters were mostly composed of CFs from only one mouse line (Figure 23D). The activated CF cluster 7 was mostly composed of CFs from HIF-1αdPA-expressing mice. In contrast, the relative contribution by CFs from the Postn-tdTomato sample to the only resident CF cluster 1 was nearly twice as high as the contribution by CFs from the Postn-Hif-1αdPA sample. All other clusters only showed slight differences in the percentages of the total sample cell count between the both mouse lines (Figure 23D).

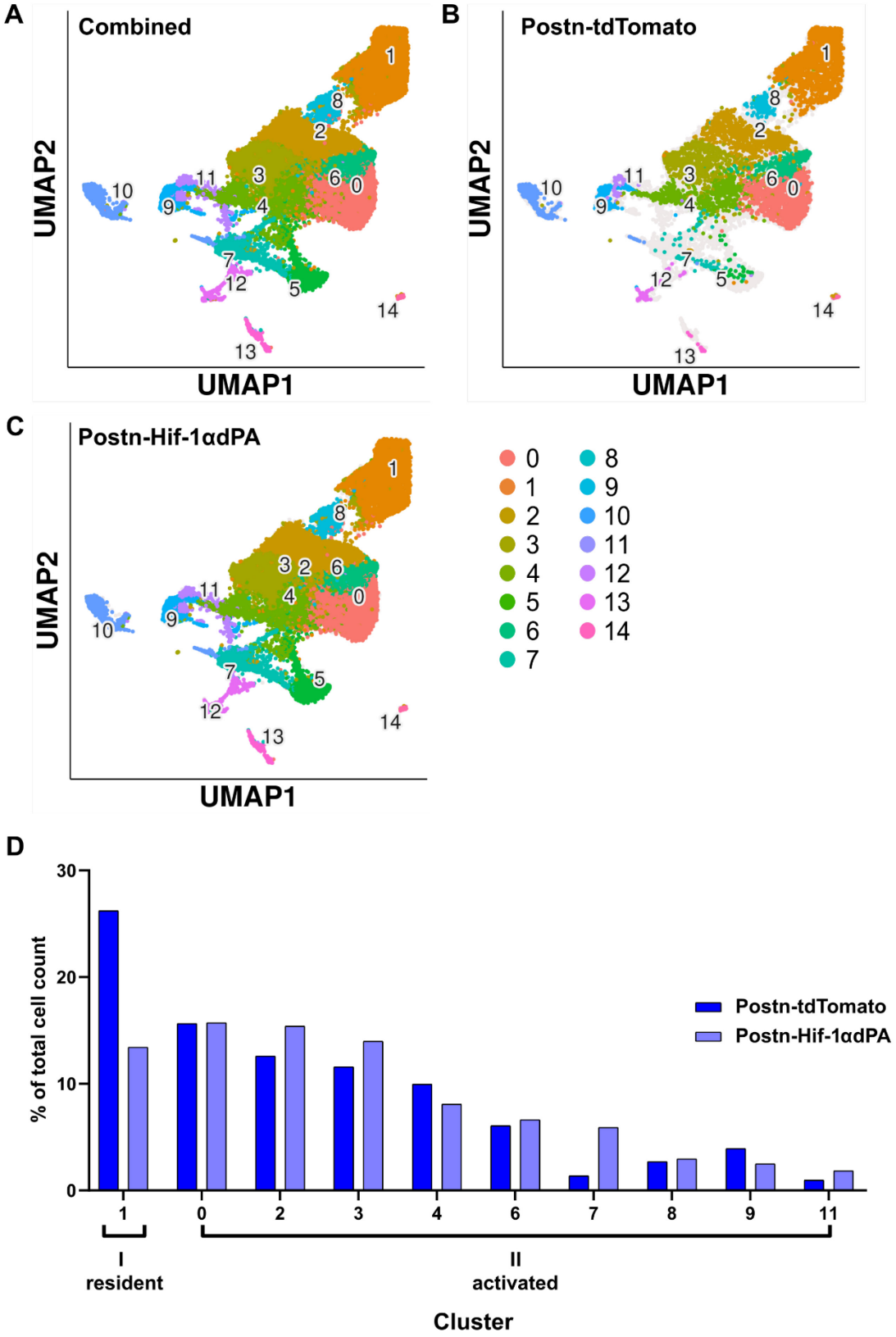
A
Combined
UMAP2
UMAP1
B
Postn-tdTomato
UMAP2
UMAP1
C
Postn-Hif-1αdPA
UMAP2
UMAP1
0
1
2
3
4
5
6
7
8
9
10
11
12
13
14
D
% of total cell count
30
20
10
0
Postn-tdTomato
Postn-Hif-1αdPA
1
0
2
3
4
6
7
8
9
11
I
resident
II
activated
Cluster

Figure 23: Clusters of the combined CF scRNAseq analysis of CFs from Postn-tdTomato mice and Postn-Hif-1αdPA mice at 5 dpMI.

The samples were from the same dataset as illustrated in Figure 15. Here the samples from 5 dpMI were analysed separately. After quality control filtering, transcriptional profiles of 6273 cells from Postn-tdTomato heart 5 dpMI (n=1) and 31443 cells from Postn-Hif-1αdPA hearts 5 dpMI (n=3) were further analysed. **A-C**: UMAP plots of the CF datasets visualizing the identified CF clusters. Shown are the data combined (A), or the individual data sets of Postn-tdTomato control mice (B) and Postn-Hif-1αdPA mice (C). Clusters were labelled according to size, starting with the largest one (cluster 0). The following non-CF clusters, as identified by expression of non-CF markers (see Figure 24), were excluded for further analysis: cluster 12 (endothelial cells), cluster 13 (macrophages), cluster 14 (epicardium). **D**: Bar chart showing the percentage of the total cell count each sample is contributing to the individual clusters. Clusters are grouped on basis of their transcription profile (see 4.4.3.2) in resident (1) and activated (0, 2, 3, 4, 6, 7, 8, 9, 11) CF clusters.

4.4.3.2 Characterisation of cell clusters

The identification and characterisation of all CF clusters of the combined data analysis from the 5 dpMI scRNAseq samples were done according to their transcriptional profile and their determined marker genes. Where possible, the clusters were assigned to the defined CF clusters from Farbehi *et al.*[91], as in already done in 4.4.2.2. The expression of the top 5 marker genes and the top 3 enriched GO annotations, which were determined as already done in 4.4.2.2, within each CF cluster are visualised in Figure 24.

The two highest expressed marker genes within cluster 0 were the myofibroblast-specific genes *Sfrp2* and *Ptn*[91]. Not in the top 10 marker genes but also significantly high expressed were *Ccn5* and *Comp*. Both genes are known to be expressed in CFs during the proliferative phase or maturation phase after MI[52,144]. In contrast, also specific genes for resident fibroblasts like *Ddr2*, *Col1a1*, *Tcf21*, *Sparc* and *Col3a1* were among the marker genes[70,74,135,156]. The top 3 enriched GO annotations for cluster 0 were “regulation of cell motility”, “regulation of cell migration” and “regulation of locomotion”.

Cluster 1 was characterised by *Gsn*, a resident fibroblast marker geneas the top marker gene, followed by *Pi16* which has been assigned as marker gene for the F-SH population[91]. Among the marker genes beyond the top 10 were *Pdgfra* and *Tcf21* as resident fibroblast markers. Interestingly, other marker genes for the F-SH population

like *Cd248*, *Efhd1*, *Gfpt2* and *Tmem100* but also marker genes for the F-SL population like *Hsd11b1*, *Cxcl14*, *G0s2*, *Lpl* and *Smoc2* were among the significant marker genes of this cluster. The search for enriched GO annotations revealed “extracellular structure organisation”, “chemotaxis” and “taxis” as the top 3.

Among the top 10 marker genes of cluster 2 were mitochondrial genes, indicating that some cells were dying[141,142], together with *Col11a1*. The top 10 marker genes showed no clear signature for a specific fibroblast population. *Postn*, *Cilp* and *Col8a1* assigned to the F-Act population were found among the further significant markers. The top 3 enriched GO annotations found for this cluster were “biological adhesion”, “cell adhesion” and “synapse organisation”.

Cluster 3 could be assigned to the F-Act population described in Farbehi *et al*.[91]. *Cilp* and *Meox1* were among the top 10 marker genes. Additionally, *Col8a1*, *Cst6* and *Postn* were also significantly higher expressed in this cell cluster. No enriched GO annotations were found for cluster 3.

Cluster 4 was characterised by expression of *Acta2*, *H2afz*, *Cenpa* and *Stmn1* which were found under the top 5 markers. These genes have been assigned to the F-Cyc population. The top 3 enriched GO annotations found for this cluster were “cytoskeleton organisation”, “mitotic cytokinesis” and “negative regulation of actin filament bundle assembly”.

The top 10 markers of cluster 5 only contained mitochondrial and ribosomal genes, indicating that this cluster mainly consisted of dying cells. Thus, cluster 5 was excluded from further analysis.

In cluster 6 *Sfrp2* and *Cthrc1* belonged to the top 10 marker genes, giving a hint that this cell cluster contains myofibroblasts. Also, other myofibroblast-specific gene transcripts like *Fn1* and *Ddah1* as well as the activation marker *Postn* were significantly higher expressed. This cluster also showed a gene signature for *Wnt*-signalling by expressing *Eln* as the top marker gene and also expressing *Frzb*, *Mfap4* and *Timp3* significantly higher. The search for enriched GO annotations revealed “supramolecular fiber organisation”, “regulation of protein kinase activity” and “positive regulation of transferase activity”.

Cluster 7 was characterised by a high number of ribosomal genes among the marker genes, but also markers indicating an activated state of CFs, like *Postn*, *Acta2*, *Cthrc1*, and *Ptn* were significantly higher expressed. The top 3 enriched GO annotations included “generation of precursor metabolites and energy”, “monovalent inorganic cation transport” and “proton transmembrane transport”.

The top 10 markers of Cluster 8 included *Ifit1*, *Ifit3*, *Iigp1*, *Isg15* and *Rsad2*, which have been assigned to the interferon-responding F-IFNS population[91]. The top 3 enriched GO annotations were “response to external biotic stimulus”, “response to biotic stimulus” and “response to other organism”.

Cluster 9 was characterised by the presence of *Stmn1* and *H2afz*, known as markers for the F-Cyc population, and *Top2a* and *Mki67*, known as proliferation markers, among the top 10 marker genes. *Timp1*, *Cenpa*, and *Acta2*, which also known as markers for the F-Cyc population, were among the other significant markers of this cluster. The search for enriched GO annotations revealed “mitotic cell cycle process”, “cell cycle” and “cell cycle process” as top 3.

Cluster 10 was showed a perivascular cell gene expression pattern. The top 10 marker genes included the pericyte marker genes *Rgs5*, *Abcc9*, and *Kcnj8*[151], as well as the smooth muscle cell marker *Notch3*. In line with this also the smooth muscle cell markers *Acta2*, *Myh11*[151], *Vtn*, and *Tagln* were significantly higher expressed in cluster 10. With this gene expression pattern typical for pericytes and smooth muscle cells, cluster 10 was as a non-fibroblast cluster excluded from further analysis.

Cluster 11 was characterised by the proliferation markers *Top2a*[157], *Mki67*[158] and *Anln*[159] in the top 10 marker genes. In addition, other proliferation markers as *Ccnb2* and *Cdk1* were also expressed at significantly higher levels, as well as the genes *Stmn1*, *H2afz* and *Cenpa*, which indicated that the cluster belonged to the F-Cyc population. The top 3 enriched GO annotations for this cluster consisted of “mitotic cell cycle process”, “cell cycle process” and “cell division”.

Cluster 12 was identified as a cluster of endothelial cells. The top 10 marker genes included *Fabp4*, *CD36*, *Gpihbp1*, and *Cav1*, which are all known as endothelial cell marker genes. This non-fibroblast cluster was excluded from further analysis.

A

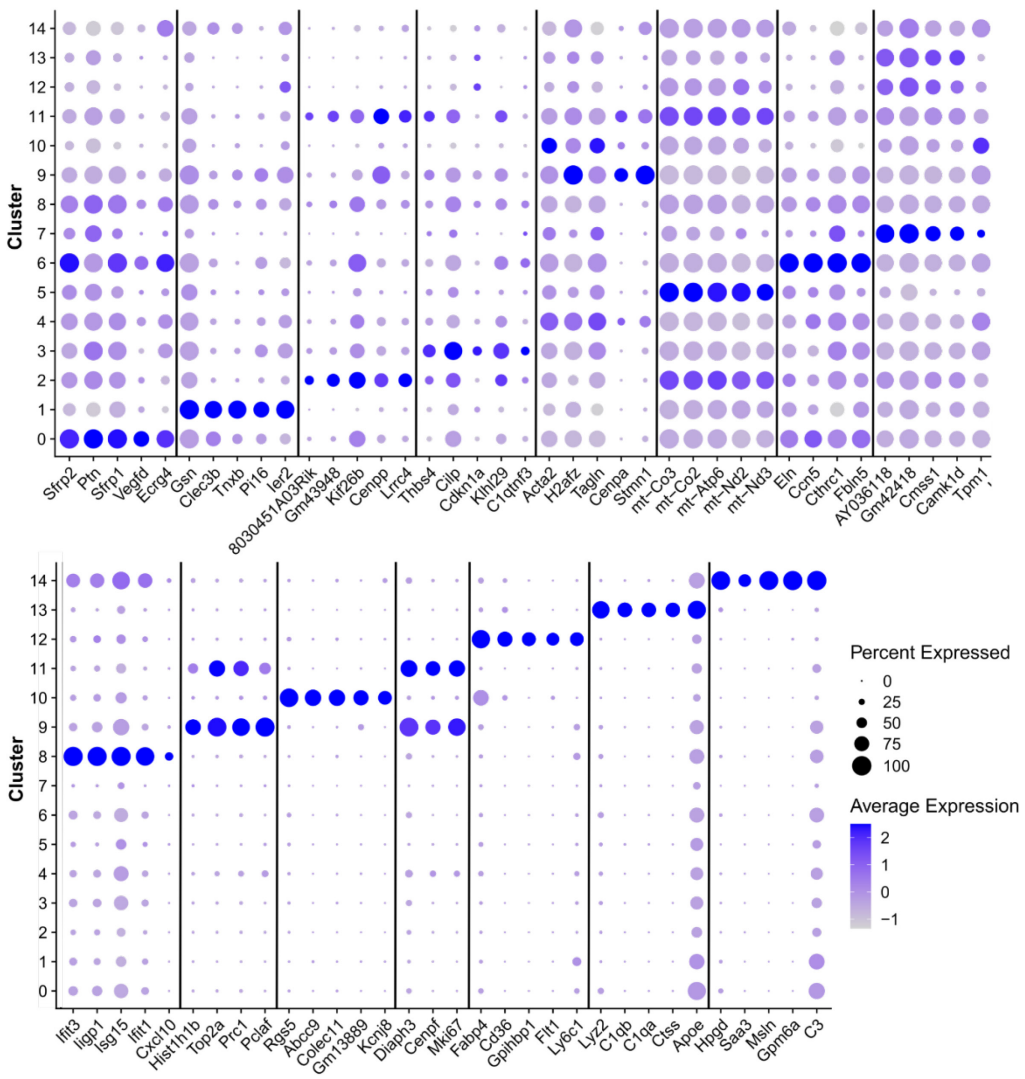

B

CF cluster	GO annotations	FDR q-value
0	regulation of cell motility	2.05E-2
	regulation of cell migration	1.02E-2
	regulation of locomotion	1.23E-2
1	extracellular structure organization	1.36E-2
	chemotaxis	1.2E-2
	taxis	7.99E-3
2	biological adhesion	1.41E-7
	cell adhesion	7.06E-8
	synapse organization	6.26E-5
3	/	/
4	cytoskeleton organization	3.23E-2
	mitotic cytokinesis	6.12E-2
	negative regulation of actin filament bundle assembly	5.7E-2
5	amide biosynthetic process	7.24E-7
	translation	3.62E-7
	peptide biosynthetic process	2.41E-7
6	supramolecular fiber organization	1.28E-1
	regulation of protein kinase activity	6.51E-1
	positive regulation of transferase activity	4.79E-1
7	generation of precursor metabolites and energy	6.95E-6
	monovalent inorganic cation transport	1.51E-3
	proton transmembrane transport	5.88E-3

CF cluster	GO annotations	FDR q-value
8	response to external biotic stimulus	6.11E-6
	response to biotic stimulus	3.06E-6
	response to other organism	2.44E-6
9	mitotic cell cycle process	1.75E-11
	cell cycle	1.63E-11
	cell cycle process	3.47E-9
10	muscle system process	2.71E-4
	regulation of multicellular organismal process	1.06E-3
	muscle contraction	1.19E-3
11	mitotic cell cycle process	5.65E-23
	cell cycle process	1.4E-21
	cell division	3.3E-18
12	regulation of locomotion	1.66E-7
	regulation of cell motility	8.74E-8
	regulation of cellular component movement	1.86E-7
13	immune system process	1.73E-13
	immune response	7.54E-12
	regulation of immune system process	9.58E-10
14	developmental process	7.11E-3
	regulation of multicellular organismal process	1.2E-2
	cellular developmental process	2.19E-2

Figure 24: Top 5 marker genes and top 3 GO annotations of each cell cluster of the combined analysis of scRNAseq CF datasets 5 dpMI.

A: Dotplot showing the expression levels of the top 5 marker genes of each cluster. **B:** Table listing the top 3 enriched GO annotations of the marker genes of each cell cluster.

In cluster 13 the macrophage marker genes *Lyz2*, *Ctss*, *Spp1*, and *Lgals3* were found in the top 10 marker genes. As a macrophage cluster it was not further analysed.

Cluster 14 was identified as an epicardial cluster with the epicardial marker genes *Saa3*, *Clu*, *Msln*, and *Gpm6a* among the top 10 markers. Also, this cluster was as non-fibroblast cluster excluded from further analysis.

4.4.3.3 Correlation of *Hif1a* and *Postn* expression in CF clusters at 5 dpMI

To compare *Hif1a* and *Postn* expression in the CFs from Postn-Hif-1αdPA mice and the CFs from the control (Postn-tdTomato mouse) in this combined 5 dpMI analysis, their gene expression in the individual clusters is displayed in Figure 25. As already observed in the scRNAseq analysis together with the basal heart sample and the 21 dpMI samples (4.4.2.3, Figure 18), the *Postn* gene expression was significantly higher in the CFs from the Postn-Hif-1αdPA mice compared to CFs from the control at 5 dpMI. *Hif-1α* gene expression showed a significantly higher value in the CFs from Postn-Hif-1αdPA mice in clusters 0, 4, 6, and 9. As reported above, clusters 4 and 9 were clusters of proliferating CFs (F-Cyc), while Cluster 0 was characterised as a mixed cluster of myofibroblasts and resident fibroblasts, and cluster 6 likely contained myofibroblasts with the special signature for *Wntx* signalling (4.4.3.2). Additionally, the clusters 1, 3, 7, and 8 showed a trend for a higher *Hif1a* expression in CFs from Postn-Hif-1αdPA mice. Only in clusters 2 and 11, CFs from Postn-Hif-1αdPA mice showed no higher *Hif-1α* expression than CFs from the control. Thus, the increased *Postn* expression in CFs from Hif-1αdPA-expressing mice did not in all clusters correlate with a clear increase in *Hif-1α* expression but in 4 of them significantly. The results from this timepoint analysis confirm the results already seen in the combined time course analysis in Figure 18.

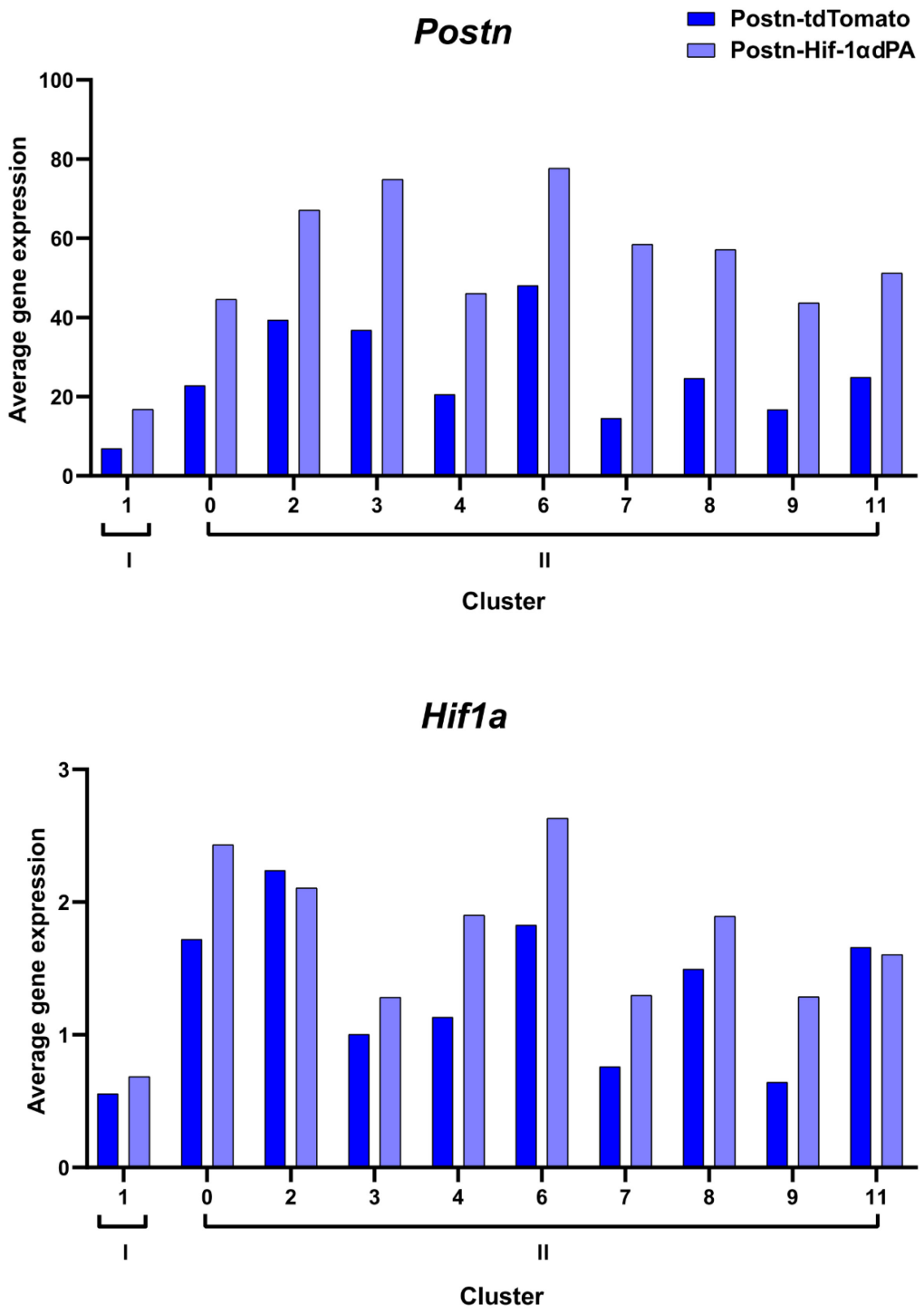

Figure 25: Gene expression of *Hif1a* und *Postn* in the combined analysis of scRNAseq CF datasets at 5 dpMI.

The gene expression was analysed in the same combined data set displayed in Figure 23. The bar charts show the average gene expression of *Postn* and *Hif1a* in every CF cluster, separated for cells from Postn-tdTomato (control) and Postn-Hif-1αdPA mice at 5 dpMI. CF clusters are grouped into the resident (I) and activated (II) CF clusters.

4.4.3.4 HIF-1α-dependent changes in the gene expression level

To investigate the HIF-1αdPA-induced effects at 5 dpMI, gene expression of HIF response-, fibrosis- and angiogenesis-associated genes as well as chemokines were compared between CFs from the control sample (Postn-tdTomato mouse line) and CFs from Postn-Hif-1αdPA mice.

To explore, whether in addition to *Hif1a* (see Figure 25*)* also expression of genes associated with the HIF response was modulated, which might indicate HIF-1α protein activity, a group of HIF response genes were selected and analysed (Figure 26, upper left panel). Interestingly, only two of these genes, *Chd2* and *Egfr*, were significantly higher expressed in CFs from Postn-Hif-1αdPA mice in comparison to CFs from the control among all clusters, except for cluster 7 and 11. Gene expression of the other genes of the HIF response was either not significantly affected or downregulated, like *Aldoa*, *Eno1*, *Fxyd1*, *Ldha*, *Slc29a1*, and *Tpi1,* compared to the control CFs. Cluster 9, as one of the clusters with a profound difference in *Hif-1α* expression (see Figure 25), showed the most changes in gene expression of the HIF response genes (Figure 26, upper left panel). Altogether, the majority of the selected HIF response genes showed a downregulated expression in CFs of Postn-Hif-1αdPA mice.

As shown in Figure 26, upper right panel, the majority of the selected pro-fibrotic genes were higher expressed in CFs from Postn-Hif-1αdPA mice compared to CFs from the control. The expression levels of *Col3a1*, *Fn1*, *Lox*, and *Postn* were significantly increased in the CFs from Postn-Hif-1αdPA mice throughout all clusters. Expression of *Col1a1*, *Col1a2*, *Tgfb3*, *Thbs1*, and *Tnc* was upregulated in all clusters except for one each. Additionally, anti-fibrotic gene expression of *Airn*, *Smad7* and *Timp3* was also significantly upregulated in CFs from Postn-Hif-1αdPA mice in the majority of resident and activated clusters. Only *Il33* expression was consistently downregulated in CFs from Postn-Hif-1αdPA mice, in those of the resident cluster 1 as well as the activated clusters 0, 2, and 8.

Among the angiogenic genes, expression of *Fgfr2*, *Piezo2*, *Ptn*, and *Sulf1* was significantly increased in CFs from Postn-Hif-1αdPA mice in all clusters (Figure 26, lower left panel). The expression of *Cxcl12* and *Fbln1* was decreased in Postn-Hif-1αdPA CFs in the resident cluster 1 as well as in a few activated clusters (0 and 0, 2,

6, 8, respectively), while *Apoe* expression was downregulated in the activated clusters 0, 6, and 8.

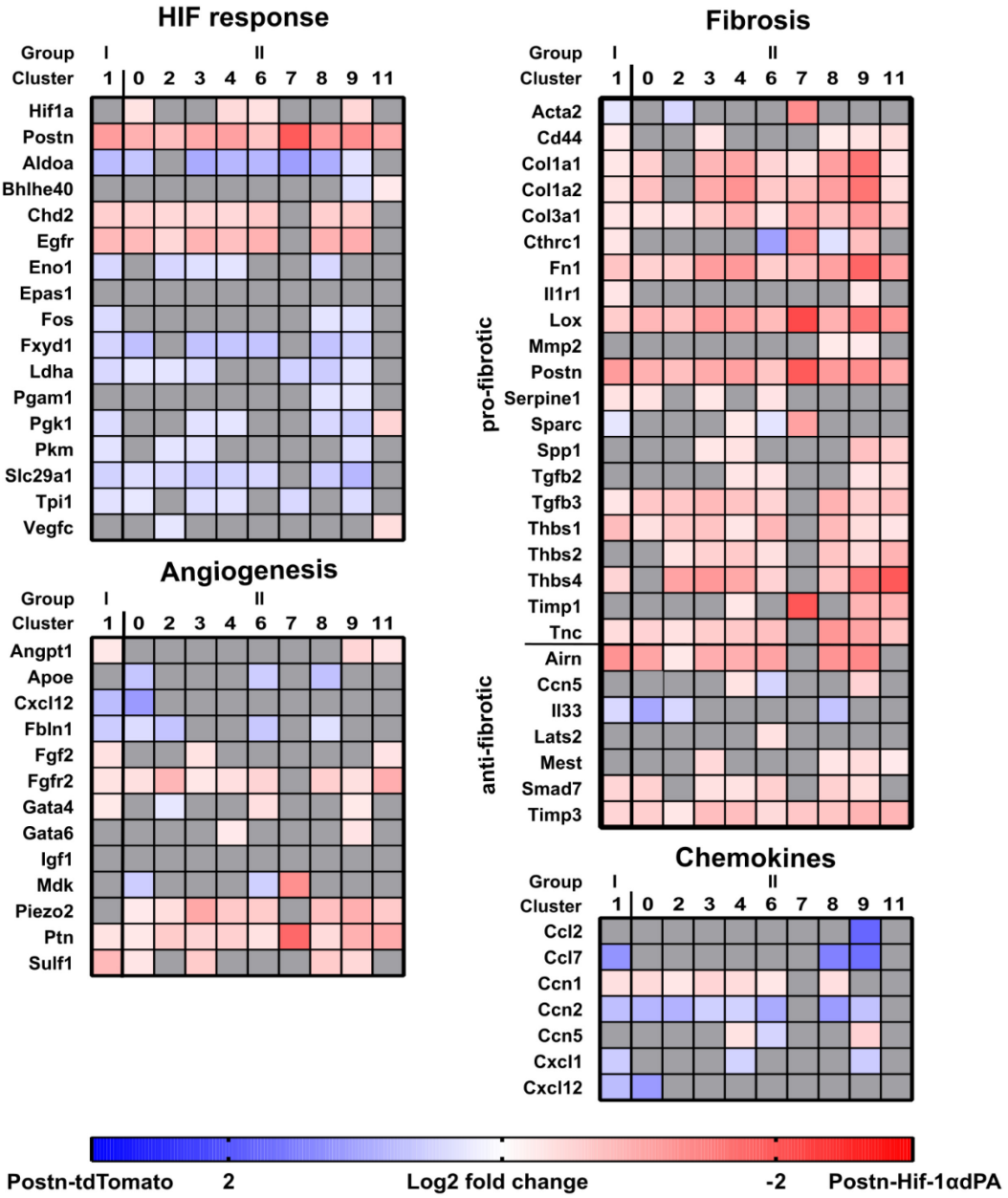

Figure 26: Hif-1αdPA-mediated changes in expression of genes associated with the HIF response, angiogenesis, fibrosis, and chemokines in the combined analysis of CF scRNAseq datasets at 5 dpMI.

The gene expression was analysed in the same combined data set displayed in Figure 23. The heatmaps show the differences in gene expression of HIF response genes, chemokines, angiogenesis- and fibrosis-associated genes in each cluster comparing the CFs from the Postn-tdTomato control and the Postn-Hif-1αdPA mice with HIF-1αdPA expression. CF clusters are grouped into resident (group I)

and activated (group II) CF clusters. The differences in gene expression are displayed as log2 fold change (Postn-Hif-1αdPA to Postn-tdTomato) and only significant differences are shown in the heatmaps. Blue: higher gene expression in the cells from Postn-tdTomato mice. Red: higher gene expression in cells from Postn-Hif-1αdPA mice. Grey: no significant differences in gene expression.

Significant changes in expression of chemokines and other important signalling factors were hardly detected (Figure 26, lower right panel). Only the expression of *Ccn1,* which is known to increase the number of senescence cells and to inhibit the proliferation of CFs in the heart after MI[160], was increased in CFs from Postn-Hif-1αdPA mice compared to CFs of the control in most of the clusters. Interestingly, its family member *Ccn2* showed the opposite and was significantly downregulated in Postn-Hif-1αdPA CFs in the same clusters in which *Ccn1* expression was upregulated. In summary, direct comparison of CFs from the Postn-Hif-1αdPA sample with CFs from the Postn-tdTomato control sample at 5 dpMI revealed several differences in gene expression. Particularly striking were the differences within the fibrotic genes: a significant increase in pro-fibrotic gene expression in CFs from Hif-1αdPA animals was observed. In the other gene groups, expression was both upregulated and downregulated between the samples, showing no clear gene regulation pattern.

4.4.4 Effects of HIF-1α protein stabilisation in aCFs on heart function after MI

So far, the effects of HIF-1αdPA stabilisation in POSTN-expressing cells has been only analysed on gene expression level. To explore the effects on heart function *in vivo*, MRI measurements were carried out. To investigate the potential cardioprotective effects of stabilised HIF-1αdPA protein in aCFs, infarct size and cardiac function of Postn-Hif-1αdPA mice with tamoxifen-induced Hif-1αdPA expression (i.p. injections at -1, 0, 1, 2, 3 dpMI) was quantified and compared to mice of the same strain without tamoxifen induction as control group. Cardiac function was measured over a time course of 21 days after MI. Before MI the cardiac function of each mouse was measured. One day after MI, infarct size was quantified using late gadolinium enhancement (LGE) (3.3.1).

The infarct size of control and HIF-1αdPA-induced mice did not differ 1 day post MI (Figure 27 A), indicating that the HIF-1αdPA stabilisation had no impact on infarct size. Measurements of cardiac functional parameters were performed at 1, 7, 14 and 21 dpMI. At day 1 pMI, the ejection fraction (EF), representing the percentage of the whole

left ventricular blood amount pumped out with one heartbeat, was at nearly significantly (p value = 0.0516) increased in the HIF-1αdPA-induced mice compared to the controls (Figure 27 B). At 7 dpMI, there was still a trend for an increase visible. 21 dpMI, the EF of HIF-1αdPA-induced mice was comparable to the EF of the control mice (Figure 27 B). The end diastolic volume (EDS), which represents the volume of blood that fills the left ventricle at the end of the diastole, increased after MI and over time in both control and HIF-1αdPA-induced mice at a comparable rate (Figure 27 C). The end systolic volume (ESV) represents the volume of blood that fills the left ventricle at the end of the systole. After MI the ESV increased in both control and HIF-1αdPA-induced mice but in different ways: At 1 dpMI, the ESV of HIF-1αdPA-induced mice also increased compared to the basal value but was significantly smaller than the increased ESV of the control mice (Figure 27 D). Interestingly, at 7 dpMI this difference was no longer visible and the ESVs of both mouse groups were nearly the same. Altogether, a significant difference in cardiac function was observed for endsystolic volume at 1 dpMI, which did not translate in a significant difference of EF.

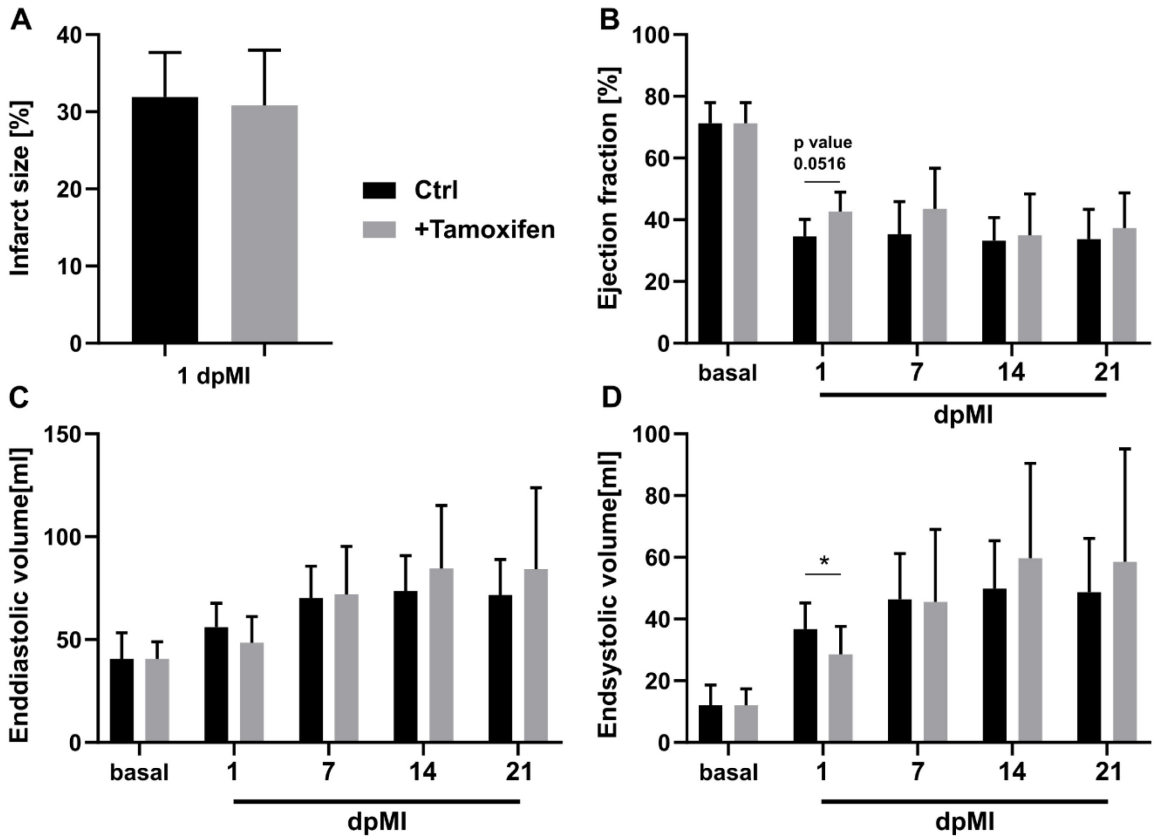

Figure 27: Effects of Hif-1αdPA protein stabilisation in POSTN-positive aCFs on cardiac function post MI.

The MI in Postn-Hif-1αdPA mice w/o (control) and with tamoxifen treatment was induced by 50 min I/R. The HIF-1αdPA expression in POSTN-expressing aCFs was induced by i.p. tamoxifen injections at -1, 0, 1, 2, 3 dpMI. Infarct size and cardiac function of control (Ctrl, n=5) and HIF-1αdPA-induced (+Tamoxifen, n=7) mice were analysed at indicated time points post MI by MRI. **A**: The bar chart shows the infarct size of control and HIF-1αdPA-induced mice as quantified 1 dpMI using gadolinium to label the ischemic region in the myocardium. **B-D:** Bar charts showing the ejection fraction (B), end diastolic volume (C) and end systolic volume (D) of control (black) and tamoxifen-treated (grey) mice before MI (basal), 1, 7, 14 and 21 dpMI. Unpaired Welch's t-test was used for statistical analysis (p-value: * < 0.05).

5 Discussion

MI is among the leading causes of death worldwide[1]. CFs play a crucial role in the different phases of cardiac remodelling post MI. Due to their essential role during remodelling CFs and aCFs are promising targets for new therapeutical approaches. In the past it has been shown that HIF has several cardioprotective effects including the induction of expression of beneficial target genes[154] or a reduction of collagen synthesis leading to a partial recovery of left ventricular function[161]. Cell-specific HIF stabilisation in CMs and ECs improved cardiac function[129,131]. The present study investigated the effects of HIF signalling in CFs and aCFs in order to define potential differences in their response. In addition, the effects of an aCF-specific HIF-1α stabilisation were explored on gene expression at single cell level and cardiac function.

5.1 Differences in *Hif1a* gene expression and HIF-1α-associated energy metabolism between CFs and aCFs

Ischemia during MI induces HIF-1α signalling in cells within the ischemic area including CFs leading to target gene expression which protects the cells from hypoxic stress[96]. An induced HIF-1α signalling, independent of the trigger stabilising HIF-1α, might facilitate the adaptation of energy metabolism of CFs and aCFs to low oxygen levels. Therefore, one aim of this study was to investigate differences in *Hif1a* gene expression and the HIF-1α-associated metabolic switch between CFs and aCFs.

While the basal *Hif1a* expression of isolated total CFs from healthy wildtype hearts and aCFs from wildtype hearts 5 dpMI did not show significant differences in the qRT-PCR analysis (Figure 6A), the scRNAseq data from the Postn-tdTomato control samples 5 dpMI revealed an increase in *Hif1a* expression in the majority of aCF clusters (group II) compared to the resident CFs (group I) of the same hearts (Figure 18, Figure 25). This effect most likely becomes obscured in the *in vitro* qRT-PCR approach because the Langendorff isolation procedure does not allow separation of remote myocardium and the infarcted area, so that the sample “aCFs” includes all CFs, resident and infarct activated. Differences in *Hif1a* expression between CFs and aCFs, however, could be detected in the *in vivo* scRNAseq data with clearly separated clusters of resident CFs and aCFs. It is known that in the first 24 h post MI HIF-1α protein expression is increased in the peri-infarcted area but not in the non-infarcted

area[162]. The *in vivo* results showed a difference in *Hif1a* gene expression between resident CF clusters, likely representing CFs from non-infarcted tissue, and aCFs from the peri-infarcted area even 5 days after MI. This might indicate active HIF-1α signalling in aCFs still at 5 dpMI. Additionally, *Hif1a* expression was found to be increased in aCFs 5 dpMI in comparison to the aCFs already present in hearts without MI in low numbers (Figure 18).

Besides the MI-induced difference in *Hif1a* expression between resident CFs and aCFs, an increase of *Hif1a* expression was also detected in aCFs of group II clusters 5 dpMI comparing in the transgenic model with HIF-1α stabilisation in POSTN positive aCFs to the respective transgenic control model (Figure 25). This suggests that HIF-1α signalling was upregulated in this in-vivo model.

The effect of increased *Hif1a* expression in aCFs of Postn-Hif-1αdPA mice was transitory and was found to diminished at 21 dpMI (Figure 18), which might be due to either a negative feedback mechanism downregulating *Hif1a* expression or cell death of HIF-1αdPA-expressing aCF. While the regulation of HIF-1α protein has already been extensively studied, not much is known about the transcriptional regulation of *Hif1a* mRNA[163]. In lung epithelial cells it was shown that during prolonged hypoxia HIF-1α signalling decreases *Hif1a* expression due to an increase in natural antisense *Hif1a* and destabilisation of *Hif1a* mRNA[164]. Since natural antisense transcripts of *Hif1a* has been shown to be conserved in mice[165] this could represent a possible negative feedback mechanism activated by the stabilisation of HIF-1α due to the dPA mutation in the Postn-Hif-1αdPA mice. Another explanation for the loss of the effect at 21 dpMI might be a HIF-1α-induced apoptotic cell death of aCFs with the HIF-1α stabilisation over time. The involvement of HIF-1α in hypoxia-induced apoptosis by increasing the tumour suppressor gene p53 has been already shown[166]. It should also be noted that the maturation phase of post-MI remodelling takes place 21 days after infarction, during which mainly matrifibrocytes in the infarct area stabilize the scar and reparative aCFs are deactivated and undergo apoptosis[23,167]. These reparative aCF include the POSTN-expressing aCFs with the HIF-1α stabilisation which are present during the proliferation phase of cardiac remodelling. The deactivation of aCFs is also reflected in the scRNAseq results, which show that in addition to *Hif1a* expression, *Postn* expression also decreased at 21 dpMI compared to the time point 5 dpMI (Figure 18).

Differences in *Hif1a* expression between CFs and aCFs came along with differences in their metabolism. Metabolic differences between CFs and aCFs were seen in the *in vitro* as well as in the *in vivo* approaches. Under basal cell culture conditions with 20% O_2, CFs and aCFs only slightly differed in their energy level (Figure 6B). However, activated CFs from hearts 5 dpMI showed a higher oxygen consumption than CFs from healthy hearts but in parallel were also slightly more glycolytic than CFs which on the first look seems to be contradictory. Note, however, that the aCFs were examined 5 dpMI considered a time point in the proliferative phase of cardiac remodelling. In line with a proliferative phenotype is also the observation that the proliferation-associated cluster 10 in the scRNAseq analysis was mainly composed of cells from the 5 dpMI samples (Figure 15). Proliferating cells are known to use both oxidative phosphorylation and aerobic glycolysis during proliferation[168,169]. Therefore, the higher basal glycolysis (Figure 6C) of aCFs compared to CFs might directly reflect a higher proliferation rate of these cells. Interestingly, only the gene expression of lactate dehydrogenase A (LDHA), which maintains glycolysis, was significantly increased in aCFs compared to CFs under basal conditions (Figure 9). The majority of examined glycolytic genes showed comparable gene expression levels in CFs and aCFs. These findings suggest that the functional differences in metabolism between CFs and aCFs seen in Figure 6 are not caused by changes in metabolic gene expression but may have another level of regulation. One possible other way of glycolytic regulation might be the metabolic reprogramming due to post-translational modification by ubiquitination and deubiquitination of glycolytic enzymes which has been discussed in cancer[170].

Besides the basal metabolic differences between CFs and aCFs, changes induced by A_{2B}R-induced HIF-1α signalling were detected in both cell types. The normoxic HIF-1α induction by A_{2B}R activation raised *Hif1a* expression in both CFs and aCFs to the same extent (Figure 6A). Additionally, the A_{2B}R-mediated HIF-1α induction led to a maximum increase of glycolysis in both CFs and aCFs, accompanied by the expected significant reduction in oxygen consumption (Figure 6B-E). The proton efflux rate from glycolysis significantly increased in both CFs and aCFs to over 90% (Figure 6E). This indicates that both CFs and aCFs completely switched to glycolytic metabolism after A_{2B}R-mediated HIF-1α induction despite oxygen was still available. The difference in

energy metabolism between CFs and aCFs seen under basal conditions was diminished after A_{2B}R-mediated induction of HIF-1α.

While no major differences in metabolic gene expression were detected between CFs and aCFs despite their functional differences under basal conditions (see above), metabolic gene expression differences between both cell types were detected after hypoxia-induced HIF-1α induction (Figure 8). In aCFs, hypoxia-induced HIF-1α signalling caused more significant changes in metabolic gene expression compared to CFs (Figure 8).

Differences that are difficult to categorize were observed for metabolic genes *in vivo* by the aCF-specific HIF-1α stabilisation. At 5 dpMI the HIF-1α stabilisation led to a downregulation of glycolytic genes encoding e.g., aldolase A (*Aldoa*), LDHA (*Ldha*), phosphoglycerate mutase 1 (*Pgam1*), phosphoglycerate kinase 1 (*Pgk1*), pyruvate kinase M1/2 (*Pkm*), solute carrier family 29 member 1 (*Slc29a1*) and triosephosphate isomerase 1 (*Tpi1*) in aCF clusters (group II), as seen in the comparison of cells from Postn-Hif-1αdPA mice to cells from the control mice (Figure 26). These results suggest a negative regulation of glycolysis in aCFs with HIF-1α stabilisation, which might represent a compensatory mechanism that needs to be clarified in further studies. Besides the proteasomal degradation of HIF-1α which can be excluded due to the mutation in the stabilised HIF-1α, there are a number of mechanisms known to negatively regulate HIF-1α and its signalling. Especially, protein-protein interactions can either abrogate the interaction of HIF-1α with transcriptional co-activators or cause modulations to inactivate the HIF-1α protein[171]. One possible mechanism is the potential of HIF-1α to downregulate its own activity[171]. It has been reported that a dominant-negative HIF-1α deletion mutant (dnHIF-1α) negatively regulates HIF-1α activity by inhibiting the formation of the HIF-1 complex[172]. Additionally, the expression of dnHIF-1α led to a suppression of glucose metabolism and cells had a lower glucose uptake[173]. This mechanism could explain the downregulation of glycolytic genes in the aCFs of Postn-Hif-1αdPA mice.

Taken together, the three different approaches to induce HIF-1α in CFs and aCFs affected metabolic gene expression in different ways. While the A_{2B}R-mediated HIF-1α induction resulted in the expected metabolic switch towards glycolysis in both CFs an aCFs (Figure 6), the hypoxia-induced HIF-1α protein (Figure 7) affected metabolic

gene expression more in aCFs than in CFs (Figure 8). Surprisingly, the increase in glycolytic gene expression was not as high as expected. This could be due to the fact that, on the one hand, pharmacological activation of the $A_{2B}R$ might not be fully specific[107] and could have also activated other signalling pathways in addition to HIF-1α induction. On the other hand, it is possible that 6h of hypoxia represents the peak in *Hif1a* expression, so that this time point is too early to detect the full extent of HIF signalling on glycolytic gene expression. In contrast to the two *in vitro* approaches in which the induced HIF-1α is not rescued for degradation, HIF-1α signalling is constantly active in the POSTN positive aCFs in the *in vivo* approach. Therefore, the different effects on metabolic gene expression in the *in vivo* approach compared to the *in vitro* approaches might involve differences in time course of active HIF-1α signalling in the cells (acute vs. stabilised HIF-1α protein expression).

5.2 HIF-1α-induced changes in ECM deposition by CFs and aCFs

One main task of CFs in the healthy heart is to sustain ECM homeostasis. Resident CFs are characterised by a basal ECM turnover and they are part of a complex communications network with the surrounding cells[82–84]. After MI, homeostasis is disturbed and aCFs play a crucial role in cardiac remodelling including the formation of the scar[26]. In the present study differences in ECM deposition between CFs and aCFs were assessed as modulated by HIF signalling using gene expression analysis of fibrosis-associated genes. This included proliferation-associated genes and the identification of proliferative cell clusters post MI. After MI the activation of CFs is well known to be accompanied by an increased proliferation to populate the infarct border zone with ECM-secreting aCFs[174,175].

The activation of CFs after MI led to an increase in fibrotic gene expression especially in aCFs at 5 dpMI: in the *in vitro* approach all tested fibrotic genes showed a trend to be increased in their gene expression in aCFs 5 dpMI compared to CFs from healthy hearts (Figure 9). These results were confirmed in about two thirds of the analysed pro-fibrotic genes when comparing *in vivo* changes in gene expression 5 dpMI in aCFs (group II) from Postn-tdTomato mice with the basal time point (Figure 19). As expected, the expression of genes playing a role in synthesis and deposition of ECM proteins (Table 17) like collagens, collagen triple helix repeat containing 1 (*Cthrc1*), fibronectin 1 (*Fn1*), lysyl oxidase (*Lox*), periostin (*Postn*), tenascin-C (*Tnc*) and tissue inhibitor of

metalloproteinases 1 (*Timp1*) showed higher changes in gene expression at 5 dpMI in aCFs as compared to resident CFs (Figure 19). Tissue inhibitor of metalloproteinases 3 (*Timp3*), which is known to be anti-inflammatory[176,177] as well as anti-fibrotic[178] (Table 17), was found to be decreased in aCFs 5 dpMI which might suggest that the anti-inflammatory response during the transition from the inflammation to the proliferation phase was completed 5 dpMI[41].

Table 17: Known fibrosis-associated functions of significantly altered gene expression in CFs and aCFs from Postn-tdTomato and Postn-Hif-1αdPA mice 5 dpMI.

Protein (*gene*)	Functions	Ref.
Actin alpha 2, smooth muscle (*Acta2*)	assembled into stress fibers, myofibroblast marker post MI	179
Antisense of IGF2R non-protein coding RNA (*Airn*)	anti-fibrotic	180
Collagen triple helix repeat containing 1 (*Cthrc1*)	synthesis and deposition of the fibrotic scar	181
Fibronectin 1 (*Fn1*)	regulates deposition, maturation and stabilisation of ECM proteins	182,183
Lysyl oxidase (*Lox*)	remodelling of ECM	184
Mothers Against Decapentaplegic Homolog 7 (*Smad7*)	anti-fibrotic, protects against TGF-β1-mediated fibrosis	185,186
Periostin, POSTN (*Postn*)	role in cardiac fibrosis, regulator of cellular reorganisation, crucial scaffold for assembling ECM	187,188
Tenascin-C (*Tnc*)	pivotal role in myocardial repair post MI	138
Thrombospondin-1, TSP-1 (*Thbs1*)	promotes cardiac fibrosis by TGF-β1 activation, inhibition of MMPs, anti-angiogenic	189 190
Thrombospondin-2, TSP-2 (*Thbs2*)	pro-fibrotic, anti-angiogenic	191
Thrombospondin-4, TSP-4 (*Thbs4*)	modulates activation of CFs, modification of ECM	192 193
Tissue inhibitor of metalloproteinase 1 (*Timp1*)	promotes myocardial fibrosis	194

Tissue inhibitor of metalloproteinase 3 (*Timp3*)	anti-fibrotic, anti-inflammatory	178 176,177
WNT1-inducible-signaling pathway protein 2 (*Ccn5*)	anti-fibrotic through Smad6-CCN2 pathway	195

Since cardiac remodelling at 5 dpMI is in the proliferation phase, it was expected to observe proliferating aCFs as well as aCFs that transdifferentiate into the myofibroblast phenotype[28,29]. This view was confirmed by the identified proliferative aCF clusters (cluster 10 and 18) and myofibroblast clusters (cluster 3, 4 and 9) which showed the highest proportion of cells 5 dpMI (Figure 15E). The increase in the proportion of cells in the myofibroblast clusters indicates more aCFs with an involvement in ECM deposition and scar formation. At 21 dpMI the cell proportions in aCF clusters (2, 3, 4, 9, 10, 11, 12, 14 and 18) return to nearly the same level as seen in samples from healthy hearts. Interestingly, the cell proportion in the proliferating clusters decreased to a lower level compared to the basal condition. The data are in line with the current model of cardiac remodelling in which aCFs in the maturation phase do not further proliferate and undergo apoptosis[167] and myofibroblasts transform into matrifibrocytes which are closely related to quiescent CFs but differ by being resistant to proliferative stimuli[52].

HIF-1α is rapidly induced *in vivo* by cardiac hypoxia[97] during the ischemic event of MI which leads to the activation of numerous hypoxia-associated signalling pathways. Additionally, HIF-induced changes in gene expression were investigated *in vivo* using a permanent aCF-specific HIF-1α stabilisation due to a mutation in the *Hif1a* sequence. While after a 6 h hypoxia treatment of CFs and aCFs nearly no changes in fibrotic gene expression were detected in both CFs and aCFs (Figure 8), ischemia during MI affected fibrosis-associated gene expression either as direct or indirect effects in aCFs 5 dpMI. As already described above, ischemia induced the activation of CFs which was reflected by the increase of the proportion of cells in group II clusters comparing the Postn-tdTomato samples 5 dpMI with the basal control samples from healthy hearts (Figure 15E). Comparing the CF samples from infarcted hearts 5 dpMI with endogenous hypoxia-mediated HIF-signalling (Postn-tdTomato) and with introduced aCF-specific HIF-1α stabilisation (Postn-Hif-1αdPA mice), differences were detected in the cell proportion in the resident CF (group I) cluster (Figure 23D). The

cell proportion in this cluster (cluster 1) of CFs from Postn-Hif-1αdPA mice was about half the size of CFs from the control Postn-tdTomato mice (Figure 23D). This result suggests that the aCF-specific HIF-1α stabilisation increases the activation of CFs post MI. HIF-1α has already been shown to activate the TGF-β/SMAD pathway in different cell types[196,197]. TGF-β induces the activation of CFs and further the differentiation into myofibroblasts[198]. Gene expression of *Tgfb2* and *Tgfb3* in aCFs from Postn-Hif-1αdPA mice 5 dpMI was found to be upregulated compared to respective controls (Figure 26), suggesting that this axis might contribute to the increased activation of CFs in Postn-Hif-1αdPA mice.

Similar to changes in the proportion of activation of CFs, HIF-1αdPA induction triggered significant changes in fibrosis-associated gene expression in aCFs. MI resulted in upregulated fibrotic gene expression in aCFs 5 dpMI compared to the basal level. As already mentioned above the log2 FCs of the upregulated gene expression appeared to be higher in the aCF clusters (group II) as compared to those in the CF clusters (group I) (Figure 19). Even resident CFs 5 dpMI the majority of which can be assumed to be located in the remote area showed a significantly higher gene expression in the activation markers *Postn* and *Acta2* compared to the basal resident CFs (Figure 19). It is known that after MI not only CFs in the infarct area and border zone are proliferating but also CFs in the remote area[175,199], albeit to a lesser extent. This suggests a higher activation status of CFs also in the remote area without direct exposure to ischemia. The additional HIF-1α stabilisation in aCFs of Postn-Hif-1αdPA mice led to a further increase in gene expression of the genes associated with ECM deposition (collagens, *Fn1*, *Postn*, *Lox* and *Tnc*) (Figure 26) 5 dpMI, which were already upregulated in aCF clusters of Postn-tdTomato mice (Figure 19) 5 dpMI in comparison to respective time controls. Interestingly, HIF-1α stabilisation in Postn-Hif-1αdPA mice affected gene expression of a larger number of fibrosis-associated genes (Figure 26) compared to ischemia alone in CFs 5 dpMI (Figure 19). Genes of three different members of the thrombospondin (TSP, *Thbs*) family were increased in aCFs 5 dpMI from Postn-Hif-1αdPA mice (Figure 26**)**. TSP-1 and TSP-2 are known to promote cardiac fibrosis and have an anti-angiogenic potential[189,191] but also have protective effects in the infarcted heart[190] (see Table 17). TSP-1 has been suggested to play a crucial role in the limitation of the expansion of cardiac fibrosis into the remote area and to decrease adverse cardiac remodelling by inhibiting MMPs[190]. Thus, the

increase in *Thbs1* and *Thbs2* expression in aCFs from Postn-Hif-1αdPA mice might contribute to the limitation of cardiac fibrosis expansion. Besides *Thbs-1* and *-2*, also the expression of *Thbs-4*, which is slightly different in function compared to its family members, was increased in aCFs from Postn-Hif-1αdPA mice. TSP-4 was reported to play a role in the modification of ECM[193] and was also shown to activate CFs[192] which appears to correlate to the increased number of aCFs in Postn-Hif-1αdPA mice post MI (Figure 23). In contrast, HIF-1α stabilisation also induced the expression of antisense of IGF2R non-protein coding RNA (*Airn*), which is anti-fibrotic by inhibition of CF activation[180] and this may counterbalance the possible fibrotic effects of increased aCF numbers in Postn-Hif-1αdPA mice. Other anti-fibrotic genes whose expression levels were upregulated 5 dpMI were *Timp3* and *Smad7,* which are known to inhibit especially TGF-β1-mediated fibrosis[185,186] and therefore might be involved in counteracting excessive fibrosis.

Taken together, hypoxia during the ischemic event of MI induced as expected the activation and proliferation of CFs as well as increased gene expression of genes involved in ECM synthesis and deposition. Additional HIF-1α stabilisation further increased the activation of aCFs along with the expression of ECM-related genes. The parallel increase in anti-fibrotic gene expression might indicate a compensatory mechanism to prevent excessive fibrosis as consequence of increased activation of CFs and pro-fibrotic gene expression. HIF-1α stabilisation in aCFs also increased the expression of fibrosis-associated genes like *Thbs1* and *Thbs2* known to have cardioprotective effects[190]. Comparing both approaches, the *in vitro* and the *in vivo*, the induction of HIF-1α signalling led to different effects on fibrosis-associated gene expression. The lower effects in the *in vitro* data could either be due to the short duration of the *in vitro* hypoxia treatment (6 h) or the *in vivo* approach might involve additional signalling pathways.

5.3 HIF-1α-induced changes in paracrine signalling of CFs and aCFs

In addition to ECM synthesis and deposition another main task of CFs and aCFs is the release of paracrine factors for intercellular communication in tissue homeostasis and as well as in orchestration of cardiac remodelling after MI including modulation of inflammation and angiogenesis[23,51].

Similar to fibrosis-associated genes, CFs and aCFs differed in their expression profile of angiogenesis-associated genes. *In vitro* aCFs 5 dpMI expressed significantly more insulin-like growth factor (*Igf2*) known to promote fibroblast proliferation[200] but also the pro-angiogenic factors insulin-like growth factor binding protein 2 (*Igfbp2*) and platelet-derived growth factor C (*Pdgfc*) compared to CFs from healthy hearts (Figure 9). The additional downregulation of the anti-angiogenic insulin-like growth factor binding protein 3 [201] gene (*Igfbp3*) expression in aCFs compared to CFs (Figure 9) is in support of the view that aCFs are more angiogenic than healthy CFs. This is further supported by scRNAseq *in vivo* data: genes encoding pro-angiogenic factors (Table 18) like collagen 1A1 (*Col1a1*), midkine (MDK, *Mdk*) and pleiotrophonin (PTN, *Ptn*) showed a higher log2 FCs of the upregulation in gene expression after MI in the aCF clusters (group II) than in the resident CF clusters (Figure 21). Interestingly, MDK whose gene expression is induced by HIF-1α[202] has been shown to increase cell survival in response to acute hypoxia and the myocardial injection of MDK had a protective effect against I/R injury[203,204]. The enhanced expression of MDK by aCFs could lead to a positive effect on other cell types in the surrounding area and might decrease the ischemic induced cell deaths. The ischemia-induced upregulation of the pro-angiogenic *Mdk* expression seen in aCFs after MI was not further enhanced by HIF-1α stabilisation in Postn-Hif-1αdPA mice (Figure 26. Interestingly, aCF-specific HIF-1α stabilisation led to a further increase in *Ptn* expression which has been demonstrated to promote cardiac vascularisation after an ischemic event[205]. Additionally, the release of PTN due to cell stress by CMs was shown to inhibit the AKT pathway and potentiated apoptosis[206]. Therefore, an increased release of PTN by aCFs might have positive effects on revascularisation in the infarct and border zone but could also enhance CM apoptosis. In the aCFs with the HIF-1αdPA stabilisation the two additional pro-angiogenic genes fibroblast growth factor receptor 2 (*Fgfr2*) and piezo-type mechanosensitive ion channel component 2 (*Piezo2*) were increased in expression (Figure 26), which were not differentially expressed between CFs and ischemia-induced aCFs (Figure 21). In rat and mouse models *Piezo2* has been identified to be upregulated in cardiac tissue due to mechanical and pharmacological stress, however, its function in cardiac tissue is presently unclear[207].

Table 18: Known angiogenesis-associated functions of significantly altered genes in CFs and aCFs from Postn-tdTomato and Postn-Hif-1αdPA mice 5 dpMI.

Protein (*Gene*)	Functions	Ref.
Collagen 1A1 (*Col1a1*)	stimulates angiogenesis	208
Fibroblast growth factor receptor 2 (*Fgfr2*)	pro-angiogenic through *Fgf2* binding	209
Fibulin 1 (*Fbln1*)	indirect role in angiogenesis by regulating ADAMTS-1	210
Insulin-like growth factor 2 (*Igf2*)	paracrine-acting mitogen, promotes proliferation of fibroblasts	211 200
Insulin-like growth factor binding protein 2 (*Igfbp2*)	manages transport and regulates bioavailability of IGF-1, promotes angiogenesis via PI3K/AKT/VEGFA pathway	212,213 214
Insulin-like growth factor binding protein 3 (*Igfbp3*)	anti-angiogenic by regulating THBS1	201
Midkine (*Mdk*)	heparin-binding growth factor promotes angiogenesis, increased cell survival with acute hypoxia, protective against I/R injury	215 203 204
Platelet-derived growth factor C (*Pdgfc*)	pro-angiogenic factor	216
Piezo-type mechanosensitive ion channel component 2 (*Piezo2*)	pro-angiogenic	217
Pleiotrophin (*Ptn*)	pro-angiogenic, potentiates cardiomyocyte apoptosis	206
Tissue inhibitor of metalloproteinase 3 (*Timp3*)	anti-angiogenic	218

While angiogenic proteins may serve as paracrine signals for the surrounding tissue, cytokines and chemokines are well established paracrine factors. However, in both the *in vitro* (Figure 9) and the *in vivo* (Figure 22) approach, no differences in gene expression of the selected chemokines and cytokines were detected between CFs

and aCFs. Yet gene expression was altered in both resident CF and aCF cluster groups of Postn-tdTomato samples 5 dpMI compared to healthy controls (Figure 22). Hypoxia induced a slight but significant downregulation of the cytokine interleukin 6 (*Il6*) and the chemokine C-X3-C motif chemokine ligand 1 (*Cx3cl1*) in aCFs 5 dpMI *in vitro* (Figure 8) which was not observed in the *in vivo* data from Postn-tdTomato mice 5 dpMI compared to the basal level (Figure 22). Ischemia-associated HIF induction affected the expression of only a low range of the selected paracrine factors. The two genes encoding connective tissue growth factor (CCN2, *Ccn2*) and WNT1 inducible signalling pathway protein 2 (CCN5, *Ccn5*) are involved in intercellular signalling[219], and were significantly upregulated 5 dpMI in both CFs and aCFs (Figure 22). While CCN2 regulates cardiac fibrosis in a pro-fibrotic manner together with its autocrine and paracrine function[220], CCN5 represents an antagonist of CCN2 and can diminish pro-fibrotic gene expression along with inhibition of transdifferentiation of CFs into myofibroblasts[221,222]. The upregulated expression of *Ccn5* might balance the effects of *Ccn2* to prevent excessive cardiac fibrosis. The additional aCF-specific HIF-1α stabilisation in Postn-Hif-1αdPA mice did not affect the *Ccn5* expression, but led to a significant decrease in *Ccn2* expression in both aCF and CF clusters compared to the cells from the control mice 5 dpMI (Figure 26). In combination with the increased expression of the cysteine-rich protein 61 (*Ccn1*) (Figure 26), which regulates fibrogenesis and is thought to inhibit fibrosis[223], this may indicate that the HIF-1α stabilisation can additionally decrease the pro-fibrotic signalling by paracrine factors. One might speculate that the increase in profibrotic gene expression leads to the upregulation of paracrine factors which act in an anti-fibrotic fashion to protect the cells in order to avoid excessive fibrosis.

Taken together, like already seen for fibrosis-associated and metabolic genes, the changes in gene expression differ within the two different approaches to induce HIF-1α. As it was already discussed above (5.2), the *in vitro* approach might not show the full extent of HIF-1α on paracrine signalling due to the short time exposure to hypoxia. In contrast to gene expression of paracrine factors, angiogenic gene expression differed between CFs and aCFs suggesting that aCFs are more angiogenic than CFs. Thus, HIF-1α induced effects on angiogenic gene expression might begin at an early phase of HIF signalling but also is long lasting. Additionally, the increase of pro-

angiogenic gene expression by the HIF-1α stabilisation in the transgenic model suggest a role of HIF-1α in regulating aCF communication with other cell types.

5.4 Influence of HIF-1α signalling in aCFs on cardiac function post MI

In the present study, the influence of HIF-1α signalling on energy metabolism, ECM deposition, and paracrine signalling at the gene expression level has provided evidence that aCF-specific HIF-1α stabilisation seems to influence all these processes. It therefore was consequential to investigate whether these changes in aCF might translate into improved cardiac remodelling over a period of 3 weeks post MI.

Stabilisation of aCF-specific HIF-1α in a transgenic model had no effect on the infarct size (Figure 27), indicating that all observed effects on cardiac function were independent of infarct size. To assess cardiac function, ejection fraction (EF), enddiastolic and the endsystolic volume (EDV and ESV, respectively) of hearts from control mice and Postn-Hif-1αdPA mice were analysed before MI and 1, 7, 14, and 21 dpMI. In the clinic, EF - defined as the ratio of stroke volume to EDV - is the standard parameter to assess systolic function of the heart[224]. MI-induced necrosis of CM leads to a marked decrease in EF indicative of a decrease in systolic heart function[225]. In the present study it was observed that in mice with the aCF-specific HIF-1α stabilisation, EF at day 1 after MI was decreased, however, it did not reach the level of significance (Figure 27). This difference is also mirrored by a significant decrease in EDV at 1dpMI. This initial effect tended to fade away with time: at 21 dpMI the EF and EDV were comparable to the control mice (Figure 27). Together these results suggest that HIF-1α stabilisation in aCF was initially slightly cardioprotective.

This positive short-term effect of Hif-1αdPA stabilisation in CF is similar to the beneficial outcome after acute HIF-signalling induction by ischemic preconditioning which affects the entire heart[118]. Note, however, that long-term stabilisation of HIF-1α in CMs results in a cardiomyopathy[132]. Similarly, it might also be possible that the long-term HIF-1α stabilisation in aCFs may lead to cellular apoptosis and cell renewal over time[226]. The underlying mechanisms by which Hif-1αdPA stabilisation in aCFs alters cardiac function remains to be investigated in future studies.

5.5 Outlook

In this thesis, HIF signalling in CFs and aCFs was characterised by induction of hypoxia under *in vitro* conditions, and by HIF-1αdPA stabilisation *in vivo* in a transgenic model. Numerous differences between CFs and aCFs in their response to HIF-1α protein expression have been identified. Additionally, this study is the first to investigate the influence of cell-specific HIF-1a stabilisation in aCFs on cardiac remodelling after MI.

It was discovered that HIF signalling switches the metabolic state of CFs as well as aCFs on the same extent towards glycolysis even in the presence of oxygen. Interestingly, the long-term stabilisation of HIF-1α in aCFs resulted in a decrease in metabolic genes in both CFs and aCFs suggesting a negative feedback mechanism. To further examine the underlying mechanism of this metabolic switch, which might play a role in cell protection, it might be interesting to perform different metabolic assays in isolated aCFs which are stably transfected to express HIF-1αdPA. Since the present study with chemical transfection of CFs and aCFs was not successful, a viral transduction approach might be more promising. Since the aCF-specific HIF-1α stabilisation affected metabolic gene expression of cells from the CF and aCF clusters to the same extent, it would be interesting to know whether aCFs from the infarct/border zone communicate with CFs from the remote area. Along this line it might be interesting to investigate cell-cell interaction between aCFs and CFs but also with other cardiac cell types.

Using scRNAseq, this study identified the impact of HIF signalling on transcriptional profiles of the different identified CF and aCF clusters. Effects of HIF signalling induced in the ischemic region by MI showed a clear difference between CFs and aCFs with regard to gene expression which was associated with ECM deposition and fibrosis. The additional aCF-specific Hif-1α stabilisation increased fibrosis-associated genes as well as anti-fibrotic genes in cells of the aCF clusters but also in cells from the CF cluster compared to the control Postn-tdTomato samples. The anti-fibrotic genes and corresponding proteins could represent potential targets for drug development to treat cardiac fibrosis. To this end further analyses on the protein level have to be performed. Ideally, the secretome of CFs and aCFs of Postn-Hif-1αdPA mice with aCF-specific HIF-1α stabilisation should be analysed by mass spectrometry.

In addition to the effects on fibrosis-associated genes, the HIF-induced increase in pro-angiogenic and decrease in anti-angiogenic gene expression seen in aCFs suggest a potential role of HIF-1α in communication with ECs, thereby regulating neovascularisation post MI. Thus, HIF-induced pro-angiogenic genes in aCFs could be targeted for therapeutical neovascularisation.

Within this study the transcriptional effects of induced HIF signalling by aCF-specific Hif-1α stabilisation has been investigated in the proliferation (5 dpMI) and maturation (21 dpMI) phase of cardiac remodelling by using scRNAseq. Since the functional heart measurements identified some initial cardioprotective effect of the aCF-specific Hif-1α stabilisation, it would be interesting to further investigate the effects of Hif-1 on gene and protein level in aCFs in the early inflammation phase post MI. Since our transcriptional analysis at day 5 pMI identified changes in paracrine signalling by HIF stabilisation, the effects on communication of CFs and aCFs with ICs could be interesting to further explore during the inflammatory response. Using scRNAseq could give novel insights into the role of HIF-1α-regulated genes during cardiac remodelling.

6 References

1. Roth, G. A. *et al.* Global Burden of Cardiovascular Diseases and Risk Factors, 1990-2019: Update From the GBD 2019 Study. *Journal of the American College of Cardiology* **76,** 2982–3021; 10.1016/j.jacc.2020.11.010 (2020).
2. Thygesen, K. *et al.* Fourth Universal Definition of Myocardial Infarction (2018). *Journal of the American College of Cardiology* **72,** 2231–2264; 10.1016/j.jacc.2018.08.1038 (2018).
3. Ooi, D. S., Isotalo, P. A. & Veinot, J. P. Correlation of Antemortem Serum Creatine Kinase, Creatine Kinase-MB, Troponin I, and Troponin T with Cardiac Pathology. *Clinical Chemistry* **46,** 338–344; 10.1093/clinchem/46.3.338 (2000).
4. Physiologie von Rainer Klinke | ISBN 978-3-13-796006-5 | Fachbuch online kaufen - Lehmanns.de. Available at https://www.lehmanns.de/shop/veterinaermedizin/11485024-9783137960065-physiologie (2024).
5. Vaupel, P., Schaible, H.-G. & Mutschler, E. *Anatomie, Physiologie, Pathophysiologie des Menschen. 158 Tabellen.* 7th ed. (Wissenschaftliche Verlagsgesellschaft Stuttgart, Stuttgart, 2017).
6. Orogo, A. M. & Gustafsson, Å. B. Cell death in the myocardium: my heart won't go on. *IUBMB life* **65,** 651–656; 10.1002/iub.1180 (2013).
7. Lemos, J. A. de, Newby, L. K. & Mills, N. L. A Proposal for Modest Revision of the Definition of Type 1 and Type 2 Myocardial Infarction. *Circulation* **140,** 1773–1775; 10.1161/CIRCULATIONAHA.119.042157 (2019).
8. Bentzon, J. F., Otsuka, F., Virmani, R. & Falk, E. Mechanisms of plaque formation and rupture. *Circulation research* **114,** 1852–1866; 10.1161/CIRCRESAHA.114.302721 (2014).
9. Falk, E., Nakano, M., Bentzon, J. F., Finn, A. V. & Virmani, R. Update on acute coronary syndromes: the pathologists' view. *European heart journal* **34,** 719–728; 10.1093/eurheartj/ehs411 (2013).

10. Saw, J., Mancini, G. B. J. & Humphries, K. H. Contemporary Review on Spontaneous Coronary Artery Dissection. *Journal of the American College of Cardiology* **68,** 297–312; 10.1016/j.jacc.2016.05.034 (2016).

11. Thygesen, K. *et al.* Recommendations for the use of cardiac troponin measurement in acute cardiac care. *European heart journal* **31,** 2197–2204; 10.1093/eurheartj/ehq251 (2010).

12. Thygesen, K. *et al.* How to use high-sensitivity cardiac troponins in acute cardiac care. *European heart journal* **33,** 2252–2257; 10.1093/eurheartj/ehs154 (2012).

13. Daubert, M. A. & Jeremias, A. The utility of troponin measurement to detect myocardial infarction: review of the current findings. *Vascular health and risk management* **6,** 691–699; 10.2147/vhrm.s5306 (2010).

14. Thygesen, K. *et al.* Third universal definition of myocardial infarction. *European heart journal* **33,** 2551–2567; 10.1093/eurheartj/ehs184 (2012).

15. Apple, F. S. *et al.* IFCC educational materials on selected analytical and clinical applications of high sensitivity cardiac troponin assays. *Clinical biochemistry* **48,** 201–203; 10.1016/j.clinbiochem.2014.08.021 (2015).

16. Schmid, J. *et al.* Elevated Cardiac Troponin T in Patients With Skeletal Myopathies. *Journal of the American College of Cardiology* **71,** 1540–1549; 10.1016/j.jacc.2018.01.070 (2018).

17. Vestergaard, K. R. *et al.* Prevalence and significance of troponin elevations in patients without acute coronary disease. *International journal of cardiology* **222,** 819–825; 10.1016/j.ijcard.2016.07.166 (2016).

18. Roberts, W. L. *et al.* Prevention of Analytical False-Positive Increases of Cardiac Troponin I on the Stratus II Analyzer. *Clinical Chemistry* **43,** 860–861; 10.1093/clinchem/43.5.860 (1997).

19. Lum, G., Solarz, D. E. & Farney, L. False Positive Cardiac Troponin Results in Patients Without Acute Myocardial Infarction. *Lab Med* **37,** 546–550; 10.1309/T94UUXTJ3TX5Y9W2 (2006).

20. Anderson, J. L., Karagounis, L. A. & Califf, R. M. Metaanalysis of five reported studies on the relation of early coronary patency grades with mortality and

outcomes after acute myocardial infarction. *The American journal of cardiology* **78,** 1–8; 10.1016/s0002-9149(96)00217-2 (1996).

21. Schäfer, A., König, T., Bauersachs, J. & Akin, M. Novel Therapeutic Strategies to Reduce Reperfusion Injury After Acute Myocardial Infarction. *Current problems in cardiology* **47,** 101398; 10.1016/j.cpcardiol.2022.101398 (2022).
22. Heusch, G. Myocardial ischaemia-reperfusion injury and cardioprotection in perspective. *Nature reviews. Cardiology* **17,** 773–789; 10.1038/s41569-020-0403-y (2020).
23. Prabhu, S. D. & Frangogiannis, N. G. The Biological Basis for Cardiac Repair After Myocardial Infarction: From Inflammation to Fibrosis. *Circulation research* **119,** 91–112; 10.1161/CIRCRESAHA.116.303577 (2016).
24. Gil, H. *et al.* Defining the timeline of periostin upregulation in cardiac fibrosis following acute myocardial infarction in mice. *Scientific Reports* **12,** 21863; 10.1038/s41598-022-26035-y (2022).
25. Creemers, E. E. & Pinto, Y. M. Molecular mechanisms that control interstitial fibrosis in the pressure-overloaded heart. *Cardiovascular research* **89,** 265–272; 10.1093/cvr/cvq308 (2011).
26. Frangogiannis, N. G. Pathophysiology of Myocardial Infarction. *Comprehensive Physiology* **5,** 1841–1875; 10.1002/cphy.c150006 (2015).
27. Humeres, C. & Frangogiannis, N. G. Fibroblasts in the Infarcted, Remodeling, and Failing Heart. *JACC. Basic to translational science* **4,** 449–467; 10.1016/j.jacbts.2019.02.006 (2019).
28. Frangogiannis, N. G. Regulation of the inflammatory response in cardiac repair. *Circulation research* **110,** 159–173; 10.1161/CIRCRESAHA.111.243162 (2012).
29. Arslan, F., Kleijn, D. P. de & Pasterkamp, G. Innate immune signaling in cardiac ischemia. *Nature reviews. Cardiology* **8,** 292–300; 10.1038/nrcardio.2011.38 (2011).
30. Haan, J. J. de, Smeets, M. B., Pasterkamp, G. & Arslan, F. Danger signals in the initiation of the inflammatory response after myocardial infarction. *Mediators of inflammation* **2013,** 206039; 10.1155/2013/206039 (2013).

31. Rossen, R. D. *et al.* Cardiolipin-protein complexes and initiation of complement activation after coronary artery occlusion. *Circulation research* **75,** 546–555; 10.1161/01.res.75.3.546 (1994).

32. Timmers, L. *et al.* The innate immune response in reperfused myocardium. *Cardiovascular research* **94,** 276–283; 10.1093/cvr/cvs018 (2012).

33. Newton, K. & Dixit, V. M. Signaling in innate immunity and inflammation. *Cold Spring Harbor Perspectives in Biology* **4**; 10.1101/cshperspect.a006049 (2012).

34. Shinde, A. V. & Frangogiannis, N. G. Fibroblasts in myocardial infarction: a role in inflammation and repair. *Journal of molecular and cellular cardiology* **70,** 74–82; 10.1016/j.yjmcc.2013.11.015 (2014).

35. Yan, X. *et al.* Temporal dynamics of cardiac immune cell accumulation following acute myocardial infarction. *Journal of molecular and cellular cardiology* **62,** 24–35; 10.1016/j.yjmcc.2013.04.023 (2013).

36. White, G. E., Iqbal, A. J. & Greaves, D. R. CC chemokine receptors and chronic inflammation--therapeutic opportunities and pharmacological challenges. *Pharmacological reviews* **65,** 47–89; 10.1124/pr.111.005074 (2013).

37. Sandanger, Ø. *et al.* The NLRP3 inflammasome is up-regulated in cardiac fibroblasts and mediates myocardial ischaemia-reperfusion injury. *Cardiovascular research* **99,** 164–174; 10.1093/cvr/cvt091 (2013).

38. Saxena, A. *et al.* IL-1 induces proinflammatory leukocyte infiltration and regulates fibroblast phenotype in the infarcted myocardium. *Journal of immunology (Baltimore, Md. : 1950)* **191,** 4838–4848; 10.4049/jimmunol.1300725 (2013).

39. Mantovani, A., Cassatella, M. A., Costantini, C. & Jaillon, S. Neutrophils in the activation and regulation of innate and adaptive immunity. *Nature reviews. Immunology* **11,** 519–531; 10.1038/nri3024 (2011).

40. Geering, B., Stoeckle, C., Conus, S. & Simon, H.-U. Living and dying for inflammation: neutrophils, eosinophils, basophils. *Trends in immunology* **34,** 398–409; 10.1016/j.it.2013.04.002 (2013).

41. Horckmans, M. *et al.* Neutrophils orchestrate post-myocardial infarction healing by polarizing macrophages towards a reparative phenotype. *European heart journal* **38,** 187–197; 10.1093/eurheartj/ehw002 (2017).

42. Kino, T., Khan, M. & Mohsin, S. The Regulatory Role of T Cell Responses in Cardiac Remodeling Following Myocardial Infarction. *International journal of molecular sciences* **21**; 10.3390/ijms21145013 (2020).

43. Frangogiannis, N. G., Michael, L. H. & Entman, M. L. Myofibroblasts in reperfused myocardial infarcts express the embryonic form of smooth muscle myosin heavy chain (SMemb). *Cardiovascular research* **48,** 89–100; 10.1016/s0008-6363(00)00158-9 (2000).

44. Turner, N. A. & Porter, K. E. Function and fate of myofibroblasts after myocardial infarction. *Fibrogenesis & tissue repair* **6,** 5; 10.1186/1755-1536-6-5 (2013).

45. Hinz, B. Formation and function of the myofibroblast during tissue repair. *The Journal of investigative dermatology* **127,** 526–537; 10.1038/sj.jid.5700613 (2007).

46. Hinz, B. The myofibroblast: paradigm for a mechanically active cell. *Journal of biomechanics* **43,** 146–155; 10.1016/j.jbiomech.2009.09.020 (2010).

47. Cleutjens, J. P., Verluyten, M. J., Smiths, J. F. & Daemen, M. J. Collagen remodeling after myocardial infarction in the rat heart. *The American Journal of Pathology* **147,** 325–338 (1995).

48. Dobaczewski, M. *et al.* Smad3 signaling critically regulates fibroblast phenotype and function in healing myocardial infarction. *Circulation research* **107,** 418–428; 10.1161/CIRCRESAHA.109.216101 (2010).

49. Nikolov, A. & Popovski, N. Extracellular Matrix in Heart Disease: Focus on Circulating Collagen Type I and III Derived Peptides as Biomarkers of Myocardial Fibrosis and Their Potential in the Prognosis of Heart Failure: A Concise Review. *Metabolites* **12**; 10.3390/metabo12040297 (2022).

50. Mouton, A. J. *et al.* Fibroblast polarization over the myocardial infarction time continuum shifts roles from inflammation to angiogenesis. *Basic research in cardiology* **114,** 6; 10.1007/s00395-019-0715-4 (2019).

51. Daseke, M. J., Tenkorang, M. A. A., Chalise, U., Konfrst, S. R. & Lindsey, M. L. Cardiac fibroblast activation during myocardial infarction wound healing: Fibroblast polarization after MI. *Matrix biology : journal of the International Society for Matrix Biology* **91-92,** 109–116; 10.1016/j.matbio.2020.03.010 (2020).

52. Fu, X. *et al.* Specialized fibroblast differentiated states underlie scar formation in the infarcted mouse heart. *The Journal of clinical investigation* **128,** 2127–2143; 10.1172/JCI98215 (2018).

53. Venugopal, H., Hanna, A., Humeres, C. & Frangogiannis, N. G. Properties and Functions of Fibroblasts and Myofibroblasts in Myocardial Infarction. *Cells* **11**; 10.3390/cells11091386 (2022).

54. van den Borne, S. W. M. *et al.* Myocardial remodeling after infarction: the role of myofibroblasts. *Nature reviews. Cardiology* **7,** 30–37; 10.1038/nrcardio.2009.199 (2010).

55. Burke, R. M., Burgos Villar, K. N. & Small, E. M. Fibroblast contributions to ischemic cardiac remodeling. *Cellular signalling* **77,** 109824; 10.1016/j.cellsig.2020.109824 (2021).

56. Hanna, A., Shinde, A. V. & Frangogiannis, N. G. Validation of diagnostic criteria and histopathological characterization of cardiac rupture in the mouse model of nonreperfused myocardial infarction. *American journal of physiology. Heart and circulatory physiology* **319,** H948-H964; 10.1152/ajpheart.00318.2020 (2020).

57. Murry, C. E., Reinecke, H. & Pabon, L. M. Regeneration gaps: observations on stem cells and cardiac repair. *Journal of the American College of Cardiology* **47,** 1777–1785; 10.1016/j.jacc.2006.02.002 (2006).

58. Becker, R. O., Chapin, S. & Sherry, R. Regeneration of the ventricular myocardium in amphibians. *Nature* **248,** 145–147; 10.1038/248145a0 (1974).

59. Poss, K. D., Wilson, L. G. & Keating, M. T. Heart regeneration in zebrafish. *Science (New York, N.Y.)* **298,** 2188–2190; 10.1126/science.1077857 (2002).

60. Wernly, B. *et al.* Regenerative Cardiovascular Therapies: Stem Cells and Beyond. *International journal of molecular sciences* **20**; 10.3390/ijms20061420 (2019).

61. Orlic, D. *et al.* Bone marrow cells regenerate infarcted myocardium. *Nature* **410,** 701–705; 10.1038/35070587 (2001).

62. Fisher, S. A., Zhang, H., Doree, C., Mathur, A. & Martin-Rendon, E. Stem cell treatment for acute myocardial infarction. *The Cochrane database of systematic reviews* **2015,** CD006536; 10.1002/14651858.CD006536.pub4 (2015).

63. Furtado, M. B., Nim, H. T., Boyd, S. E. & Rosenthal, N. A. View from the heart: cardiac fibroblasts in development, scarring and regeneration. *Development (Cambridge, England)* **143,** 387–397; 10.1242/dev.120576 (2016).

64. Nam, Y.-J. *et al.* Induction of diverse cardiac cell types by reprogramming fibroblasts with cardiac transcription factors. *Development (Cambridge, England)* **141,** 4267–4278; 10.1242/dev.114025 (2014).

65. Ieda, M. *et al.* Direct reprogramming of fibroblasts into functional cardiomyocytes by defined factors. *Cell* **142,** 375–386; 10.1016/j.cell.2010.07.002 (2010).

66. Takeda, N. *et al.* Cardiac fibroblasts are essential for the adaptive response of the murine heart to pressure overload. *The Journal of clinical investigation* **120,** 254–265; 10.1172/JCI40295 (2010).

67. Fu, J.-D. *et al.* Direct reprogramming of human fibroblasts toward a cardiomyocyte-like state. *Stem cell reports* **1,** 235–247; 10.1016/j.stemcr.2013.07.005 (2013).

68. Sluijter, J. P. G. *et al.* MicroRNA-1 and -499 regulate differentiation and proliferation in human-derived cardiomyocyte progenitor cells. *Arteriosclerosis, thrombosis, and vascular biology* **30,** 859–868; 10.1161/ATVBAHA.109.197434 (2010).

69. Jayawardena, T. M. *et al.* MicroRNA-mediated in vitro and in vivo direct reprogramming of cardiac fibroblasts to cardiomyocytes. *Circulation research* **110,** 1465–1473; 10.1161/CIRCRESAHA.112.269035 (2012).

70. Furtado, M. B. *et al.* Cardiogenic genes expressed in cardiac fibroblasts contribute to heart development and repair. *Circulation research* **114,** 1422–1434; 10.1161/CIRCRESAHA.114.302530 (2014).

71. Hesse, J. *et al.* Single-cell transcriptomics defines heterogeneity of epicardial cells and fibroblasts within the infarcted murine heart. *eLife* **10**; 10.7554/eLife.65921 (2021).

72. Haldar, S. M. A mighty "MyD" guardian of heart function. *Sci. Transl. Med.* **7**; 10.1126/scitranslmed.aaa9139 (2015).

73. Combs, M. D. & Yutzey, K. E. Heart valve development: regulatory networks in development and disease. *Circulation research* **105,** 408–421; 10.1161/CIRCRESAHA.109.201566 (2009).

74. Moore-Morris, T. *et al.* Resident fibroblast lineages mediate pressure overload-induced cardiac fibrosis. *The Journal of clinical investigation* **124,** 2921–2934; 10.1172/JCI74783 (2014).

75. Moore-Morris, T., Guimarães-Camboa, N., Yutzey, K. E., Pucéat, M. & Evans, S. M. Cardiac fibroblasts: from development to heart failure. *Journal of molecular medicine (Berlin, Germany)* **93,** 823–830; 10.1007/s00109-015-1314-y (2015).

76. Doppler, S. A. *et al.* Cardiac fibroblasts: more than mechanical support. *Journal of thoracic disease* **9,** S36-S51; 10.21037/jtd.2017.03.122 (2017).

77. Tarbit, E., Singh, I., Peart, J. N. & Rose'Meyer, R. B. Biomarkers for the identification of cardiac fibroblast and myofibroblast cells. *Heart failure reviews* **24,** 1–15; 10.1007/s10741-018-9720-1 (2019).

78. Nag, A. C. Study of non-muscle cells of the adult mammalian heart: a fine structural analysis and distribution. *Cytobios* **28,** 41–61 (1980).

79. Pinto, A. R. *et al.* Revisiting Cardiac Cellular Composition. *Circulation research* **118,** 400–409; 10.1161/CIRCRESAHA.115.307778 (2016).

80. Camelliti, P., Borg, T. K. & Kohl, P. Structural and functional characterisation of cardiac fibroblasts. *Cardiovascular research* **65,** 40–51; 10.1016/j.cardiores.2004.08.020 (2005).

81. Kohl, P., Camelliti, P., Burton, F. L. & Smith, G. L. Electrical coupling of fibroblasts and myocytes: relevance for cardiac propagation. *Journal of electrocardiology* **38,** 45–50; 10.1016/j.jelectrocard.2005.06.096 (2005).

82. Camelliti, P., Green, C. R., LeGrice, I. & Kohl, P. Fibroblast network in rabbit sinoatrial node: structural and functional identification of homogeneous and heterogeneous cell coupling. *Circulation research* **94,** 828–835; 10.1161/01.RES.0000122382.19400.14 (2004).

83. Goldsmith, E. C. *et al.* Organization of fibroblasts in the heart. *Developmental dynamics : an official publication of the American Association of Anatomists* **230,** 787–794; 10.1002/dvdy.20095 (2004).

84. Manso, A. M., Kang, S.-M. & Ross, R. S. Integrins, focal adhesions, and cardiac fibroblasts. *Journal of investigative medicine : the official publication of the American Federation for Clinical Research* **57,** 856–860; 10.2310/JIM.0b013e3181c5e61f (2009).

85. Acharya, A. *et al.* The bHLH transcription factor Tcf21 is required for lineage-specific EMT of cardiac fibroblast progenitors. *Development (Cambridge, England)* **139,** 2139–2149; 10.1242/dev.079970 (2012).

86. Zeisberg, E. M. *et al.* Endothelial-to-mesenchymal transition contributes to cardiac fibrosis. *Nature medicine* **13,** 952–961; 10.1038/nm1613 (2007).

87. Smith, C. L., Baek, S. T., Sung, C. Y. & Tallquist, M. D. Epicardial-derived cell epithelial-to-mesenchymal transition and fate specification require PDGF receptor signaling. *Circulation research* **108,** e15-26; 10.1161/CIRCRESAHA.110.235531 (2011).

88. Baum, J. & Duffy, H. S. Fibroblasts and myofibroblasts: what are we talking about? *Journal of cardiovascular pharmacology* **57,** 376–379; 10.1097/FJC.0b013e3182116e39 (2011).

89. Leslie, K. O., Taatjes, D. J., Schwarz, J., vonTurkovich, M. & Low, R. B. Cardiac myofibroblasts express alpha smooth muscle actin during right ventricular pressure overload in the rabbit. *The American Journal of Pathology* **139,** 207–216 (1991).

90. Ivey, M. J. & Tallquist, M. D. Defining the Cardiac Fibroblast. *Circulation journal : official journal of the Japanese Circulation Society* **80,** 2269–2276; 10.1253/circj.CJ-16-1003 (2016).

91. Farbehi, N. *et al.* Single-cell expression profiling reveals dynamic flux of cardiac stromal, vascular and immune cells in health and injury. *eLife* **8**; 10.7554/eLife.43882 (2019).

92. Bordin, S., Page, R. C. & Narayanan, A. S. Heterogeneity of normal human diploid fibroblasts: isolation and characterization of one phenotype. *Science (New York, N.Y.)* **223,** 171–173; 10.1126/science.6691142 (1984).

93. Lekic, P. C., Pender, N. & McCulloch, C. A. Is fibroblast heterogeneity relevant to the health, diseases, and treatments of periodontal tissues? *Critical reviews in oral biology and medicine : an official publication of the American Association of Oral Biologists* **8,** 253–268; 10.1177/10454411970080030201 (1997).

94. Tallquist, M. D. Cardiac Fibroblast Diversity. *Annual review of physiology* **82,** 63–78; 10.1146/annurev-physiol-021119-034527 (2020).

95. Chong, J. J. H. *et al.* Adult cardiac-resident MSC-like stem cells with a proepicardial origin. *Cell stem cell* **9,** 527–540; 10.1016/j.stem.2011.10.002 (2011).

96. Lee, J. W., Ko, J., Ju, C. & Eltzschig, H. K. Hypoxia signaling in human diseases and therapeutic targets. *Experimental & molecular medicine* **51,** 1–13; 10.1038/s12276-019-0235-1 (2019).

97. Janbandhu, V. *et al.* Hif-1a suppresses ROS-induced proliferation of cardiac fibroblasts following myocardial infarction. *Cell stem cell* **29,** 281-297.e12; 10.1016/j.stem.2021.10.009 (2022).

98. Bruick, R. K. & McKnight, S. L. A conserved family of prolyl-4-hydroxylases that modify HIF. *Science (New York, N.Y.)* **294,** 1337–1340; 10.1126/science.1066373 (2001).

99. Maxwell, P. H. *et al.* The tumour suppressor protein VHL targets hypoxia-inducible factors for oxygen-dependent proteolysis. *Nature* **399,** 271–275; 10.1038/20459 (1999).

100. Mahon, P. C., Hirota, K. & Semenza, G. L. FIH-1: a novel protein that interacts with HIF-1alpha and VHL to mediate repression of HIF-1 transcriptional activity. *Genes & development* **15,** 2675–2686; 10.1101/gad.924501 (2001).

101. Lando, D. *et al.* FIH-1 is an asparaginyl hydroxylase enzyme that regulates the transcriptional activity of hypoxia-inducible factor. *Genes & development* **16,** 1466–1471; 10.1101/gad.991402 (2002).

102. Déry, M.-A. C., Michaud, M. D. & Richard, D. E. Hypoxia-inducible factor 1: regulation by hypoxic and non-hypoxic activators. *The international journal of biochemistry & cell biology* **37,** 535–540; 10.1016/j.biocel.2004.08.012 (2005).

103. Richard, D. E., Berra, E. & Pouyssegur, J. Nonhypoxic pathway mediates the induction of hypoxia-inducible factor 1alpha in vascular smooth muscle cells. *The Journal of biological chemistry* **275,** 26765–26771; 10.1074/jbc.M003325200 (2000).

104. Feldser, D. *et al.* Reciprocal positive regulation of hypoxia-inducible factor 1alpha and insulin-like growth factor 2. *Cancer research* **59,** 3915–3918 (1999).

105. Görlach, A. *et al.* Thrombin activates the hypoxia-inducible factor-1 signaling pathway in vascular smooth muscle cells: Role of the p22(phox)-containing NADPH oxidase. *Circulation research* **89,** 47–54; 10.1161/hh1301.092678 (2001).

106. Hellwig-Bürgel, T., Rutkowski, K., Metzen, E., Fandrey, J. & Jelkmann, W. Interleukin-1beta and tumor necrosis factor-alpha stimulate DNA binding of hypoxia-inducible factor-1. *Blood* **94,** 1561–1567 (1999).

107. Hesse, J. *et al.* Normoxic induction of HIF-1α by adenosine-A2B R signaling in epicardial stromal cells formed after myocardial infarction. *FASEB journal : official publication of the Federation of American Societies for Experimental Biology* **35,** e21517; 10.1096/fj.202002545R (2021).

108. Kim, W. Y. *et al.* Failure to prolyl hydroxylate hypoxia-inducible factor alpha phenocopies VHL inactivation in vivo. *The EMBO journal* **25,** 4650–4662; 10.1038/sj.emboj.7601300 (2006).

109. Semenza, G. L. HIF-1 and mechanisms of hypoxia sensing. *Current opinion in cell biology* **13,** 167–171; 10.1016/s0955-0674(00)00194-0 (2001).

110. Masoud, G. N. & Li, W. HIF-1α pathway: role, regulation and intervention for cancer therapy. *Acta pharmaceutica Sinica. B* **5,** 378–389; 10.1016/j.apsb.2015.05.007 (2015).

111. Kierans, S. J. *et al.* Hypoxia induces a glycolytic complex in intestinal epithelial cells independent of HIF-1-driven glycolytic gene expression. *Proc. Natl. Acad. Sci. U.S.A.* **120,** e2208117120; 10.1073/pnas.2208117120 (2023).

112. Forsythe, J. A. *et al.* Activation of vascular endothelial growth factor gene transcription by hypoxia-inducible factor 1. *Molecular and cellular biology* **16,** 4604–4613; 10.1128/MCB.16.9.4604 (1996).

113. LaGory, E. L. & Giaccia, A. J. The ever-expanding role of HIF in tumour and stromal biology. *Nature cell biology* **18,** 356–365; 10.1038/ncb3330 (2016).

114. Tamamori, M., Ito, H., Hiroe, M., Marumo, F. & Hata, R. I. Stimulation of collagen synthesis in rat cardiac fibroblasts by exposure to hypoxic culture conditions and suppression of the effect by natriuretic peptides. *Cell biology international* **21,** 175–180; 10.1006/cbir.1997.0130 (1997).

115. Semenza, G. L. Hypoxia-inducible factor 1 and cardiovascular disease. *Annual review of physiology* **76,** 39–56; 10.1146/annurev-physiol-021113-170322 (2014).

116. Sousa Fialho, Maria da Luz, Abd Jamil, A. H., Stannard, G. A. & Heather, L. C. Hypoxia-inducible factor 1 signalling, metabolism and its therapeutic potential in cardiovascular disease. *Biochimica et biophysica acta. Molecular basis of disease* **1865,** 831–843; 10.1016/j.bbadis.2018.09.024 (2019).

117. Schreiber, T., Salhöfer, L., Quinting, T. & Fandrey, J. Things get broken: the hypoxia-inducible factor prolyl hydroxylases in ischemic heart disease. *Basic research in cardiology* **114,** 16; 10.1007/s00395-019-0725-2 (2019).

118. Murry, C. E., Jennings, R. B. & Reimer, K. A. Preconditioning with ischemia: a delay of lethal cell injury in ischemic myocardium. *Circulation* **74,** 1124–1136; 10.1161/01.cir.74.5.1124 (1986).

119. Cai, Z., Luo, W., Zhan, H. & Semenza, G. L. Hypoxia-inducible factor 1 is required for remote ischemic preconditioning of the heart. *Proceedings of the National Academy of Sciences of the United States of America* **110,** 17462–17467; 10.1073/pnas.1317158110 (2013).

120. Cai, Z. *et al.* Hearts from rodents exposed to intermittent hypoxia or erythropoietin are protected against ischemia-reperfusion injury. *Circulation* **108,** 79–85; 10.1161/01.CIR.0000078635.89229.8A (2003).

121. Cai, Z. *et al.* Complete loss of ischaemic preconditioning-induced cardioprotection in mice with partial deficiency of HIF-1 alpha. *Cardiovascular research* **77,** 463–470; 10.1093/cvr/cvm035 (2008).

122. Eckle, T., Köhler, D., Lehmann, R., El Kasmi, K. & Eltzschig, H. K. Hypoxia-inducible factor-1 is central to cardioprotection: a new paradigm for ischemic preconditioning. *Circulation* **118,** 166–175; 10.1161/CIRCULATIONAHA.107.758516 (2008).

123. Kalakech, H. *et al.* Role of hypoxia inducible factor-1α in remote limb ischemic preconditioning. *Journal of molecular and cellular cardiology* **65,** 98–104; 10.1016/j.yjmcc.2013.10.001 (2013).

124. Ockaili, R. *et al.* HIF-1 activation attenuates postischemic myocardial injury: role for heme oxygenase-1 in modulating microvascular chemokine generation. *American journal of physiology. Heart and circulatory physiology* **289,** H542-8; 10.1152/ajpheart.00089.2005 (2005).

125. Zhao, H.-X. *et al.* Attenuation of myocardial injury by postconditioning: role of hypoxia inducible factor-1alpha. *Basic research in cardiology* **105,** 109–118; 10.1007/s00395-009-0044-0 (2010).

126. Dendorfer, A. *et al.* Deferoxamine induces prolonged cardiac preconditioning via accumulation of oxygen radicals. *Free radical biology & medicine* **38,** 117–124; 10.1016/j.freeradbiomed.2004.10.015 (2005).

127. Xi, L., Taher, M., Yin, C., Salloum, F. & Kukreja, R. C. Cobalt chloride induces delayed cardiac preconditioning in mice through selective activation of HIF-1alpha and AP-1 and iNOS signaling. *American journal of physiology. Heart and circulatory physiology* **287,** H2369-75; 10.1152/ajpheart.00422.2004 (2004).

128. Kido, M. *et al.* Hypoxia-inducible factor 1-alpha reduces infarction and attenuates progression of cardiac dysfunction after myocardial infarction in the mouse. *Journal of the American College of Cardiology* **46,** 2116–2124; 10.1016/j.jacc.2005.08.045 (2005).

129. Hölscher, M. *et al.* Cardiomyocyte-specific prolyl-4-hydroxylase domain 2 knock out protects from acute myocardial ischemic injury. *The Journal of biological chemistry* **286,** 11185–11194; 10.1074/jbc.M110.186809 (2011).

130. Zieseniss, A. *et al.* Cardiomyocyte-Specific Transgenic Expression of Prolyl-4-Hydroxylase Domain 3 Impairs the Myocardial Response to Ischemia. *Cellular physiology and biochemistry : international journal of experimental cellular physiology, biochemistry, and pharmacology* **36,** 843–851; 10.1159/000430260 (2015).

131. Fan, Q. *et al.* Depletion of Endothelial Prolyl Hydroxylase Domain Protein 2 and 3 Promotes Cardiomyocyte Proliferation and Prevents Ventricular Failure Induced by Myocardial Infarction. *Circulation* **140,** 440–442; 10.1161/CIRCULATIONAHA.118.039276 (2019).

132. Moslehi, J. *et al.* Loss of hypoxia-inducible factor prolyl hydroxylase activity in cardiomyocytes phenocopies ischemic cardiomyopathy. *Circulation* **122,** 1004–1016; 10.1161/CIRCULATIONAHA.109.922427 (2010).

133. Lei, L. *et al.* Hypoxia-inducible factor-dependent degeneration, failure, and malignant transformation of the heart in the absence of the von Hippel-Lindau protein. *Molecular and cellular biology* **28,** 3790–3803; 10.1128/MCB.01580-07 (2008).

134. Uscategui Calderon, M., Gonzalez, B. A. & Yutzey, K. E. Cardiomyocyte-fibroblast crosstalk in the postnatal heart. *Frontiers in cell and developmental biology* **11,** 1163331; 10.3389/fcell.2023.1163331 (2023).

135. Kaur, H. *et al.* Targeted Ablation of Periostin-Expressing Activated Fibroblasts Prevents Adverse Cardiac Remodeling in Mice. *Circulation research* **118,** 1906–1917; 10.1161/CIRCRESAHA.116.308643 (2016).

136. Hao, Y. *et al.* Integrated analysis of multimodal single-cell data. *Cell* **184,** 3573-3587.e29; 10.1016/j.cell.2021.04.048 (2021).

137. Erickson, H. P. Tenascin-C, tenascin-R and tenascin-X: a family of talented proteins in search of functions. *Current opinion in cell biology* **5,** 869–876; 10.1016/0955-0674(93)90037-q (1993).

138. Imanaka-Yoshida, K. *et al.* Tenascin-C modulates adhesion of cardiomyocytes to extracellular matrix during tissue remodeling after myocardial infarction. *Laboratory investigation; a journal of technical methods and pathology* **81,** 1015–1024; 10.1038/labinvest.3780313 (2001).

139. Eden, E., Navon, R., Steinfeld, I., Lipson, D. & Yakhini, Z. GOrilla: a tool for discovery and visualization of enriched GO terms in ranked gene lists. *BMC bioinformatics* **10,** 48; 10.1186/1471-2105-10-48 (2009).

140. Tallquist, M. D. & Molkentin, J. D. Redefining the identity of cardiac fibroblasts. *Nature reviews. Cardiology* **14,** 484–491; 10.1038/nrcardio.2017.57 (2017).

141. Ilicic, T. *et al.* Classification of low quality cells from single-cell RNA-seq data. *Genome biology* **17,** 29; 10.1186/s13059-016-0888-1 (2016).

142. Lun, A. T. L., McCarthy, D. J. & Marioni, J. C. A step-by-step workflow for low-level analysis of single-cell RNA-seq data with Bioconductor. *F1000Research* **5,** 2122; 10.12688/f1000research.9501.2 (2016).

143. Hu, C. *et al.* CellMarker 2.0: an updated database of manually curated cell markers in human/mouse and web tools based on scRNA-seq data. *Nucleic acids research* **51,** D870-D876; 10.1093/nar/gkac947 (2023).

144. Zolfaghari, S. *et al.* Tissue distribution and transcriptional regulation of CCN5 in the heart after myocardial infarction. *Journal of cell communication and signaling* **16,** 377–395; 10.1007/s12079-021-00659-7 (2022).

145. Kretzschmar, K. *et al.* Profiling proliferative cells and their progeny in damaged murine hearts. *Proceedings of the National Academy of Sciences of the United States of America* **115,** E12245-E12254; 10.1073/pnas.1805829115 (2018).

146. Kanisicak, O. *et al.* Genetic lineage tracing defines myofibroblast origin and function in the injured heart. *Nature communications* **7,** 12260; 10.1038/ncomms12260 (2016).

147. Bochmann, L. *et al.* Revealing new mouse epicardial cell markers through transcriptomics. *PloS one* **5,** e11429; 10.1371/journal.pone.0011429 (2010).

148. Liang, R. *et al.* Elevated CDKN1A (P21) mediates β-thalassemia erythroid apoptosis, but its loss does not improve β-thalassemic erythropoiesis. *Blood advances* **7,** 6873–6885; 10.1182/bloodadvances.2022007655 (2023).

149. He, W. *et al.* MiR-155 Knockout in Fibroblasts Improves Cardiac Remodeling by Targeting Tumor Protein p53-Inducible Nuclear Protein 1. *Journal of cardiovascular pharmacology and therapeutics* **21,** 423–435; 10.1177/1074248415616188 (2016).

150. Nechushtan, A., Smith, C. L., Hsu, Y. T. & Youle, R. J. Conformation of the Bax C-terminus regulates subcellular location and cell death. *The EMBO journal* **18,** 2330–2341; 10.1093/emboj/18.9.2330 (1999).

151. Kirkwood, P. M. *et al.* Single-cell RNA sequencing redefines the mesenchymal cell landscape of mouse endometrium. *FASEB journal : official publication of the Federation of American Societies for Experimental Biology* **35,** e21285; 10.1096/fj.202002123R (2021).

152. Chen, H. *et al.* Functional analysis of a novel potassium channel (KCNA1) mutation in hereditary myokymia. *Neurogenetics* **8,** 131–135; 10.1007/s10048-006-0071-z (2007).

153. Patyal, P., Fil, D. & Wight, P. A. Plp1 in the enteric nervous system is preferentially expressed during early postnatal development in mouse as DM20, whose expression appears reliant on an intronic enhancer. *Frontiers in cellular neuroscience* **17,** 1175614; 10.3389/fncel.2023.1175614 (2023).

154. Schreiber, T., Salhöfer, L., Quinting, T. & Fandrey, J. Things get broken: the hypoxia-inducible factor prolyl hydroxylases in ischemic heart disease. *Basic research in cardiology* **114,** 16; 10.1007/s00395-019-0725-2 (2019).

155. Zhang, H. *et al.* NSA2, a novel nucleolus protein regulates cell proliferation and cell cycle. *Biochemical and biophysical research communications* **391,** 651–658; 10.1016/j.bbrc.2009.11.114 (2010).

156. Ali, S. R. *et al.* Developmental heterogeneity of cardiac fibroblasts does not predict pathological proliferation and activation. *Circulation research* **115,** 625–635; 10.1161/CIRCRESAHA.115.303794 (2014).

157. Wang, T., Lu, J., Wang, R., Cao, W. & Xu, J. TOP2A promotes proliferation and metastasis of hepatocellular carcinoma regulated by miR-144-3p. *Journal of Cancer* **13,** 589–601; 10.7150/jca.64017 (2022).

158. Gerdes, J., Schwab, U., Lemke, H. & Stein, H. Production of a mouse monoclonal antibody reactive with a human nuclear antigen associated with cell proliferation. *International journal of cancer* **31,** 13–20; 10.1002/ijc.2910310104 (1983).

159. Piekny, A. J. & Maddox, A. S. The myriad roles of Anillin during cytokinesis. *Seminars in cell & developmental biology* **21,** 881–891; 10.1016/j.semcdb.2010.08.002 (2010).

160. Feng, T. *et al.* CCN1-Induced Cellular Senescence Promotes Heart Regeneration. *Circulation* **139,** 2495–2498; 10.1161/CIRCULATIONAHA.119.039530 (2019).

161. Nwogu, J. I. *et al.* Inhibition of collagen synthesis with prolyl 4-hydroxylase inhibitor improves left ventricular function and alters the pattern of left ventricular dilatation after myocardial infarction. *Circulation* **104,** 2216–2221; 10.1161/hc4301.097193 (2001).

162. Lee, S. H. *et al.* Early expression of angiogenesis factors in acute myocardial ischemia and infarction. *The New England journal of medicine* **342,** 626–633; 10.1056/NEJM200003023420904 (2000).

163. Cavadas, M. A., Nguyen, L. K. & Cheong, A. Hypoxia-inducible factor (HIF) network: insights from mathematical models. *Cell communication and signaling : CCS* **11,** 42; 10.1186/1478-811X-11-42 (2013).

164. Uchida, T. *et al.* Prolonged hypoxia differentially regulates hypoxia-inducible factor (HIF)-1alpha and HIF-2alpha expression in lung epithelial cells: implication of natural antisense HIF-1alpha. *The Journal of biological chemistry* **279,** 14871–14878; 10.1074/jbc.M400461200 (2004).

165. Rossignol, F. *et al.* Natural antisense transcripts of HIF-1alpha are conserved in rodents. *Gene* **339,** 121–130; 10.1016/j.gene.2004.06.029 (2004).

166. Greijer, A. E. & van der Wall, E. The role of hypoxia inducible factor 1 (HIF-1) in hypoxia induced apoptosis. *Journal of clinical pathology* **57,** 1009–1014; 10.1136/jcp.2003.015032 (2004).

167. Takemura, G. *et al.* Role of apoptosis in the disappearance of infiltrated and proliferated interstitial cells after myocardial infarction. *Circulation research* **82,** 1130–1138; 10.1161/01.res.82.11.1130 (1998).

168. Lunt, S. Y. & Vander Heiden, M. G. Aerobic glycolysis: meeting the metabolic requirements of cell proliferation. *Annual review of cell and developmental biology* **27,** 441–464; 10.1146/annurev-cellbio-092910-154237 (2011).

169. Vander Heiden, M. G., Cantley, L. C. & Thompson, C. B. Understanding the Warburg effect: the metabolic requirements of cell proliferation. *Science (New York, N.Y.)* **324,** 1029–1033; 10.1126/science.1160809 (2009).

170. Xie, Y. *et al.* Ubiquitination regulation of aerobic glycolysis in cancer. *Life sciences* **292,** 120322; 10.1016/j.lfs.2022.120322 (2022).

171. Bárdos, J. I. & Ashcroft, M. Negative and positive regulation of HIF-1: a complex network. *Biochimica et biophysica acta* **1755,** 107–120; 10.1016/j.bbcan.2005.05.001 (2005).

172. Halterman, M. W. & Federoff, H. J. HIF-1alpha and p53 promote hypoxia-induced delayed neuronal death in models of CNS ischemia. *Experimental neurology* **159,** 65–72; 10.1006/exnr.1999.7160 (1999).

173. Chen, J. *et al.* Dominant-negative hypoxia-inducible factor-1 alpha reduces tumorigenicity of pancreatic cancer cells through the suppression of glucose metabolism. *The American Journal of Pathology* **162,** 1283–1291; 10.1016/s0002-9440(10)63924-7 (2003).

174. Burke, R. M. *et al.* Small proline-rich protein 2B drives stress-dependent p53 degradation and fibroblast proliferation in heart failure. *Proceedings of the National Academy of Sciences of the United States of America* **115,** E3436-E3445; 10.1073/pnas.1717423115 (2018).

175. Ivey, M. J. *et al.* Resident fibroblast expansion during cardiac growth and remodeling. *Journal of molecular and cellular cardiology* **114,** 161–174; 10.1016/j.yjmcc.2017.11.012 (2018).

176. Kandalam, V. *et al.* Early activation of matrix metalloproteinases underlies the exacerbated systolic and diastolic dysfunction in mice lacking TIMP3 following myocardial infarction. *American Journal of Physiology-Heart and Circulatory Physiology* **299,** H1012-H1023; 10.1152/ajpheart.00246.2010 (2010).

177. Smookler, D. S. *et al.* Cutting Edge: Tissue Inhibitor of Metalloproteinase 3 Regulates TNF-Dependent Systemic Inflammation. *The Journal of Immunology* **176,** 721–725; 10.4049/jimmunol.176.2.721 (2006).

178. Fan, D. *et al.* Differential role of TIMP2 and TIMP3 in cardiac hypertrophy, fibrosis, and diastolic dysfunction. *Cardiovascular research* **103,** 268–280; 10.1093/cvr/cvu072 (2014).

179. Li, Y. *et al.* Loss of Acta2 in cardiac fibroblasts does not prevent the myofibroblast differentiation or affect the cardiac repair after myocardial infarction. *Journal of molecular and cellular cardiology* **171,** 117–132; 10.1016/j.yjmcc.2022.08.003 (2022).

180. Peng, T. *et al.* LncRNA Airn alleviates diabetic cardiac fibrosis by inhibiting activation of cardiac fibroblasts via a m6A-IMP2-p53 axis. *Biology direct* **17,** 32; 10.1186/s13062-022-00346-6 (2022).

181. Pyagay, P. *et al.* Collagen triple helix repeat containing 1, a novel secreted protein in injured and diseased arteries, inhibits collagen expression and promotes cell migration. *Circulation research* **96,** 261–268; 10.1161/01.RES.0000154262.07264.12 (2005).

182. Sottile, J. *et al.* Fibronectin-dependent collagen I deposition modulates the cell response to fibronectin. *American journal of physiology. Cell physiology* **293,** C1934-46; 10.1152/ajpcell.00130.2007 (2007).

183. Valiente-Alandi, I. *et al.* Inhibiting Fibronectin Attenuates Fibrosis and Improves Cardiac Function in a Model of Heart Failure. *Circulation* **138,** 1236–1252; 10.1161/CIRCULATIONAHA.118.034609 (2018).

184. López, B. *et al.* Role of lysyl oxidase in myocardial fibrosis: from basic science to clinical aspects. *American Journal of Physiology-Heart and Circulatory Physiology* **299,** H1-H9; 10.1152/ajpheart.00335.2010 (2010).

185. Hu, H.-H. *et al.* New insights into TGF-β/Smad signaling in tissue fibrosis. *Chemico-biological interactions* **292,** 76–83; 10.1016/j.cbi.2018.07.008 (2018).

186. Miyazawa, K. & Miyazono, K. Regulation of TGF-β Family Signaling by Inhibitory Smads. *Cold Spring Harbor Perspectives in Biology* **9**; 10.1101/cshperspect.a022095 (2017).

187. Landry, N. M., Cohen, S. & Dixon, I. M. C. Periostin in cardiovascular disease and development: a tale of two distinct roles. *Basic Res Cardiol* **113**; 10.1007/s00395-017-0659-5 (2018).

188. Qiao, B., Liu, X., Wang, B. & Wei, S. The role of periostin in cardiac fibrosis. *Heart Fail Rev* **29,** 191–206; 10.1007/s10741-023-10361-y (2023).

189. Zhou, Y., Ng, D. Y. E., Richards, A. M. & Wang, P. microRNA-221 Inhibits Latent TGF-β1 Activation through Targeting Thrombospondin-1 to Attenuate Kidney Failure-Induced Cardiac Fibrosis. *Molecular Therapy. Nucleic Acids* **22,** 803–814; 10.1016/j.omtn.2020.09.041 (2020).

190. Chatila, K. *et al.* The role of the thrombospondins in healing myocardial infarcts. *Cardiovascular & hematological agents in medicinal chemistry* **5,** 21–27; 10.2174/187152507779315813 (2007).

191. Reinecke, H. *et al.* Lack of thrombospondin-2 reduces fibrosis and increases vascularity around cardiac cell grafts. *Cardiovascular pathology : the official journal of the Society for Cardiovascular Pathology* **22,** 91–95; 10.1016/j.carpath.2012.03.005 (2013).

192. Sawaki, D. *et al.* Modulation of cardiac fibrosis by Krüppel-like factor 6 through transcriptional control of thrombospondin 4 in cardiomyocytes. *Cardiovascular research* **107,** 420–430; 10.1093/cvr/cvv155 (2015).

193. Mustonen, E., Ruskoaho, H. & Rysä, J. Thrombospondin-4, tumour necrosis factor-like weak inducer of apoptosis (TWEAK) and its receptor Fn14: novel extracellular matrix modulating factors in cardiac remodelling. *Annals of medicine* **44,** 793–804; 10.3109/07853890.2011.614635 (2012).

194. Takawale, A. *et al.* Tissue Inhibitor of Matrix Metalloproteinase-1 Promotes Myocardial Fibrosis by Mediating CD63–Integrin β1 Interaction. *Hypertension* **69,** 1092–1103; 10.1161/HYPERTENSIONAHA.117.09045 (2017).

195. XU, H. *et al.* CCN5 attenuates profibrotic phenotypes of fibroblasts through the Smad6-CCN2 pathway: Potential role in epidural fibrosis. *International Journal of Molecular Medicine* **36,** 123–129; 10.3892/ijmm.2015.2190 (2015).

196. Mingyuan, X. *et al.* Hypoxia-inducible factor-1α activates transforming growth factor-β1/Smad signaling and increases collagen deposition in dermal fibroblasts. *Oncotarget* **9,** 3188–3197; 10.18632/oncotarget.23225 (2018).

197. Kushida, N. *et al.* Hypoxia-Inducible Factor-1α Activates the Transforming Growth Factor-β/SMAD3 Pathway in Kidney Tubular Epithelial Cells. *American journal of nephrology* **44,** 276–285; 10.1159/000449323 (2016).

198. Khalil, H. *et al.* Fibroblast-specific TGF-β-Smad2/3 signaling underlies cardiac fibrosis. *The Journal of clinical investigation* **127,** 3770–3783; 10.1172/JCI94753 (2017).

199. Talman, V. & Ruskoaho, H. Cardiac fibrosis in myocardial infarction-from repair and remodeling to regeneration. *Cell and tissue research* **365,** 563–581; 10.1007/s00441-016-2431-9 (2016).

200. Zhu, Y. *et al.* Insulin-like Growth Factor-2 (IGF-2) in Fibrosis. *Biomolecules* **12**; 10.3390/biom12111557 (2022).

201. Shih, H.-J., Chen, C.-L. & Torng, P.-L. IGFBP3 inhibits angiogenesis through intracellular regulation of THBS1 expression. *American Journal of Cancer Research* **10,** 1728–1744 (2020).

202. Reynolds, P. R., Mucenski, M. L., Le Cras, T. D., Nichols, W. C. & Whitsett, J. A. Midkine is regulated by hypoxia and causes pulmonary vascular remodeling. *The Journal of biological chemistry* **279,** 37124–37132; 10.1074/jbc.M405254200 (2004).

203. Bădilă, E. *et al.* Midkine proteins in cardio-vascular disease. Where do we come from and where are we heading to? *European journal of pharmacology* **762,** 464–471; 10.1016/j.ejphar.2015.06.040 (2015).

204. Horiba, M. *et al.* Midkine plays a protective role against cardiac ischemia/reperfusion injury through a reduction of apoptotic reaction. *Circulation* **114,** 1713–1720; 10.1161/CIRCULATIONAHA.106.632273 (2006).

205. Christman, K. L. *et al.* Enhanced neovasculature formation in ischemic myocardium following delivery of pleiotrophin plasmid in a biopolymer. *Biomaterials* **26,** 1139–1144; 10.1016/j.biomaterials.2004.04.025 (2005).

206. Li, J. *et al.* The pro-angiogenic cytokine pleiotrophin potentiates cardiomyocyte apoptosis through inhibition of endogenous AKT/PKB activity. *The Journal of biological chemistry* **282,** 34984–34993; 10.1074/jbc.M703513200 (2007).

207. Kloth, B. *et al.* Piezo2 is not an indispensable mechanosensor in murine cardiomyocytes. *Scientific Reports* **12,** 8193; 10.1038/s41598-022-12085-9 (2022).

208. Twardowski, T., Fertala, A., Orgel, J. P. R. O. & San Antonio, J. D. Type I collagen and collagen mimetics as angiogenesis promoting superpolymers. *Current pharmaceutical design* **13,** 3608–3621; 10.2174/138161207782794176 (2007).

209. Wu, X. Y. *et al.* Formononetin, a novel FGFR2 inhibitor, potently inhibits angiogenesis and tumor growth in preclinical models. *Oncotarget* **6,** 44563–44578; 10.18632/oncotarget.6310 (2015).

210. Aksoy, A. *et al.* A preliminary study: is fibulin 1 a friend or an enemy that needs to be silenced with siRNAs for mesothelioma? *Contemporary oncology (Poznan, Poland)* **24,** 241–246; 10.5114/wo.2020.102826 (2020).

211. Shen, H. *et al.* Mononuclear diploid cardiomyocytes support neonatal mouse heart regeneration in response to paracrine IGF2 signaling. *eLife* **9**; 10.7554/eLife.53071 (2020).

212. Kang, H. S. *et al.* Regulation of IGFBP-2 expression during fasting. *The Biochemical journal* **467,** 453–460; 10.1042/BJ20141248 (2015).

213. Wheatcroft, S. B. & Kearney, M. T. IGF-dependent and IGF-independent actions of IGF-binding protein-1 and -2: implications for metabolic homeostasis. *Trends in endocrinology and metabolism: TEM* **20,** 153–162; 10.1016/j.tem.2009.01.002 (2009).

214. Qian, S., Wang, F., Liao, W. & Liu, J. The role of HMGA2 in activating the IGFBP2 expression to promote angiogenesis and LUAD metastasis via the

PI3K/AKT/VEGFA signaling pathway. *Neoplasma* **71,** 22–36; 10.4149/neo_2024_230907N476 (2024).

215. Shin, D. H. *et al.* Midkine Is a Potential Therapeutic Target of Tumorigenesis, Angiogenesis, and Metastasis in Non-Small Cell Lung Cancer. *Cancers* **12**; 10.3390/cancers12092402 (2020).

216. Crawford, Y. *et al.* PDGF-C mediates the angiogenic and tumorigenic properties of fibroblasts associated with tumors refractory to anti-VEGF treatment. *Cancer cell* **15,** 21–34; 10.1016/j.ccr.2008.12.004 (2009).

217. Yang, H. *et al.* Piezo2 protein: A novel regulator of tumor angiogenesis and hyperpermeability. *Oncotarget* **7,** 44630–44643; 10.18632/oncotarget.10134 (2016).

218. He, M. *et al.* Overexpression of TIMP3 inhibits discogenic pain by suppressing angiogenesis and the expression of substance P in nucleus pulposus. *Molecular medicine reports* **21,** 1163–1171; 10.3892/mmr.2020.10922 (2020).

219. Kular, L., Pakradouni, J., Kitabgi, P., Laurent, M. & Martinerie, C. The CCN family: a new class of inflammation modulators? *Biochimie* **93,** 377–388; 10.1016/j.biochi.2010.11.010 (2011).

220. Charrier, A. & Brigstock, D. R. Regulation of pancreatic function by connective tissue growth factor (CTGF, CCN2). *Cytokine & growth factor reviews* **24,** 59–68; 10.1016/j.cytogfr.2012.07.001 (2013).

221. Yoon, P. O. *et al.* The opposing effects of CCN2 and CCN5 on the development of cardiac hypertrophy and fibrosis. *Journal of molecular and cellular cardiology* **49,** 294–303; 10.1016/j.yjmcc.2010.04.010 (2010).

222. XU, H. *et al.* CCN2 and CCN5 exerts opposing effect on fibroblast proliferation and transdifferentiation induced by TGF-β. *Clinical and experimental pharmacology & physiology* **42,** 1207–1219; 10.1111/1440-1681.12470 (2015).

223. Zhao, J. *et al.* Prognostic Significance of Serum Cysteine-Rich Protein 61 in Patients with Acute Heart Failure. *Cellular physiology and biochemistry : international journal of experimental cellular physiology, biochemistry, and pharmacology* **48,** 1177–1187; 10.1159/000491984 (2018).

224. Iwano, H. & Little, W. C. Heart failure: what does ejection fraction have to do with it? *Journal of cardiology* **62,** 1–3; 10.1016/j.jjcc.2013.02.017 (2013).

225. Ellis, S. G., Henschke, C. I., Sandor, T., Wynne, J. & Kloner, R. A. Relation between the transmural extent of acute myocardial infarction and associated myocardial contractility two weeks after infarction. *The American journal of cardiology* **55,** 1412–1416; 10.1016/0002-9149(85)90515-6 (1985).

226. Piret, J.-P., Mottet, D., Raes, M. & Michiels, C. Is HIF-1alpha a pro- or an anti-apoptotic protein? *Biochemical pharmacology* **64,** 889–892; 10.1016/s0006-2952(02)01155-3 (2002).

7 Acknowledgement

At the end of this thesis, I would like to thank everyone who has supported and encouraged me during this exciting and thrilling time.

Special thanks go to Prof. Dr. Jürgen Schrader, who gave me the opportunity to write my doctoral thesis in a medically relevant and interesting field of research and was always there to help and advise me. Of course, I would like to thank my entire working group, especially Julia Hesse and Christina Alter, with whom I was able to discuss my results at any time, who always gave me good food for thought and always supported me. I would also like to thank Dr. Ding for conducting all the MI surgeries, without which my work would not have been possible.

Furthermore, I want to thank Prof. Dr. Eckhard Lammert for serving as my second assessor.

I would like to specifically acknowledge the Genomics and Transcriptomics Laboratory of Prof. Dr. Karl Köhrer at the Biological-Medical Research Centre (BMFZ) for the collaboration. Special thanks to Dr. Tobias Lautwein who conducted the scRNAseq analysis and always advised me.

I would like to thank Prof. Dr. Ute Warnecke-Eberz for the opportunity to measure the TaqMan Array Cards in her working group at the University Hospital of Cologne.

Beyond this, I appreciate the opportunity of being part of the graduate school IRTG1902 with special thanks to Prof. Dr. Axel Gödecke und Sandra Berger who always supported me. In this program I was able to take part in interesting lectures and seminars and above all I had the opportunity to take part in a 3-month research exchange with UVA in Virginia, USA. I would especially like to thank Prof. Dr. Brant Isakson, whose department gave me a warm welcome and enabled me to gain valuable experience that I would never want to miss again.

I would also like to emphasise my colleagues Jasmin Bahr, Vera Flocke, Ria Zalfen and Anne Hemmers, who became good friends in a very short time and without whose support, assistance, discussions, coffee breaks and understanding, everything would

have been much more difficult. I couldn't have wished for better companions during this time.

Of course, I would like to express my heartfelt thanks to my family, who have always believed in me, have supported me in everything throughout my life and have also stood by me in my good but also difficult times. Thank you, mum, dad and grandma, I wouldn't have got this far without you!

Additionally, I want to thank my boyfriend Patrick, who met me in the hardest time during my PhD, endured all my moods and supported me in everything without restrictions. Thank you for your unconditional support and your belief in me.

Last but not least I want to thank my girls for being the best friends and always being there when I needed them. Lea, Lea, Emma, G, Vivi, Eileen, Leo, I can't even put into words how grateful I am to you for always being by my side, for cushioning my breakdowns and for always encouraging me. Thank you for everything.

8 Affidavit

I solemnly affirm, under penalty of perjury, that the dissertation titled “Impact of HIF-1α-signalling in cardiac fibroblasts on healing processes after myocardial infarction” was written by me independently and without improper outside assistance, adhering to the “principles for the assurance of good scientific practice at the Heinrich-Heine-University Düsseldorf”. The dissertation has not been submitted to any other institution or in comparable form. Furthermore, I have not made any unsuccessful attempts at obtaining a doctorate to date.

Düsseldorf, _____

Julia Steinhausen